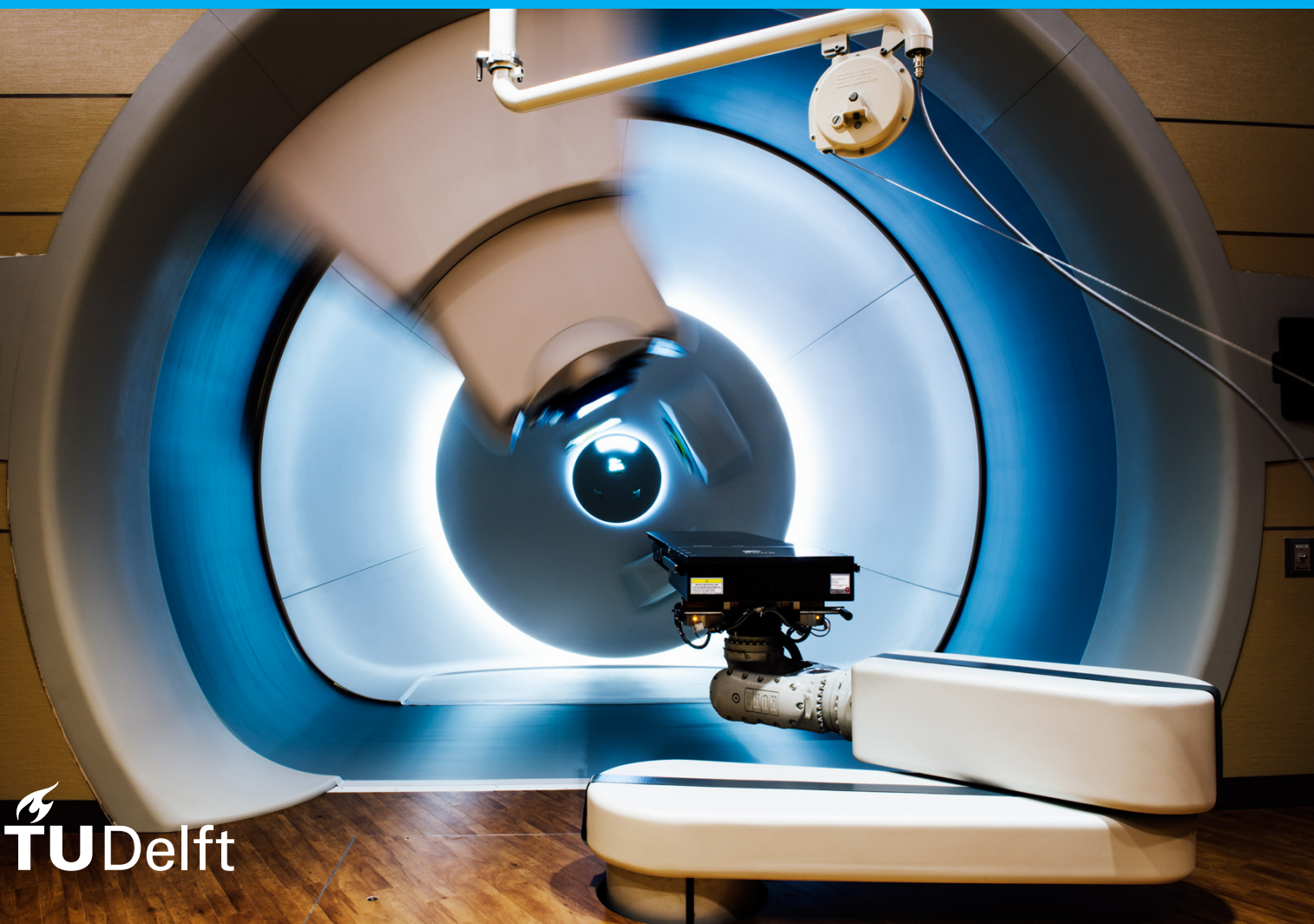


MSc Thesis

Irregular breathing in proton therapy

Erik den Boer



MSc Thesis

The effect of irregular breathing on the interplay effect in pencil beam scanning proton therapy

by

Erik den Boer

to obtain the degree of Master of Science
at the Delft University of Technology,
to be defended publicly on Monday May 25, 2020 at 09:30 AM.

Supervisors: Dr. Zoltán Perkó, Dr. Jörg Wulff (external)
Student number: 5004023
Project duration: March 18, 2019 – May 25, 2020
Thesis committee: Dr. Z. Perkó, TU Delft, supervisor
Dr. ir. D. R. Schaart, TU Delft
Dr. ir. M. C. Goorden, TU Delft
Dr. J. Wulff, Westdeutsches Protonentherapiezentrum Essen

An electronic version of this thesis is available at <http://repository.tudelft.nl/>.
Cover image source: © 2020 Texas Center for Proton Therapy

Abstract

Background Pencil beam scanning (PBS) is becoming a more common treatment modality. However, its ability to deal with moving targets is known to be limited, as beam motion and target motion can reinforce each other, deteriorating the planned dose distribution in what is called the interplay effect. Literature concerning breathing motion usually investigates regular, repeating patterns. However, human breathing is irregular. This work aims to investigate the magnitude of the interplay effect when considering irregular breathing signals.

Method In silico calculations of dose distributions were made in the treatment planning system RaySearch (version 7.99), using an XCAT phantom with 50 CT phases to model a moving patient anatomy. An interplay calculator was included in the treatment planning system, allowing calculation of disturbed doses based on an input treatment plan and an irradiation time model for an IBA Proteus Plus proton therapy accelerator. The target investigated was a spherical tumour in the liver with a diameter of 5 cm, irradiated with two beams each delivering a uniform dose to a prescription dose of 63 Gy. Plans without and with 5x layered repainting were created. Clinically realistic regular breathing patterns were generated to establish a baseline, after which irregularities were introduced. The basic form for all patterns was a \sin^4 signal, with regular signal amplitude ranging from 6 to 18 mm, period ranging from 3 to 4 s and phase between 0 and 2π . Irregularities that were considered were baseline shifts up to 34 mm, changing amplitudes ranging between 6 and 18 mm, changing periods between 1.6 and 5.2 s and some combinations thereof. Evaluation was done by looking at dose homogeneity HI_5 and the fraction of the CTV volume that received a dose outside of the clinical limits of 95% and 107%, $V_{107/95}$. For the regular patterns, both a systematic and a randomised analysis were carried out. For irregular patterns, only a systematic analysis was carried out.

Results The mean of HI_5 was found to be 31% for regular patterns; the means of all irregular patterns stay below this, even though the size of the irregularities for some breathing patterns was very large. The mean of $V_{107/95}$ was found to be 0.7 for regular patterns. Irregularities were not seen to cause further deterioration. Five times layered repainting causes a statistically significant decrease of the magnitude of the interplay effect across all breathing patterns by 50-80%, but is approximately 50% less effective against baseline shift than against all other types of breathing. Interplay effect size correlates strongly with amplitude, but this correlation can be obscured because period and phase introduce very large variance.

Conclusions The interplay effect in general is large for the investigated target size, prescription dose, beam configuration and machine performance. It can cause as much as 100% of the CTV to receive a clinically unacceptable dose and lead to large inhomogeneities. Irregular breathing was not found to be notably worse. Repainting is very effective, even against irregular breathing, but baseline shifts can undermine the effectiveness of applying repainting. Separately considering breathing irregularities for tumours similar to that investigated here is of low importance; it is more important to properly model the magnitude of the interplay effect using an accurate, individualised breathing pattern.

Acknowledgements

This thesis would never have been made if I had to do it all on my own. Over the past year, my knowledge and understanding of and interest in proton therapy have rapidly increased. That is largely thanks to all my colleagues of the physics department of the WPE, especially the QA team. Thank you all for making my year here not just educational, but also allowing me to enjoy the work. Honourable mention goes to the people I shared an office with: Max, Carina, Martial, Hilda and Lorenzo. I had a great time there.

For the research itself, I am grateful to Dr. Ulf Mader and Andreas Pfläger from the Technische Hochschule Mittelhessen, who provided me with the phantom that was the foundation of my work. The work of Erik Engwall at RaySearch has also been of vital importance, turning a rough idea I had into a working program that significantly increased the possibilities of my work

Of course, Dr. Zoltán Perkó's advice has also been indispensable. We didn't see each other as much as I think is normal for a graduate student and his supervisor, but there hasn't been a single meeting where I didn't come away with a better understanding of my problems or a bunch of new ideas to implement. Quality over quantity, as they say.

Last, but most certainly not least, I am extremely grateful to my daily supervisor, Dr. Jörg Wulff of the WPE. You have patiently spent many hours explaining a vast variety of topics to me, never losing patience or telling me you were too busy.

Preface

*Erik den Boer
Essen, May 2020*

It has been eleven long years getting up to this point... I can barely remember starting my Bachelors in Aerospace Engineering at the TU Delft in the summer of '09. I have learned a lot in the intervening years, not just in a technical sense. I think the most important aspect of my journey has been a personal one. Learning to stand on my own two feet, learning what I want to do with my life and career, discovering my core values as a person, finding out what makes me happy and coming to peace with my own flawed self.

As much as I would like to, I cannot take credit for all of it just by myself. I have been helped every step of the way, supported by friendships, some of which have fallen by the wayside since and some which I know will last a lifetime. I have tried to fit in where I couldn't, but eventually found my place in Delft with my tennis club, Obvius, where I have spent many happy hours (mostly mis-)hitting balls and just enjoying the company of everyone at the club. To my fellow board members, Francis, Jos, Lies, GJ, those days where we ruled with an iron fist were especially memorable. Well, some days, not all...

Even more important, not just during my time in Delft and Essen but also the many years before that, and for many more years to come, my family. To my sister, Sylvia, and her fiancé, Robin. It still feels weird, saying fiancé, but I am very happy you're happy together, and I hope it stays that way. Whenever I needed you, you were both there for me, and I will always cherish that and hope our bond only grows stronger. I haven't always been the best at maintaining it, but I will strive to do so in the future.

And of course... Zaneera. I am used to pulling all-nighters to meet deadlines for reports or get enough studying done for my exams, but that would never have worked here. Seriously, I could not have done this without you and I hope I will never have to.

Last but not least, om het maar in goed Hollandsch te zeggen, pa en ma. Het voelt een beetje apart om opeens naar het Nederlands te switchen (dus ik zal er waar mogelijk maar lekker leenwoorden tegenaan gooien), maar het zou denk ik nog vreemder zijn om, na alles wat jullie voor mij gedaan hebben, jullie in het Engels aan te schrijven. Dat is altijd meer mijn taal geweest dan die van jullie. Ik kan een heel lang betoog houden over alle manieren waarop jullie me geholpen en gesteund hebben, maar dat zou nog langer worden dan dit verslag en zelfs dan zou ik nog wel dingen missen, dus ik zal het kort houden. Bedankt en ik hou van jullie.

Wow, those eleven years really flew by in the blink of an eye...

Contents

Abstract	ii
1 Introduction	1
1.1 Cancer: a global problem	1
1.2 Causes and mechanisms of cancer	1
1.3 Main cancer treatment options	2
1.3.1 Surgery.	3
1.3.2 Chemotherapy.	3
1.3.3 Radiation therapy	3
1.4 External beam radiation therapy	4
1.4.1 Photons	4
1.4.2 Electrons.	5
1.4.3 Heavy particles.	5
2 Research Background	6
2.1 Proton therapy basics	6
2.1.1 The spread-out Bragg peak.	6
2.1.2 Scattering techniques	6
2.1.3 Scanning techniques.	7
2.2 Motion in radiotherapy	8
2.2.1 The interplay effect	9
2.2.2 Visualising motion using 4D CT imaging.	9
2.2.3 Motion management techniques	10
2.3 Research goal	11
3 Patient Model and Treatment Planning	12
3.1 Origin and properties of the XCAT phantom	12
3.2 Advantages and limitations	13
3.2.1 Breathing model	13
3.2.2 Contouring	13
3.2.3 Transformation accuracy	14
3.2.4 Motion range limitations.	15
3.3 General planning standards.	15
3.3.1 Structure definition	16
3.3.2 Robust planning	16
3.3.3 Intensity modulated proton therapy	17
3.4 4D treatment planning	17
3.4.1 Creating an ITV	17
3.4.2 4D planning and optimisation	17
3.4.3 Targets commonly affected by motion	17
3.5 Dose calculation algorithms	18
4 Research Method	19
4.1 Static reference plan	19
4.1.1 Input parameters	19
4.1.2 Layered repainting plan	20
4.2 Regular breathing	22
4.2.1 Randomly sampled breathing patterns.	22
4.2.2 Single variable breathing patterns	22

4.3	Irregular breathing	22
4.3.1	Baseline shift.	23
4.3.2	Amplitude change	23
4.3.3	Period variation	24
4.4	Calculating 4D dose distributions.	25
4.5	Evaluation metrics	27
4.6	Assumptions	27
5	Interplay effect with regular breathing	30
5.1	Single variable analysis	30
5.1.1	Amplitude dependence	30
5.1.2	Period dependence	30
5.1.3	Phase dependence	31
5.2	Randomised signals.	31
5.2.1	Results without repainting.	33
5.2.2	Results with 5x repainting	33
5.3	Discussion of results	34
5.3.1	Single variable analysis.	34
5.3.2	Randomised inputs	37
5.4	Statistical analysis.	37
6	Interplay effect with breathing irregularities	39
6.1	Baseline change.	39
6.2	Amplitude variation.	39
6.3	Period variation.	39
6.4	Discussion of results	40
6.5	Summary of results	43
7	Conclusions	44
7.1	Evaluation of research questions	44
7.2	Comparison to other work	45
7.3	Recommendations for future research	45
7.3.1	Testing assumptions	45
7.3.2	Increasing generality.	46
7.3.3	Further recommendations.	47

Acronyms

4DCT 4-Dimensional Computed Tomography. 9, 10, 12, 13, 15, 17, 25, 46

AP anterior-posterior. 23

BEV beam's eye view. 47

BMI Body Mass Index. 47

CDF cumulative density function. 38

CI confidence interval. 38

CT Computed Tomography. 8–10, 12, 13, 15–17, 19, 22, 25, 26, 45, 46

CTV Clinical Target Volume. 16, 17, 19, 20, 27, 35, 37, 44

DS Double Scattering. 6, 7, 17, 19, 20

DVH dose-volume histogram. 27, 28, 37

GTV Gross Tumour Volume. 16

HU Hounsfield Units. 13, 14, 16

ICRP International Commission on Radiological Protection. 12

ICRU International Commission on Radiation Units and Measurements. 16

IMPT Intensity Modulated Proton Therapy. 17

ITV Internal Target Volume. 16, 17, 19

MC Monte Carlo. 18, 28

MRI Magnetic Resonance Imaging. 12, 15, 46

NURBS non-uniform rational B-splines. 12

OARs organs at risk. 16, 17, 45, 47

PBA pencil beam algorithm. 18, 26, 28

PBS Pencil Beam Scanning. 1, 6, 7, 19, 20

PT proton therapy. 1, 6, 15

PTV Planning Target Volume. 16, 17, 19

RBE Relative Biological Effectiveness. 5, 7

ROI region of interest. 12, 15, 17, 19, 28

RS RayStation. 46

SFUD Single Field Uniform Dose. 17

SI superior-inferior. 28

SOBP Spread-Out Bragg Peak. 6, 7

SPECT single-photon emission computed tomography. 12

SS Single Scattering. 6, 7

US Uniform Scanning. 6, 7

WET water equivalent thickness. 19

WHO World Health Organization. 1

WPE Westdeutsches Protonentherapiezentrum Essen. 11, 12, 16, 18–21, 25, 28, 37, 47

XCAT extended cardiac-torso. 1, 12–15, 22, 28, 29, 45–47

Introduction

In this thesis, the effects of irregular breathing rhythms on the deposited dose distribution of Pencil Beam Scanning (PBS) proton therapy (PT) will be investigated. In order to do so, a theoretical background and explanation of relevant terms and concepts will be given in this chapter.

To start, in Section 1.1, an overview will be given of cancer as a main subject of healthcare and research worldwide, following which Section 1.2 provides more detail on the underlying biology of cancer. Section 1.3 will list the general treatment options currently available, after which Section 1.4 zooms in on the specific application of radiation therapy.

Chapter 2 will present the background of this work, detailing the relevant theoretical background before laying out the research goals. With the research goals in mind, some additional theoretical topics are discussed to establish the framework in which the research was carried out in Chapter 3, which details the extended cardiac-torso (XCAT) phantom that was used and explains the treatment planning process. The research method is discussed in Chapter 4. After that, results are presented and discussed in Chapters 5 and 6. Finally, conclusions are drawn and compared to similar work in Chapter 7.

1.1. Cancer: a global problem

Healthcare professionals around the world face many illnesses, infections and other setbacks in patient health on a daily basis. Some are minor, some are manageable, but of course there are also potentially fatal health problems. Cancer is a main contributor to loss of life worldwide, but can also severely impact quality of life even if the patient can be cured. More specifically, it is the second leading cause of death worldwide, causing 9.6 million deaths in 2018 [1]. This is roughly 1/6th of all deaths. The economic impact is also significant, being estimated at US\$ 1.16 trillion in 2010 [2]. The incidence is already high: 17 million new cases were detected in 2018. Furthermore, these numbers are still expected to rise by as much as 60% over the next ten to twenty years [3].

Cancer is itself an umbrella name for many different types of tumour. Nearly any part of the body is susceptible to some form of cancer. The most prevalent forms are lung cancer, colorectal cancer, stomach cancer, and breast cancer and cervical cancer in women and prostate cancer in men [4]. Figure 1.1 shows the number of deaths per year due to all types of cancer. It can be seen that, even though medical technology continually improves, the total death toll continues to rise. This is of course partially due to increasing populations and life expectancy, but the variety of different types of cancer also contributes to making the disease more difficult to combat.

Cancer is not a disease that can exclusively be treated in hospitals, however. The World Health Organization (WHO) reports that 30-50% of all cancer cases are preventable [5]. Worldwide, tobacco, lifestyle decisions such as diet and activity level, and alcohol list among the chief contributors to preventable cancer incidence. Age is also an important contributing factor. It is of course not part of the list of preventable aspects, but should be included in any discussion on the causes of cancer, since it has such a major influence, both on an individual's chance of developing cancer and on which types are then likely to be found [6]. Lastly, it is important to note that some cancers are truly unavoidable, as people can have a hereditary predisposition.

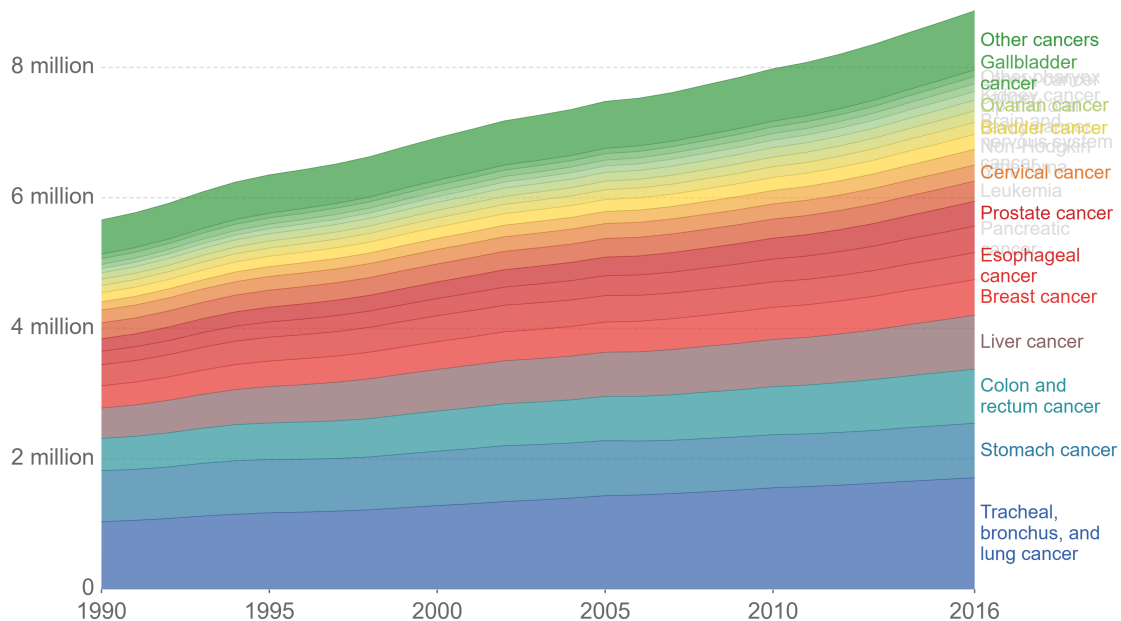
1.2. Causes and mechanisms of cancer

The root cause of cancer is a change in a DNA sequence in a cell of the body, compared to healthy tissue, called a gene mutation. This can occur due to a random error when the DNA is copied during cell reproduction, as a result of DNA damage due to for example radiation, tobacco or other environmental factors, or the defect

Cancer deaths by type, World, 1990 to 2016

Annual cancer deaths by cancer type, measured as the total number of deaths across all age categories and both sexes. Smaller categories of cancer types with global deaths <100,000 in 2016 have been grouped into a collective category 'Other cancers'. See sources for list of grouped cancers.

Our World
in Data



Source: IHME, Global Burden of Disease (GBD)

Note: All cancer types with less than 100,000 global deaths in 2016 into a collective category 'Other cancers'.

CC BY

Figure 1.1: Overview of total number of cancer deaths worldwide, split out per type of cancer. All types that caused fewer than 100,000 deaths worldwide in 2016 are grouped under 'Other cancers'. Source: [7]

could be genetic, i.e. inherited from parents [8]. These changes are likely to result in tumour growth if the change relates to a part of the DNA involved in cell reproduction or cell death. Cells that exhibit uncontrolled reproduction can multiply rapidly, pushing away healthy tissue. Cells also know when they need to die, initiating a process called apoptosis. Resisting this process allows cells to proliferate more easily than healthy cells. Combining an increased rate of reproduction and an extended lifespan, it is easy to see how tumours can start to grow. As the tumorous tissue grows, more mutations can occur, allowing some tumour cells to develop the ability to attack healthy tissue, for example. This sets the stage for the tumour to start spreading beyond its initial location, which is called metastasis. The entire process is depicted in Figure 1.2. Tumours that do not develop metastatic ability are called benign, and can often be treated well; in some cases, they are fairly harmless if left untreated, or can even resolve on their own. Only if a tumour becomes malignant, i.e. develops aggressive behaviour towards healthy tissue, is it called cancer. Malignant tumours always require treatment; if left unchecked, cancerous growth can lead to a range of health issues and even death [9].

1.3. Main cancer treatment options

Once a tumour is discovered, a biopsy is taken to determine whether it is a malignant or benign growth, after which treatment options can be assessed and discussed with the patient. There is a wide range of available treatments. The most common are surgery, chemotherapy and radiation therapy. They will be outlined in more detail in this section, with particular focus on radiation therapy, which is the subject of this report. Aside from these three main treatment methods, options include for example immunotherapy, hormone therapy and stem cell transplantation. It is possible that only one type of treatment is needed, but in most cases, a combination of treatment modalities is applied [11].

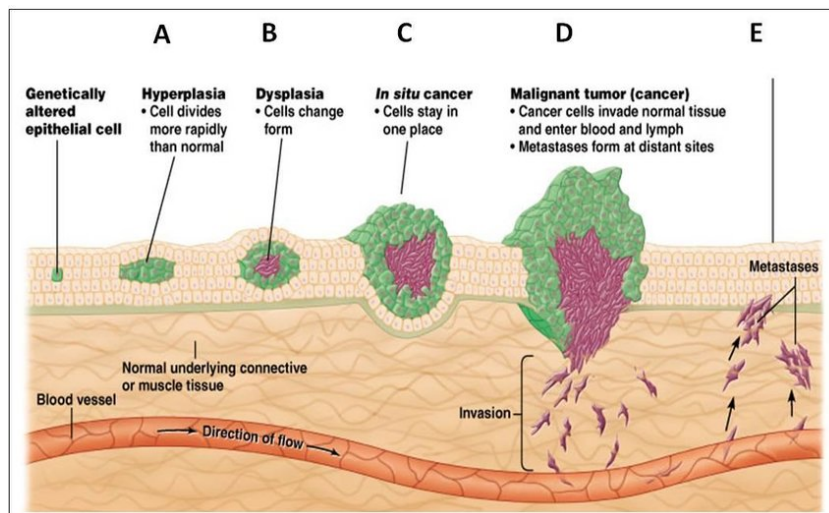


Figure 1.2: General stages of cancer growth. At first, a single cell is mutated. A: the cell divides more rapidly than its neighbours. B: Further mutations affect not just the growth rate, but also other characteristics of some of the cells. C: Benign tumour, pushing healthy tissue to the side but without actively damaging it or metastasizing. D: Malignant tumour, actively destroying surrounding healthy tissue and invading other parts of the body. E: cancer spreads throughout the body (metastasis). Source: [10]

1.3.1. Surgery

Surgery is a relatively straightforward method in theory: a surgeon can cut away tumours. Of course, there are numerous complicating factors that need to be accounted for as well. For example, this method only works well on solid tumours that have not yet spread. This means that it is not very effective against metastasised tumours or leukemia, i.e. blood cancer. Note that not the entire tumour is necessarily removed; surgery can also be used to remove a tumour partially, for example to relieve pressure or pain on nearby organs. It is also possible to remove the bulk of a tumour, leaving difficult-to-reach sections behind to be treated via alternative methods.

Surgery is commonly applied to breast, colorectal and skin cancer, for example. However, this is often dependent on the progress of the disease; if the tumour is detected early enough, surgery has the potential to be fully curative, but if the treatment starts late and the tumour has metastasised, surgery is generally supported by chemotherapy or radiotherapy [11].

1.3.2. Chemotherapy

Chemotherapy refers to the use of drugs to treat the tumour. It is a global treatment, unlike surgery and radiotherapy; the entire body will be affected. Since the drugs are designed to stop or slow down the speed of multiplication of cancer cells, other fast-dividing cell types typically suffer from chemotherapy, resulting in side effects like hair loss, a dry mouth and fatigue. However, its wide-ranging effectiveness also makes it uniquely suited for treating metastasised tumours, lymphoma and leukemia, while it is often also applied to shrink large tumours before radiotherapy or surgery is used to treat the remaining tumour volume more accurately [11].

1.3.3. Radiation therapy

Radiation can damage cells when the particles cause breaks in DNA strings, crippling cells if enough damage is done. Cancerous cells are more susceptible to this than healthy tissue, since their ability to repair the damage is reduced. The method is also called radiation oncology. This modality can be roughly divided in two: radiating from the inside out and from the outside in. The prior method is called brachytherapy, in which a radioactive substance is inserted in or near the tumour. The radiation will then damage the tumour, but some collateral damage to nearby healthy tissue is unavoidable. Brachytherapy is commonly applied to

for example cervical, prostate and eye tumours. It is important to consider that this might make the patient into a source of radiation, so additional concerns such as safety of family members must also be considered. If it is not possible or desirable to insert a radioactive substance, a beam of particles can be applied to irradiate the tumour.

For both brachytherapy and external beam radiotherapy, dose deposition occurs in the targeted tumorous tissue, but due to the dose deposition over a range of depths, it is generally impossible to avoid irradiating healthy tissue. However, healthy cells often have better repair capabilities than tumours, which is why nowadays, radiotherapy treatments are given in fractions. That means a patient is irradiated with a fraction of the total dose needed to achieve the clinical goal. In between fractions, the healthy and unhealthy tissue recover at different rates, allowing more healthy tissue to recover by the time the treatment is over than if the whole dose had been applied in a single treatment [12]–[16].

1.4. External beam radiation therapy

In general, a radiation beam can be generated using a variety of different types of particles, but photons are the most common type of beam. Dose-depth profiles are used to describe the amount of radiation dose deposited as a function of depth in a certain medium, allowing comparison of various modalities from a physics perspective. Figure 1.3 shows such a depth-dose profile graph for various modalities.

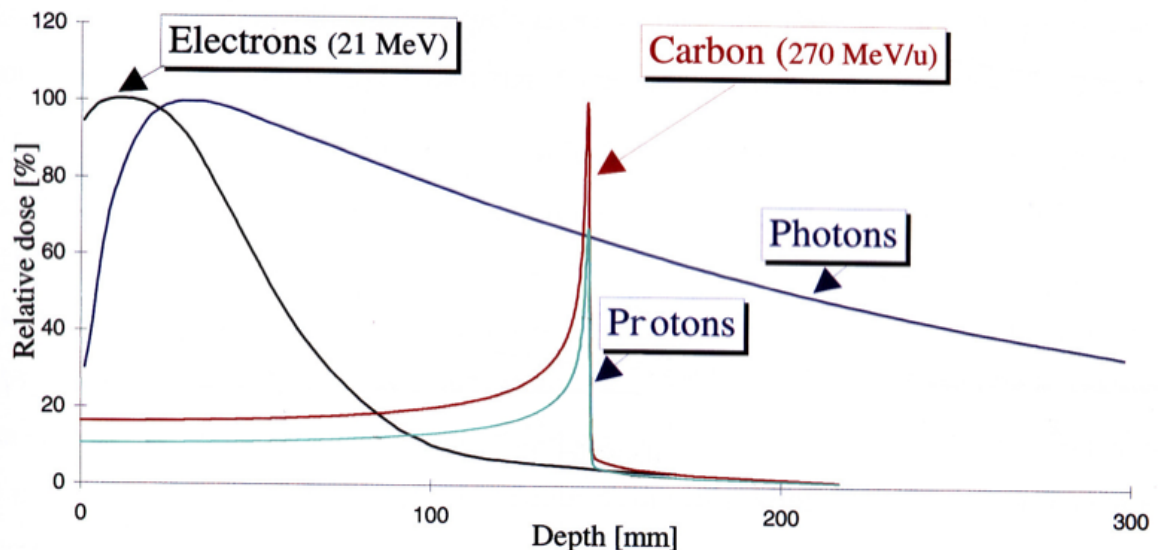


Figure 1.3: Depth-dose profiles showing the deposited dose as function of depth in water for various particles and energies. The peak in the proton and carbon profiles is called a Bragg peak. Source: [17]

1.4.1. Photons

The most commonly used type of external beam radiotherapy is photon irradiation. The main physical process by which it interacts with the patient tissue is called Compton scattering. In this process, a photon with high energy (in the order of 4-18 MeV [18]) interacts with an electron in the shell of an atom, ejecting the electron with part of its energy, while being scattered in a different angle with the remainder of its own energy. The electron then deposits its energy in the tissue after a finite range, while the photon continues on its way, causing ionisation in the tissue as it decreases in energy at an exponential rate. This yields the lengthy (theoretically infinite) tail seen in Figure 1.3 after it reaches the depth at which most energy was deposited [15], [19]. A convenient trait, however, is the relatively low entrance dose, since no secondary electrons have yet been generated at the point of entry of the beam. This is generally called the skin-sparing effect.

1.4.2. Electrons

As can be noted from Figure 1.3, electrons have a similar dose deposition curve to photons, but with two notable differences. First, the skin-sparing effect is not present, which can be explained by the fact that while photons need to interact with tissue for ionised particles to be generated, electrons are themselves ionised particles. Second, the curve drops off significantly quicker and more sharply, effectively resulting in a finite range of the electron beam, unlike the theoretically infinite range of a photon beam. For this reason, electrons can only really be used for ranges up to about 10 [cm], making it most effective for superficial targets such as melanomas [15]. However, electrons are not very commonly used anymore in clinical practise.

1.4.3. Heavy particles

Heavy ions are an emerging modality. Most commonly, carbon ions are used for irradiation, but helium and neon ions are also used. Their mass reduces straggling in the beam, resulting in sharp lateral penumbras. Combined with the Bragg peak in the depth-dose profile (illustrated in Figure 1.3 for carbon ions), these particles clearly have the potential to have a large effect on a very small volume, while barely causing any collateral damage. This accuracy is somewhat compromised by the fragmentation tail [20]. The main drawback of heavy ions is a varying Relative Biological Effectiveness (RBE); for photons and electrons, this is generally 1 and protons have an RBE roughly of 1.1. However, for carbon ions and even neutrons, the RBE can range between 5 and 20, meaning the same dose in [Gy] can cause anywhere between 5 and 20 times as much damage on a cellular level. As a result, dose prescription becomes more complicated in this scenario. Another drawback is that heavier particles require even larger accelerators, and the requirements for accuracy and robustness of the plan against uncertainties become more stringent as well [15], [19], [21].

Research Background

This chapter provides the background for the research. First, Section 2.1 elaborates on the basic principles of PT. Section 2.2 explains which types of motion can be encountered in radiotherapy and provides an overview of the currently available methods for mitigating the detrimental effects of motion. Finally, Section 2.3 sets out the research goals for this work.

2.1. Proton therapy basics

PT can roughly be divided into scattering techniques and scanning techniques. There are several different methods for delivering a proton dose to a patient, including PBS, which is the focus of this work, but also Uniform Scanning (US), Single Scattering (SS) and Double Scattering (DS) [22], [23]. For all methods, it holds that for different particle energies, the Bragg peak occurs at different depths. The greater the energy, the greater the depth, assuming the medium through which the beam travels is homogeneous, or at least has a fairly uniform density. Various reliable algorithms for dose distribution calculations are available, but high-density regions such as bone, and air cavities such as in the lungs, can complicate treatment planning.

2.1.1. The spread-out Bragg peak

The division in scattering and scanning techniques mainly refers to how the beam is shaped to fit the target in the plane orthogonal to its direction of travel. In all methods, the depth is modulated using a Spread-Out Bragg Peak (SOBP), although the mechanism by which this SOBP is created varies. The concept is shown in Figure 2.1. An SOBP can be created by stacking different beams on top of each other, varying the intensity and energy to create beams with Bragg peaks at different depths and delivering a different total dose along their path. In scattering techniques, the SOBP is created when a uniform beam with high energy passes through a range modulator wheel; this wheel has a varying thickness along its perimeter and therefore causes the beam to pass through a different thickness continually, modulating the remaining energy of the protons to vary the depth to which they penetrate. As a result, the full SOBP is applied continually, so the complete target is irradiated continuously. In scanning techniques, the SOBP is created by irradiating with distinct energies, created by slowing down the beam as necessary as it leaves the accelerator. This effectively cuts the target volume into layers, and one layer is irradiated before moving on to the next. The deeper layers tend to be more heavily weighted than shallower layers, as they need to provide the full dose nearly on their own, while the shallower depths are irradiated by multiple layers. If done correctly, the resulting sum of the beams is a profile with a range of approximately uniform dose, allowing irradiation of the whole tumour with the desired dose [24], [25]. However, because the beam needs to move to cover the entire tumour, active scanning techniques often perform poorly when the target moves.

2.1.2. Scattering techniques

SS and DS are scattering techniques, with the main variable being the size of the irradiating beam. The generation of such beams is shown schematically in Figure 2.2. In SS, the beam is small in the lateral plane, caused by passing the beam through a single scattering film. The beam intensity beyond the scattering point becomes a Bell-curve, meaning the intensity of the beam rapidly drops with distance from its central axis. To produce a beam with near-constant intensity, it is passed through a narrow opening, cutting the beam profile off beyond the roughly uniform peak of the Bell curve. As a result, SS is only able to irradiate a small target. It is also a very inefficient technique, since the vast majority of protons are blocked by the collimator. This also results in a relatively large amount of stray radiation. Therefore, it is only used for some very specific cases, such as eye tumours. As the name suggests, DS employs a second scatterer. This scatterer is shaped in such a way that it refocuses the beam after the first scatterer, delivering a beam with a uniform lateral profile. This

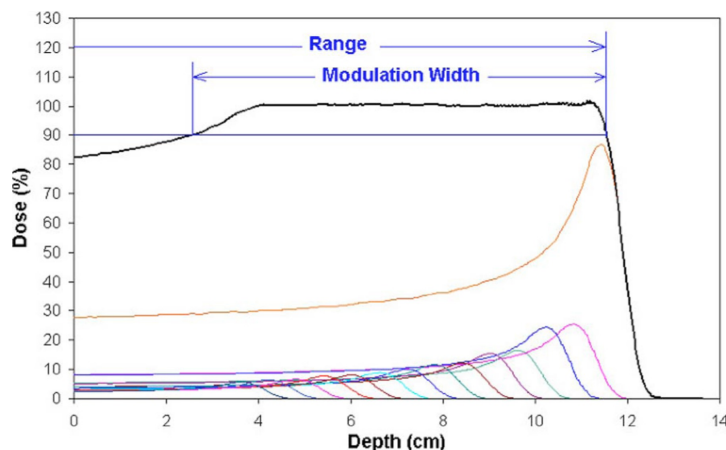
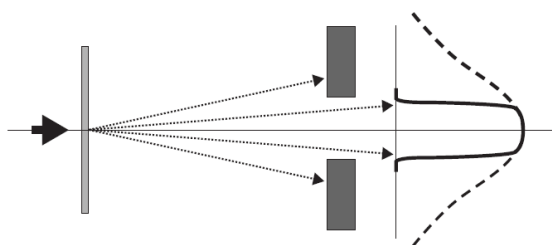


Figure 2.1: Creation of a spread-out Bragg peak with a range of approximately 12 [cm] and a width of approximately 9 [cm] by stacking many individual Bragg peaks on top of each other to generate a relatively uniform high-dose region wide enough to irradiate a three-dimensional target. Source: [25]

reduces the amount of protons that need to be blocked off, greatly increasing the efficiency compared to SS.

Once the beam leaves the nozzle, SS and DS both employ apertures and compensators. The aperture is a ring of heavy material, such as copper, to cut the beam off laterally to fit the tumour shape, while the compensator is a light material similar to water in density, such as lucite, that will change the depth of the Bragg peak to fit the beam to the tumour in the direction of travel. It is important to note that the entire tumour is irradiated simultaneously and therefore, the beam does not need to be moved [22]. A drawback of scattering methods is that they require patient-specific apertures and compensators to be created, one for each treatment field, and these pieces become activated during use, requiring additional precautions in disposal, while the interaction also generates secondary radiation in the form of neutrons, resulting in an additional dose that is difficult to model due to the varying RBE of neutrons.

A. Single Scattering with flat scatterer



B. Double Scattering with contoured scatterer

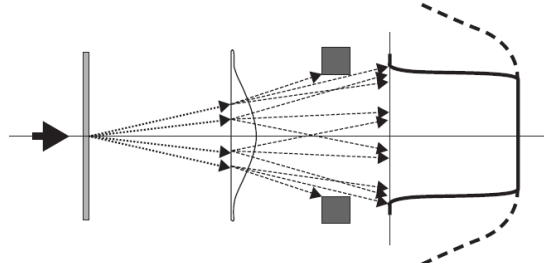


Figure 2.2: Schematic overview of single scattering and double scattering proton therapy principles, showing how the lateral beam profile is moulded to the desired shape. Source: [22]

2.1.3. Scanning techniques

Contrary to scattering techniques, PBS and US do not irradiate the entire volume simultaneously. Instead, in both cases, the beam irradiates layer by layer, with each layer being irradiated with a constant energy to generate the SOBP. Starting at the deepest part of the target volume by irradiating with the highest energy, the energy is decreased step by step until the layer closest to the surface is reached. In doing so, the beam needs to be moved laterally as well to ensure the entire tumour volume is irradiated. This is where the methods differ in approach. US sweeps a broad beam of uniform intensity across the layer, the movement or scanning speed varying to make sure that each section receives the required dose. In PBS, the layer is irradiated in discrete spots, with a single pencil beam irradiating a spot until the prescribed dose is reached, before moving on to the next spot. This process is schematically depicted in Figure 2.3.

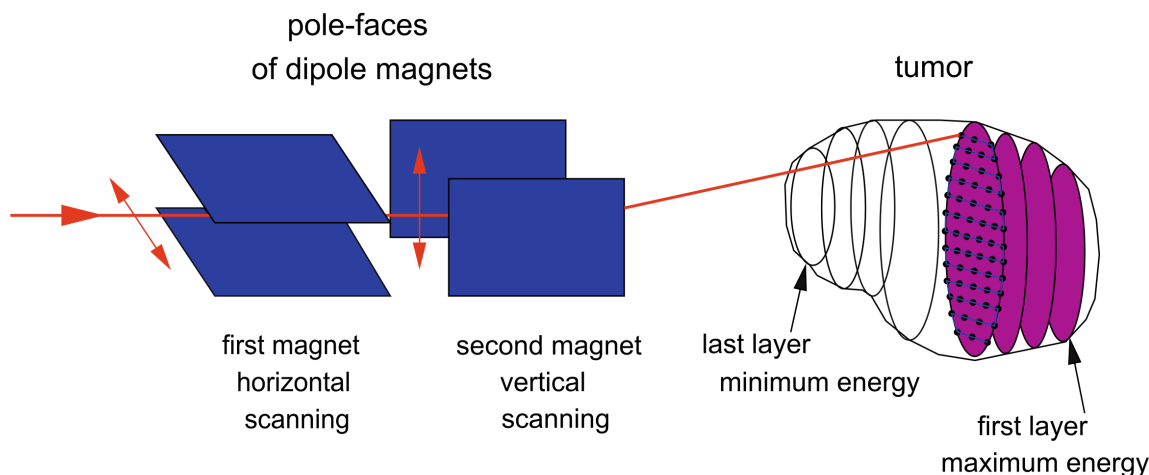


Figure 2.3: Schematic overview of pencil-beam scanning being used to irradiate a tumour layer-by-layer. The spots on the left-most coloured layer are the positions at which the beam is targeted in that layer. Source: [26]

2.2. Motion in radiotherapy

The human body is not completely rigid. In fact, it has many degrees of freedom, and most are independent of one another. For the purposes of radiotherapy, types of motion are typically divided in two main groups: interfractional and intrafractional motion [27], [28]. This refers to the concept of fractionation explained in Section 1.3. Interfractional motion is then motion between fractions, while intrafractional motion occurs within the time span of delivery of one treatment fraction [29]–[31]. Interfractional motion comprises several sources of motion, although these are not motion in the traditional sense. There is no actual motion occurring during treatment, rather, the changes with respect to planning or previous treatment fractions need to be accounted for at the start. Interfractional motion can normally be classified in four categories:

- Setup errors. These are inaccuracies in patient positioning. When the patient is placed on the treatment table before every fraction, there will generally be slight shifts and rotations every time.
- Filling and emptying of organs. As part of their function, a range of organs will fill up and then empty out again, such as the bladder and intestines. Depending on filling, the range of protons might change, since a full bladder or bowel slows the particles down more than several centimeters of air.
- Changes in patient anatomy and non-rigidity. The general shape of a patient body can change. It is common to see non-negligible weight loss if the patient receives chemotherapy simultaneously, for example. Similarly, non-rigid parts of the body such as fatty or muscle tissue may settle differently from fraction to fraction.
- Tumour shrinkage. If a treatment is effective, or if alternative modalities are applied simultaneously, it is possible to see shrinkage of the tumour over the course of treatment. This is unlikely to be noticed between concurrent fractions, but can cause a significant inaccuracy by the later fractions compared to the Computed Tomography (CT) scan on which planning was done. Of course, tumour growth while treatment is ongoing is also possible.

Intrafractional motion refers to changes that occur while the patient is on the treatment table. The main sources of intrafractional movement are breathing and cardiac function [27]. Due to the cycle of expansion and contraction of the lung, the entire thorax and a number of the abdominal organs move. This motion is the focus of this research. The beating of the heart mostly affects lung tumours, having greater frequency but smaller magnitude than breathing motion [32].

2.2.1. The interplay effect

In active scanning proton therapy, motion is of even greater concern than in modalities where the beam does not move. This is because the movement of the beam can cause an exacerbation of the target motion, a phenomenon which is called the interplay effect. This effect is well-established since the earliest days of active scanning techniques [33]–[35]. The interplay effect is the primary focus of this work, and is schematically explained in Figure 2.4. It shows two types of motion: a moving tumour and a moving beam, representing the effect these movements have on the static plan shown in white. The irradiation of a single layer can take several seconds, depending on the system, number of spots and dose per spot to be delivered. In this time, the tumour moves, causing a number of spots to be delivered to the wrong location. This can lead to certain locations being irradiated multiple times in a single layer and others receiving no dose at all. Since protons irradiating the deepest layers also deposit dose in all the layers they pass through, the effect of misplaced spots can stack up rapidly. This way, a plan that looks very homogeneous without accounting for the interplay effect, may in practise see a significant portion of its target volume either over- or underdosed. The interplay effect is capable of degrading a dose distribution in such a way that large fractions of the target volume fall outside of clinically acceptable limits. This has a detrimental effect on the chance of achieving the targeted damage to the tumour, while simultaneously increasing the risk to nearby organs [36], [37].

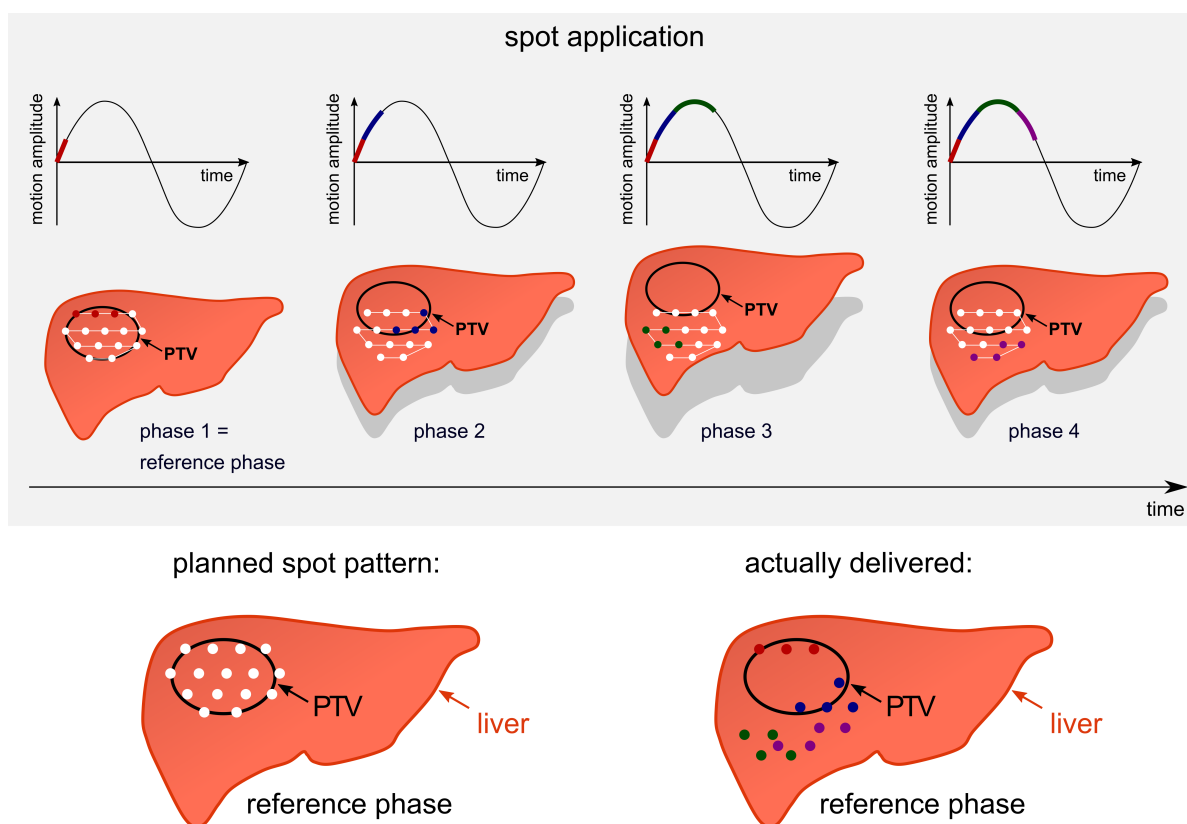


Figure 2.4: Conceptual representation of the interplay effect. In white, a planned treatment is shown in which a pencil beam is moved from spot to spot to irradiate a delineated target volume. However, while the beam traverses the planned path, the organ, and with it the target volume, is moving due to breathing motion. This causes the actual irradiation, shown by the coloured spots, to deliver a dose to other areas than was planned, and can result in over- or underdosage of certain areas, as is shown on the bottom right. This is called the interplay effect. Source: [38]

2.2.2. Visualising motion using 4D CT imaging

Many tumour sites are not very susceptible to motion, such as brain tumours. However, especially around the diaphragm, breathing motion is known to be an issue and must be accounted for in planning, but for that to be possible, motion must first be recorded. This is generally done using a 4-Dimensional Computed Tomography (4DCT) scan. A normal CT scan records the three physical dimensions; the fourth dimension in

this case is time. Figure 2.5 shows this process, which involves taking multiple 3D CTs, while recording the breathing pattern, for example by monitoring the chest wall or through markers placed on the chest. After the imaging finishes, the various 3D CTs, called the phases of the 4DCT, can be combined to create 'average' images, or the breathing signal can be analysed to find a representative point such as the mid-ventilation point, which can then be used as reference phase [39].

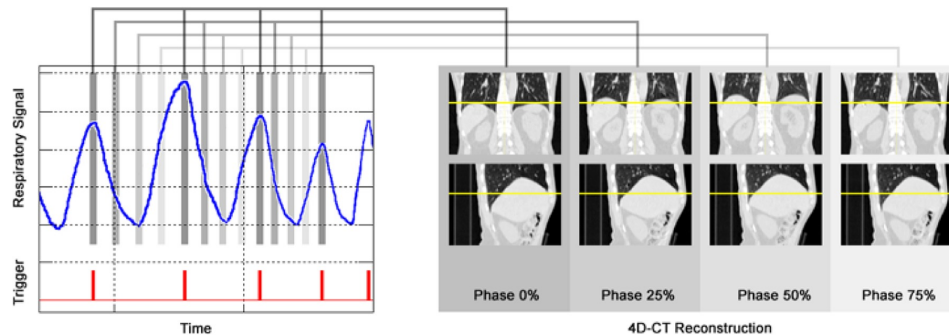


Figure 2.5: The process by which a 4DCT is obtained: several CT images are taken, while the breathing signal is monitored. The images are then linked to the breathing phase they are taken at, so that motion in the field of view can be recorded. Adapted from [40].

2.2.3. Motion management techniques

It is clear that motion is a many-sided problem, but also one of such magnitude that it cannot be ignored. Therefore, many strategies have been implemented, aimed at either mitigating the effect of motion or attempting to mitigate the motion itself [41]. For example, even though this was not why it was originally implemented, fractionation works automatically as motion management [42]. Spots can receive more than the planned dose for one fraction and less the next, since the motion, or at least its effect on the delivered dose distribution, is often random. Specialised techniques to combat the effects of motion include:

- **Immobilisation devices.** These have been commonly applied in nearly every treatment centre for many years, for all radiotherapy modalities. Their primary purpose is to create a reproducible patient setup, thus reducing setup errors and speeding up the setup process. They also serve to maintain patient position during treatment. Common immobilisation devices include masks and bags that are shaped to patient anatomy and fixed to the treatment table [43].
- **Gating.** In gating, tumour motion is monitored, usually via a surrogate such as chest wall motion or by placing markers on the chest [44]. The beam is then turned on when the signal is within a certain part of the breathing range, switching off again once the signal leaves the allowed range. This normally means the tumour is only irradiated when it is relatively close to the planning position, but this method is not always reliable if tumour motion is not measured directly, since the relationship between tumour and surrogate can often vary over the course of a full treatment or even during a single fraction [41], [45]–[47].
- **Breath holding.** A patient can be requested to hold their breath, or at least to keep the breathing shallow for the course of the irradiation, so as to minimise tumour motion. It works similar to gating in that breathing is controlled rather than tumour motion itself, so it also relies on a consistent relationship between tumour and breathing. This technique is commonly used in conjunction with gating, and patients can be trained to some extent to increase the effectiveness of the method. However, reproducibility from fraction to fraction is often poor [48], [49].
- **Repainting.** This method is specific to active scanning particle therapy, since it irradiates on a spot-by-spot basis. Repainting, sometimes also called rescanning, delivers only a fraction of the daily dose for each spot, coming back to each spot multiple times. This essentially causes additional fractionation of the treatment. It can be done by irradiating a layer in several fractions until the total dose per spot is delivered, before moving on to the next layer, or the entire volume can be irradiated, before starting back at the deepest layer to repaint. The prior method is called layered repainting, the latter is called volumetric repainting [35], [50]–[52].

- **Beam tracking.** This is theoretically the optimal method: the tumour location is monitored and the beam or treatment couch is moved in order to compensate for the motion in real time. However, this method is difficult to facilitate, since it requires a system to monitor the motion in real time with sufficient accuracy, the obtained images must then be processed quickly and reliably and finally the beam or couch motion must be generated, resulting in high hardware demands. Simplified methods are also possible which compensate only for changes in the equilibrium position that occur for a certain minimum duration [53] or that monitor tumour motion in real time but apply a gating approach rather than moving the beam or patient [54].

2.3. Research goal

In this project, the main goal will be to quantify the effect of irregularities in a breathing rhythm on the magnitude of the interplay effect. A lot of research has been carried out on quantifying breathing patterns, on the effect of breathing in radiotherapy, and on the interplay effect specifically. However, the breathing considered is regular in the vast majority of the research. Furthermore, it is often done using patient data, meaning the amount of data is limited and there is little to no ability to examine the isolated effect of various breathing parameters. Since variations in those parameters are to be studied, the use of patient data is not ideal. Therefore, several research questions are considered in this work, before the magnitude of the effect of irregularities in breathing can be adequately examined. These are:

1. What is the magnitude of the interplay effect for regular breathing?
2. Which parameters of a regular breathing pattern have the largest impact on the magnitude of the interplay effect?
3. Which parameters should be varied over the duration of a breathing pattern to obtain realistic irregular breathing patterns?
4. What is the magnitude of the interplay effect when considering irregular breathing patterns?
5. What is the magnitude of the interplay effect when applying clinical standards for mitigation of motion effects?

In order to answer these questions, several things will be needed:

- A target that is affected by breathing motion.
- Data of a moving human anatomy with high resolution.
- A clinically accepted treatment plan.
- A large number of clinically realistic breathing patterns.
- A method for calculating the interplay effect based on a breathing pattern input.

The work was done in the RayStation planning suite by RaySearch [55]. The selected target was a liver tumour. Most interplay investigations focus on the lung, since lung tumours are the most obviously affected by interplay, but lung tumours are not treated at the Westdeutsches Protonentherapiezentrum Essen (WPE), so no standardised planning process is available. Liver tumours, however, are also affected due to their close proximity to the diaphragm, and they are commonly treated and investigated at the WPE [56]–[58].

Patient Model and Treatment Planning

Patient data is difficult to obtain, often contains artefacts and regions that are difficult to contour and a 4D CT typically has only 10 phases, limiting the accuracy with which a particular breathing signal can be reconstructed [59]. These issues can all be reduced by the use of a computer-generated phantom, which is what is done in this work. The phantom that was used for this research is called the XCAT phantom. Its origin and properties will be explained in Section 3.1. Section 3.2 provides an overview of the advantages and limitations of the phantom. With the patient model in hand, a treatment plan needs to be made, which will serve as input and baseline for the calculations of the interplay effect. Section 3.3 gives some standard clinical practices from the WPE concerning general planning strategies. Section 3.4 then zooms in on the additional considerations taken when motion needs to be accounted for. Last, Section 3.5 discusses the different dose calculation algorithms available.

3.1. Origin and properties of the XCAT phantom

The XCAT phantom is a software phantom developed at the Johns Hopkins University, Baltimore, MD, USA [60], [61], by building upon an earlier phantom, the 4D NCAT phantom, designed primarily for use in single-photon emission computed tomography (SPECT) research. The phantom is a so-called hybrid phantom, combining properties of both voxelised and mathematical phantoms. Voxelised phantoms such as the NCAT are based on real patient data, allowing a very accurate representation of that particular anatomy. However, they cannot be manipulated very well to vary patient parameters or to induce organ motion. Furthermore, their resolution is often insufficient for use in high-resolution applications such as CT or Magnetic Resonance Imaging (MRI). A mathematical phantom is, as the name suggests, built by way of equations or geometric primitives, which makes them very flexible in creating different patient anatomies and enables modelling of organ motion. However, the mathematics is often a relatively poor representation of actual patient geometry. Software phantoms have potentially significant applications in medical research, to aid in improving both medical imaging devices and reconstruction techniques, and allowing evaluation of a wide range of clinical scenarios. Results are only of value if the anatomy is realistic.

Hybrid phantoms offer a middle road: they take segmented patient data as input but then fit a mathematical model to the anatomy. This combines anatomical accuracy and mathematical malleability, to create a versatile tool that can be used for large-scale research. It avoids having to irradiate patients many times, which leads to dose limitation concerns, or making physical phantoms for many different patient anatomies, which is costly and time-consuming. The XCAT phantom was created based on 4D-tagged MRI and high-resolution respiratory-gated 4DCT patient data to establish accurate models for cardiac and respiratory motion, respectively. Organ volumes were obtained from International Commission on Radiological Protection (ICRP) publication 89 [62], a wide range of body measurements was taken from the Visible Human anatomies library of the National Library of Medicine [63]. 3D polygonal surfaces were created from the anatomical structures and used as input for generating non-uniform rational B-splines (NURBS) surface structures for abdominal organs such as the bladder and prostate [64]. Tissue with highly arbitrary topology, such as the brain and vascular system, were modelled using subdivision surfaces to avoid requiring the large numbers of parameters needed to accurately define such structures using NURBS surfaces [65]. The XCAT phantom can create phantoms of both genders for a range of ages, body types and motion parameters [60], [66], [67].

For this case, a male adult phantom was created. Sagittal, coronal and transversal views of the phantom can be seen in Figure 3.1. Breathing motion for the phantom is linked to the diaphragm; it is deflected by a given input value, after which surrounding organs such as liver and heart are moved by a scaled value. Based on six such moving region of interests (ROIs), a deformation field is created to transform the rest of the phantom, such as muscle and blood vessel tissue and the remaining organs. For the phantom used here, fifty different phases were generated, corresponding to diaphragm deflections of 1 to 50 [mm], in effect creating a 4DCT with five times the common clinical resolution.

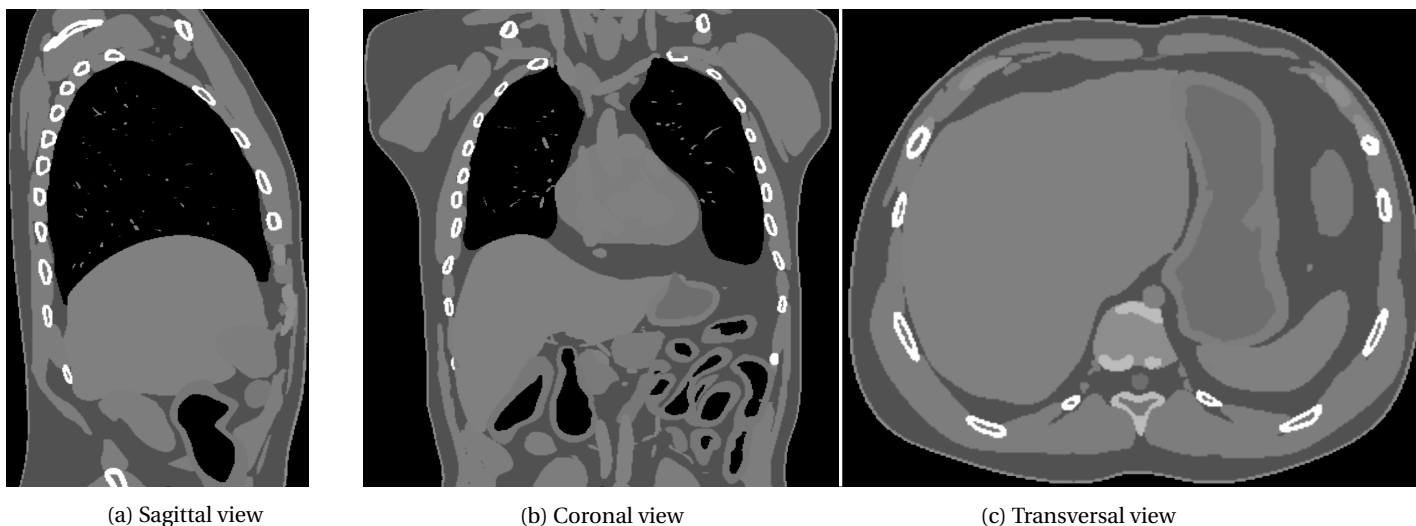


Figure 3.1: The phantom generated for use in this research. The patient anatomy is that of an adult male. It was generated by the Technische Hochschule Mittelhessen using the XCAT software [67].

3.2. Advantages and limitations

There are advantages to using the XCAT phantom. Some of these were already discussed when introducing the phantom, such as the available range of patient anatomies. On the other hand, the phantom also has limitations. Both the positive and negative aspects of the phantom as they relate to this work are discussed here.

3.2.1. Breathing model

In clinical practise, breathing models are often created using a surrogate for the tumour motion. 4DCTs often record the chest wall motion, for example, extracting the amplitude of the motion either by monitoring the surface or by tracking markers placed on the chest [68]. However, this implicitly assumes a linear relationship between tumour and surrogate motion which does not always hold. Figure 3.2 shows the relationship of chest wall markers to tumour motion for the anatomy used in this work. There is a sizeable portion where the relationship is roughly linear, but for larger amplitudes, the relationship changes very significantly. An advantage of the XCAT is that the motion of the phantom anatomy is based on diaphragm amplitude, which tends to correspond more closely to tumour motion [69], [70]. However, the phantom does not distinguish between inhalation and exhalation, merely taking diaphragm amplitude as input for its rendering of breathing motion.

3.2.2. Contouring

Since the XCAT phantom is computer-generated, it allows for perfect contouring. Two versions were created, one version with realistic attenuation coefficients, called the 'ATN' phantom, and one where each organ had a pre-defined, unique Hounsfield Units (HU) value, called the 'ACT' phantom. The individual phases were numbered based on their amplitude, e.g. the phases with 5 [mm] amplitude were named 'ATN_05' and 'ACT_05'. Using a script, the pre-set HU values were used to contour each organ perfectly on the 'ACT' phantom. These contours were then copied to the 'ATN' phantom, so that there the organs were also perfectly contoured. After this, the 'ACT' version was deleted to reduce memory usage. All subsequent steps were done on the 'ATN' set of CTs. See Figure 3.3 for a side-by-side view of the ATN phantom without and with its contours.

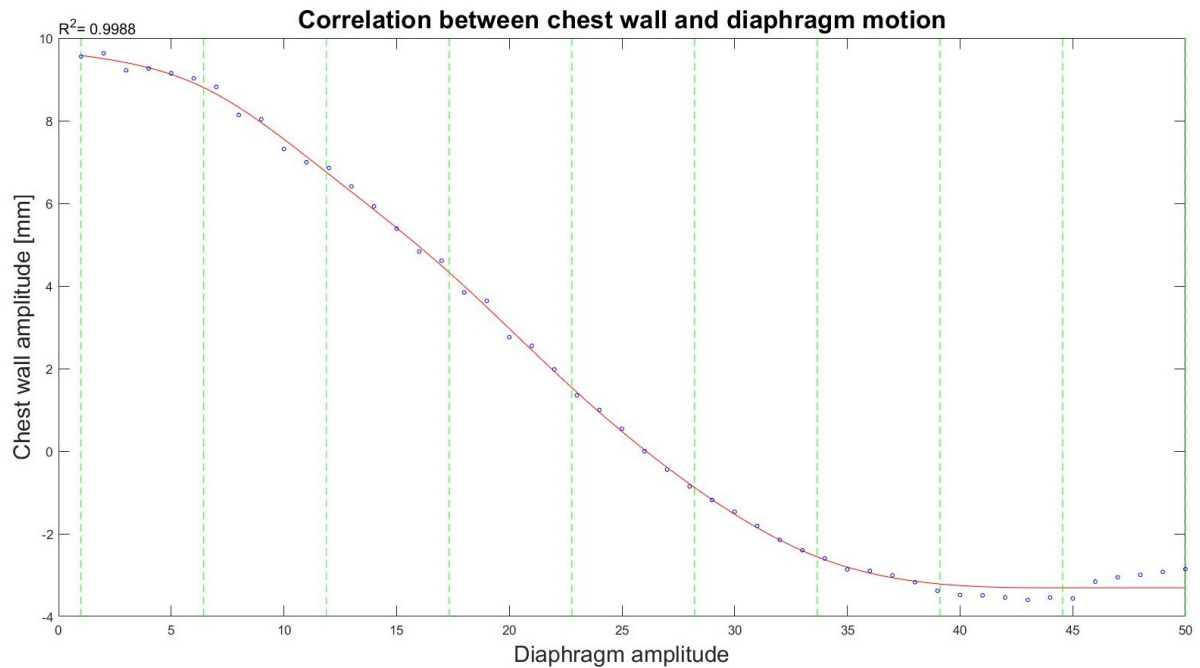
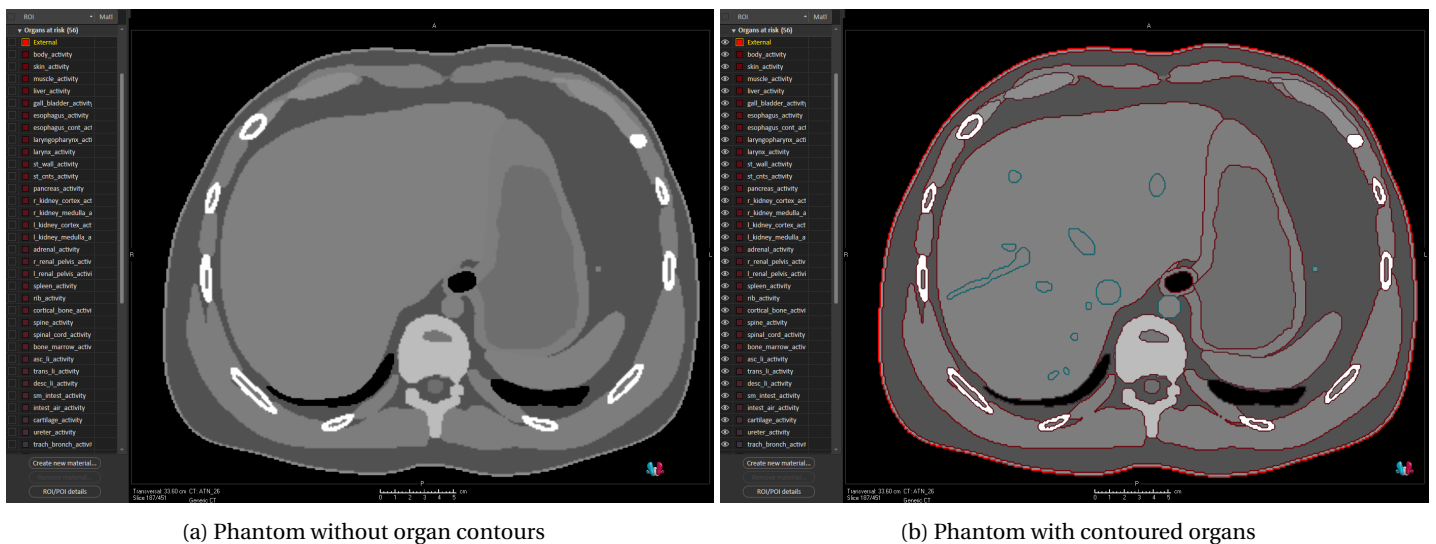


Figure 3.2: Correlation of anterior-posterior chest wall movement with inferior-superior tumour motion in the phantom used in this research, showing that the assumption of a linear relationship between the two only holds for a limited range.



(a) Phantom without organ contours

(b) Phantom with contoured organs

Figure 3.3: XCAT phantom without and with its organs contoured. Note the perfect delineation, which would not be possible when using real patient data.

3.2.3. Transformation accuracy

The deformation fields generated by the XCAT software are not always consistent [71]. Since the original deformation fields were not accessible anyway, they needed to be approximated. Various models and approaches are available within RayStation for calculating deformation fields. The first attempt used information from all organ contours as well as HU-values to establish the deformations. However, this was found to lead to a significant offset, especially around the diaphragm, reaching as much as 2 [cm] at certain locations. Since this area is of great interest in this project, the field was discarded. Three alternative options were considered:

- ROIsOnly: This deformation field was created by again using contours of all organs, but without HU-

Deformation field	Maximum similarity	Average similarity	Minimum similarity
ROIsOnly	0.9924	0.9419	0.6455
LiverLungHeartRib	0.9924	0.9801	0.9386
Unfocused	0.9931	0.9827	0.9449

Table 3.1: Maximum, average and minimum dice similarity values for the 49 XCAT phases for different deformation field settings, based on accuracy of the transformation of the liver. The reference phase result was trivial and thus excluded from the analysis. The Unfocused field was selected for further work.

value input.

- **LiverLungHeartRib:** This deformation field was created by using only the contour information for the organs in the immediate vicinity of the diaphragm. They were set to be 'Focus regions of interest', meaning the field was calculated around these organs only, with a larger window in which the deformation field slowly dropped off to zero. Portions of the phantom remained untransformed.
- **Unfocused:** The same organs as for field 'LiverLungHeartRib' were selected. However, they were not used to focus the deformation field, meaning the entire phantom was included in the calculations.

Then, for each deformation field, a copy was made of the liver contour in the reference phase and transformed to the other phases using the calculated deformation fields. Next, a union ROI was created on each phase of the transformed and contoured version. Then a similarity coefficient was computed by comparing the size of the union ROI, called the *dice similarity coefficient* d [72]:

$$d = \frac{2V(A \cup B)}{V(A) + V(B)}$$

Results are shown in Table 3.1. It was found that the 'Unfocused' deformation field had the best fit and was thus used further. Note that for the reference phase, d was always equal to one since no transformation was applied. This trivial result was excluded from the analysis.

3.2.4. Motion range limitations

The XCAT phantom has been extensively tested, with special attention being paid to accurate modelling of respiratory motion [60], [61]. However, there is no clear limit for the accuracy of this motion; the phantom will simply calculate a result based on an input, no matter what that input is. It is clear that sufficient testing was carried out for normal breathing ranges, but no limit for the inputs during validation of the breathing motion was found, meaning inaccuracies could start to occur at the end of the range of amplitudes. These extreme amplitudes could be validated by having a patient breathe as deeply as possible during a CT scan, and comparing the obtained images to the results of the XCAT with the input data set to match the particular patient. A problem of this approach, however, is that this would cause a significant dose to the patient, especially if small steps in the breathing amplitude are to be investigated, as this likely requires taking a 4DCT for several full breathing cycles to obtain the desired number of different deep-inspiration amplitudes. Therefore, validating the assumption of continued XCAT reliability throughout the amplitude range used in this work seems ethically undesirable, unless a modality is used that does not require ionising radiation. MRI seems suitable for this, since it also has a sufficiently high accuracy, and conversion to CT is well-established [73]–[75].

3.3. General planning standards

A variety of different tumours are treated with PT. Furthermore, the patient age ranges from infants to elderly patients of both genders. As such, a variety of different requirements and steps must by necessity be considered in planning. However, there are some practices commonly used around the world.

3.3.1. Structure definition

Treatment planning typically considers four volumes to delineate the tumour and to include various types of margins, as defined by the International Commission on Radiation Units and Measurements (ICRU) [76], [77]. These are shown in Figure 3.4. The smallest volume is the Gross Tumour Volume (GTV), which encompasses the extent of macroscopic disease as seen on the planning CT scan. However, it is known that the tumour may spread microscopically, which means it is not visible on planning images. To account for this microscopic growth, a margin is applied, creating the Clinical Target Volume (CTV). This is the tumour volume which must be irradiated to achieve local control. However, it is possible for the tumour to move, for example due to breathing or changes in nearby anatomy. To ensure the CTV will be covered adequately in all scenarios, additional margins are applied, corresponding to the range of the motion, yielding the Internal Target Volume (ITV). Finally, the patient setup before each fraction induces uncertainties, which are encompassed by additional margins on top of the ITV, or on top of the CTV in case no ITV needs to be defined. This volume, the largest of the target volumes defined by the ICRU, is called the Planning Target Volume (PTV). The planning process can then be roughly summarised as the striking of a balance between irradiating the target and ensuring the dose to nearby organs at risk (OARs) remains below their tolerance [78].

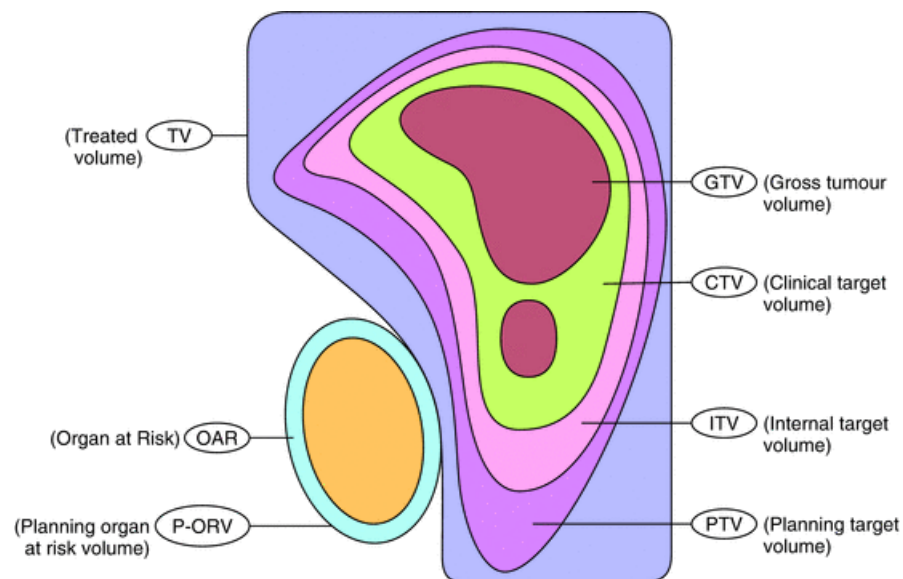


Figure 3.4: Standard clinical planning volumes, as defined by the ICRU. GTV = Gross Tumour Volume, corresponding to the detectable borders of the tumour. CTV = Clinical Target Volume, corresponding to the GTV plus a margin for unnoticeable, microscopic spread. ITV = Internal Target Volume, corresponding to the CTV plus additional margins to compensate for physiological changes such as motion and changes to tumour shape. PTV = Planning Target Volume, corresponding to the ITV or, if this is not defined, to the CTV, plus additional margins to account for setup and range uncertainties [76], [77]. Image source: [79]

3.3.2. Robust planning

Proton therapy is known to have a highly localised dose deposition, making it susceptible to errors. Therefore, it is important to account for uncertainties. These are introduced when considering the accuracy with which the setup during planning CT can be reproduced for treatment, but uncertainties in the recorded HU and its subsequent conversion to proton path length must also be accounted for. At the WPE, this is done according to ICRU standards [80], by applying a 3.5% correction to account for range uncertainties. Sources of range uncertainty are the acquired HU values used in the planning CT, the conversion from HU to proton stopping power and variation in the proton range during irradiation. Furthermore, a 5 [mm] uncertainty in every direction is used to account for setup uncertainties, provided the margin between the CTV and PTV is at least 5 [mm]. For brain tumours, a margin of just 3 [mm] is applied between CTV and PTV, since patients wear a mask and there is negligible motion involved. The setup uncertainty margins are set to 3 [mm] as well in that case, but the range uncertainty is kept at 3.5%.

3.3.3. Intensity modulated proton therapy

Many plans are created using a combination of beams, each of which delivers a roughly uniform dose, adding up to the total prescribed dose. This method is called Single Field Uniform Dose (SFUD). However, it is also possible to apply several non-uniform fields, which together still add up to the prescribed dose at any point in the target volume. This method is called Intensity Modulated Proton Therapy (IMPT) and is a commonly used planning technique. Its sharper dose gradients generally allow for better sparing of OARs, but density gradients in the irradiated tissue, such as in the lungs, can have a strong deteriorating effect, so in such cases, SFUD planning is often considered a more robust choice.

3.4. 4D treatment planning

Standard robustness is applied to every plan, whether the CTV is moving or not. To account for motion, additional steps are taken, starting with recording the motion through a 4DCT. Once the resulting images have been imported to the planning software, a reference phase must be selected. This phase will then be used for planning. This can be done either by creating an ITV or by 4D planning.

3.4.1. Creating an ITV

An ITV is essentially another uncertainty margin, similar to the construction of a PTV. While a PTV accounts for setup uncertainties, the ITV accounts for motion uncertainties. It is created by delineating a CTV on each phase and then combining all CTVs on the reference phase, resulting in an ITV that contains the full range of CTV motion over all phases in a single ROI, after which planning can proceed normally with the calculation of the PTV. Naturally, the PTV is larger when generated this way than without ITV calculation, so this means the dose will be applied to a larger area, resulting in poorer planning results for OARs in general than if motion were not accounted for. However, if the motion were left unchecked, the dose to both OARs and CTV would be unpredictable. This could potentially lead to underdosage of certain parts of the target volume, resulting in reduced tumour control, or to increased dose to healthy tissue, increasing the chance of complications. This inherent trade-off is one of the reasons why proton therapy is less commonly applied to moving targets. Moreover, an ITV is often based on a snapshot of the motion during a 4DCT and therefore may not accurately represent the motion [81].

3.4.2. 4D planning and optimisation

Using an ITV, all motion is summarised on one reference phase, after which planning proceeds normally. However, this method only accounts for CTV motion but neglects all OARs, thereby inducing uncertainties in the dose to OARs as well as in the range of protons due to density changes in their path. Alternatively, full 4D planning is an option: a plan is made on an averaged version of the 4DCT set and evaluated on the phases with the most extreme breathing, allowing for a clearer picture of the dose to all regions of interest [82]. However, this requires more time, both for planning and for evaluation by physicists and doctors. The method is also still relatively new and consensus guidelines are still being drafted. Any tumour that would absolutely require 4D planning is therefore more likely to be treated with a different modality instead, such as DS.

3.4.3. Targets commonly affected by motion

There is a range of organs which are affected by motion, and tumours in any of these are generally considered moving targets. Note that this refers to intrafractional motion, that is, motion during treatment. Interfractional motion such as filling/emptying of bladder and bowels and patient weight gain are disregarded. These are often accounted for by, for example, asking patients not to eat or drink for a certain amount of time before treatment or by taking a verification CT and adapting the plan in case of notable changes in patient anatomy. Organs for which breathing motion is significant include the lungs and heart and most of the abdominal organs, such as pancreas and liver [27]. However, intrafractional motion is not limited to breathing. Motion

can also be induced by the heart, for example. These contributions are generally smaller and more localised, however, and are therefore noted but otherwise neglected for the purposes of this work [32].

3.5. Dose calculation algorithms

RayStation offers two algorithms to calculate the final dose distribution: the pencil beam algorithm (PBA) and Monte Carlo (MC)-based dose calculation. PBA is generally faster than MC-based methods, but has known inaccuracies when handling tissue heterogeneities because it uses relatively straightforward density scaling, modelling the proton path as water with varying density. In regions where this approximation is valid, results tend to correspond well with MC, but it fails for many regions of the body as well. Another drawback is that PBA does not model particle interactions, and so does poorly in calculating secondary particle radiation. MC does model the physics of particle interactions, and it models material properties based on material composition, mass or electron density or ionisation potential, resulting in a highly accurate model of the inhomogeneities in the proton path and allowing for accurate calculation of secondary radiation [83]. This is relevant in the case of implanted markers, which are often metal implants in soft tissue, and at any air cavities in the patient anatomy. The prime example of an air cavity is of course the lung, and indeed PBA is known to perform badly when optimising for lung tumours [84], [85]. For liver plans, the error is in general more acceptable, but there is still a clearly notable error that should not be neglected entirely [86]. For proton therapy, the difference between the models is even more important than for photon therapy, owing to the prevalence of sharp dose gradients, often near healthy tissue, which form a large part of the appeal of proton therapy.

At the WPE, no plans are clinically approved using the PBA for optimisation; only MC-optimised plans are eligible for approval by doctors and physicists [87]. Therefore, from a purely scientific or clinical perspective, MC dose calculations would be the optimal choice. However, the increased accuracy comes at a considerable cost in terms of calculation time. In the case of the plan investigated here, evaluating a single breathing pattern with the MC engine was found to take between two and four hours for the plan without repainting, depending on server load caused by other activities such as the calculations run by the planning team members. This yielded a stark contrast with the run time of an interplay evaluation using PBA, which ranged between 10 and 20 minutes for the plan without repainting. Due to the increased number of spots, the plan with 5x layered repainting saw an increase of approximately 75%, ranging from 18 to 35 minutes. No MC optimisation was carried out for the 5x layered repainting plan, but it can be extrapolated that each calculation would then take anywhere between 3.5 and 7 hours. Since the calculations were divided equally between the plans with and without repainting, a quick ballpark figure would be that almost 6000 calculations at an average of approximately 4 hours each would result in a total calculation time of well over 20,000 hours. Clearly, this is a prohibitive computational load, which would have resulted in a drastic decrease in the variety of breathing patterns that could be investigated. The purpose of this work was to evaluate the magnitude of the impact various types of breathing irregularities have compared to regular breathing; in essence, this was an investigation into the relative magnitudes of both effects. Since the inaccuracies of PBA apply to each calculation equally and the beams did not pass through any air cavities or other sharp tissue density gradients, they were deemed acceptable, and the additional amount of scenarios that could be evaluated was considered to be of sufficient value to offset the drawbacks when comparing with MC.

Research Method

It is clear that organ and tumour motion due to breathing is an issue. In order to quantify the severity of interplay, a static reference plan is required. This is created in Section 4.1. A baseline for the interplay effect is established using regular breathing, which is discussed in Section 4.2, before the generation of irregular patterns in Section 4.3. The algorithm with which the disturbed dose distributions are calculated is laid out in Section 4.4. The metrics for evaluation of the distributions are listed in Section 4.5. The assumptions that were made are discussed in Section 4.6.

4.1. Static reference plan

The static reference plan was copied from earlier work at the WPE [38]. This means a CTV was prescribed with a dose of 6300 [cGy], to be administered in 15 fractions of 420 [cGy] each. Spreading the total prescribed dose out over a period of several weeks through fractionation is standard, but since interfractional effects were neglected, this was not considered.

4.1.1. Input parameters

Figure 4.1 shows all regions of interest that were used for planning. The target was a manually generated spherical CTV of 5 [cm] diameter located in the liver, which was deemed representative for hepatocellular carcinoma [88]. This target suffers significantly from breathing motion and would therefore normally be treated with DS. However, since the liver is relatively homogeneous, it is possible to treat the volume with PBS. This is desirable since many proton therapy centres are switching to or only building PBS rooms, but before patient treatment is possible, it is necessary to investigate the magnitude of the effect of target motion on the dose delivered by PBS [56]. An ITV was created based on CT phases ATN_20, ATN_22, ATN_24, ATN_26, ATN_28, ATN_30 and ATN_32. This corresponds to a 12 [mm] motion range around reference phase ATN_26. Some trial-and-error was required to generate the CTV in such a way that the ITV never reached into the lung cavity on the reference phase, to avoid problems with optimisation. The CTV material properties were then set equal to water. Once the ITV was defined, two beams were introduced, with 250 and 340 degree gantry angles. The 250 degree beam required a 51 [mm] water equivalent thickness (WET) range shifter to be inserted to get layers with deliverable energies. Air gap between the snout and the patient surface was reduced as much as possible for both beams. Once the beams were aimed at the CTV isocentre, a beam-specific PTV was calculated for each of them. This was done using the 3.5% and 5 [mm] margins introduced in Section 3.3, except at the distal edge of the ITV, where a margin of 7 [mm] was applied to account for additional range uncertainty. One support ROI was created, consisting of the liver contour minus the CTV, with a 1 [cm] padding applied to the CTV in the calculation to ensure a margin between the two regions of interest. This contour, called 'LiverMinusCTV+1cm', was used to set an optimisation goal for the dose to the healthy liver tissue.

The optimisation criteria, shown in Figure 4.2, can be divided in three categories. The dose requirements on the ITV and beam-specific PTVs aim to create a homogeneous dose distribution in the CTV equal to the specified dose prescription. The dose fall-off requirement and dose limit for the 'LiverMinusCTV+1cm' ROI were set to ensure a steep dose fall-off outside the ITV, limiting the dose to healthy tissue. Last, the dose constraints applied to the CTV ensure the target does not receive a dose outside of the clinical limits (5985 and 6741 [cGy] correspond to 95% and 107% of the prescribed dose, respectively). The resulting plan was approved by a medical physicist at the WPE. The resulting dose distribution is shown in Figure 4.3. As explained in Section 3.5, all optimisation was done using the pencil beam algorithm.

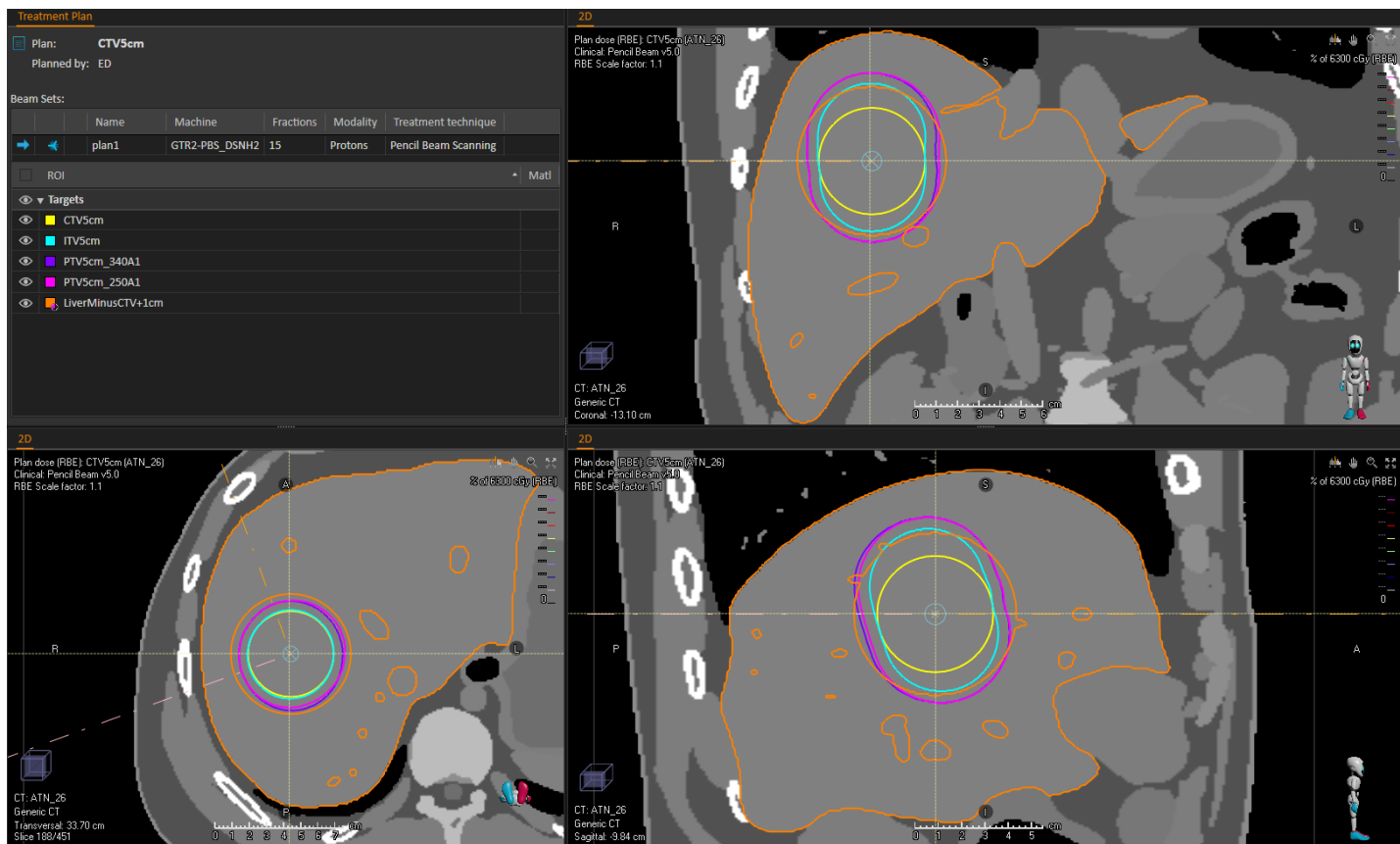


Figure 4.1: Overview of all relevant contours used in treatment planning

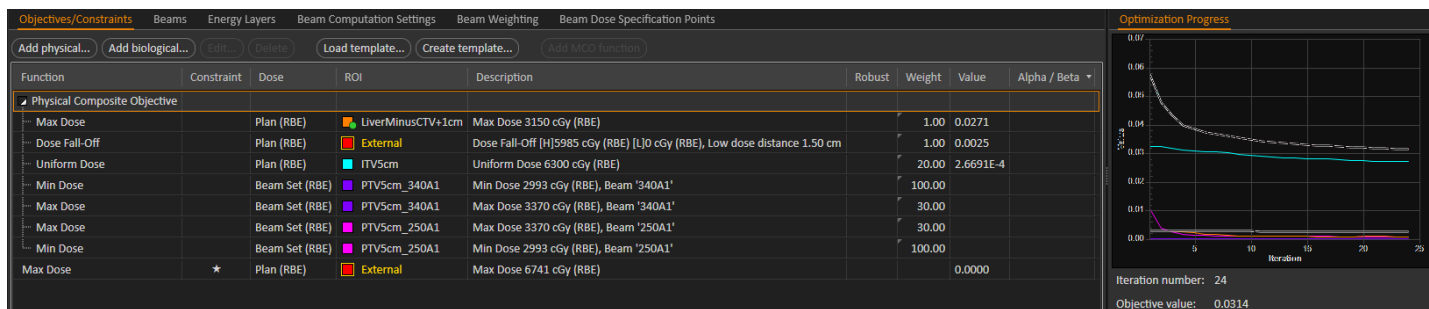


Figure 4.2: List of the criteria fed into the optimisation engine of RayStation. The combination of the criteria was chosen to ensure a homogeneous dose distribution in the CTV while balancing the weight of each beam and limiting the dose to the surrounding healthy tissue.

4.1.2. Layered repainting plan

A liver tumour suffering from motion as investigated here would generally be treated using DS at the WPE. If PBS would be used, the presented plan would usually be executed with five times layered repainting, one of the methods available to mitigate motion effects described in Section 2.2. To investigate the effectiveness of this practise, a copy of the patient data and plan were made, so that two calculations could be run simultaneously, with the second plan set to repainting. Since RayStation v7.99 only includes repainting instructions as a 'note', but does not actually adapt the spots it has calculated, an additional script was provided by RaySearch. This script takes several inputs:

- Repainting method: volumetric or layered?
- Number of repaints

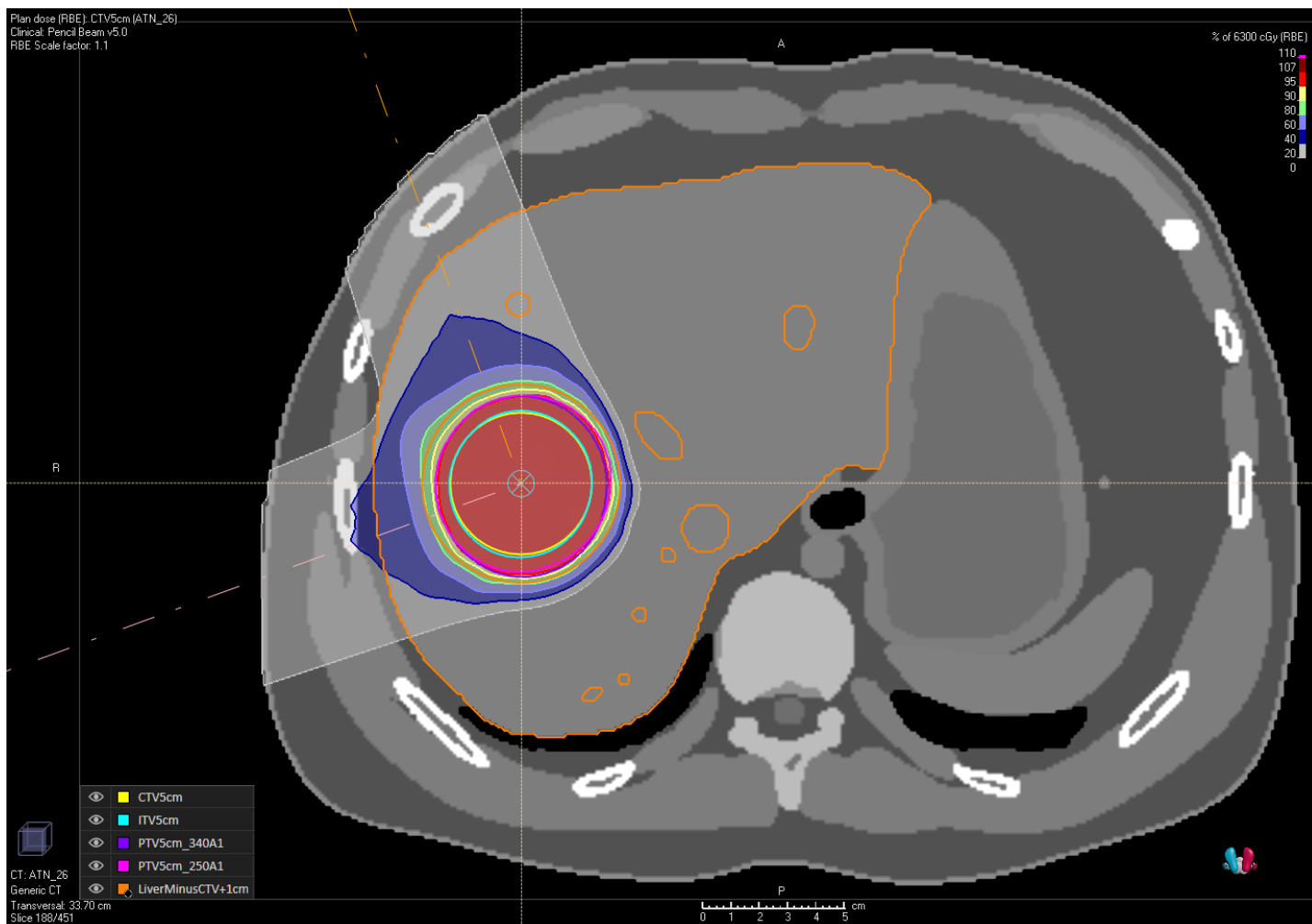


Figure 4.3: Dose distribution of the approved static plan that was used as reference. Its spot weights and locations were used to calculate the beam model for the interplay evaluations.

- Minimum spot weight

For this plan, 5x layered repainting with a minimum spot weight of 0.025 [MU] was selected. This is the lower limit that the treatment system at the WPE is capable of providing. The original plan was then copied by the script and each layer was split into five new layers of the same energy, with spots equal to 1/5 of their original weight, unless this fell below the setting for minimum allowed spot weight. In that case, the spot would be distributed over 4 layers (or even less if the new weights were still too low). This resulted in a near-quintupling of the number of spots. As a result, calculation times for the repainting plan were notably longer for the repainting plan than for the plan without repainting. However, since the transformation from the 50 phases back to the reference phase was also very computationally demanding, the increase was not a factor of five, but rather varied between roughly 50% and 80%. The total irradiation time also increased, but since layered repainting requires no additional energy layer switching, which is one of the most time-consuming parts of the beam time model, the total irradiation time increased by approximately 100%. This brought the maximum irradiation time of any beam to 65 [s], and since the program starts over at the start of the signal when calculating for the next beam, signals with a length of 100 [s] were generated. The exact beam time models for both beams and both plans are provided in the repository [89].

4.2. Regular breathing

The problem of breathing motion is well established. A lot of research has already focused on the impact of breathing on a wide range of medical procedures, including proton therapy [52], [90], [91]. The purpose of this work is to investigate the effect of irregularities in a breathing rhythm on the magnitude of the interplay effect. For that purpose, a baseline of regular signals was investigated, after which irregularities were introduced [92]. In this work, the base model was a sinusoid. Use of trigonometric functions to model breathing is well-established, with the \sin^4 especially being popular [93]. Putting this base model into an equation form:

$$d(t) = \left(A_{ref} - \frac{A}{2} \right) + A \cdot \sin^4 \left(\frac{1}{T} (t - \theta) \right) \quad (4.1)$$

Here, $d(t)$ is the deflection in [mm], A_{ref} is the deflection in [mm] of the reference CT phase, A is the amplitude in [mm], T is the period in [s], t is the time variable in [s] and θ is the phase offset in [rad]. For the purposes of this work, regular motion is defined as motion that repeats periodically, without change in any of the parameters over time. More specifically, the XCAT phantom bases breathing motion on the average diaphragm motion. The conversion between actual diaphragm motion in [mm] and CT phase is 1:1. Since the tumour is close to the diaphragm, its motion is approximately equal to the diaphragm motion, so no conversion factors between motion signal and CT phase were applied. A_{ref} is the deflection in [mm] for the phase that was chosen as reference phase. This is often either the average over all phases or the end-of-exhalation phase [94]–[96]. However, since in this project the phases and breathing patterns were generated independently from the CT phases, the reference phase could also be chosen independently. Phase 26, with an amplitude of 26 [mm], was selected, being in the middle of the available range. The time vector t was created with a length of 100 [s] for every breathing pattern, both regular and irregular.

4.2.1. Randomly sampled breathing patterns

With the basic model known, realistic values for the individual parameters needed to be established. The parameters that could be varied are all on the right-hand side of Equation 4.1; the only parameter that was not varied was the reference phase, which was kept constant at phase 26 and was the equilibrium value of the sinusoid for all regular patterns. From literature, realistic values for the amplitude of tumour motion and the period of one breathing cycle were found to be normally distributed around $\mu_{amp} = 12[mm]$; $\sigma_{amp} = 1.8[mm]$ and $\mu_T = 3.4[s]$; $\sigma_T = 0.17[s]$ [97]–[99]. Since the start phase is dependent on exactly when the beam is activated, which is essentially a random process, this ranged from zero to 2π [rad]. To create a breathing signal, the amplitude and period were taken pseudo-randomly from a normal distribution, while the phase offset was obtained from a uniform distribution. The resulting signal was then stored in a file. In this way, a total of 1000 clinically realistic signals were generated and their input parameter values were stored in a separate file for analysis. To give an idea of the signals investigated, the input values are shown in Figure 4.4.

4.2.2. Single variable breathing patterns

For the randomised input signals, all three parameters were varied simultaneously. In order to investigate the effect of the individual parameters, breathing patterns were generated that vary only one parameter at a time, with the other two at their respective mean values, or 0 [rad] phase offset. First, amplitude was varied from 1 to 20 in 1mm increments. The maximum amplitude generated by the randomised signals was roughly 18 [mm], so the limit of 20 [mm] ensures the full range of clinical signals was covered. Period ranged from 1.6 to 5.2 [s], in 0.3 [s] increments. For phase, the range was naturally taken from 0 to 2π , in steps of 0.3 [rad].

4.3. Irregular breathing

A clear definition for regular signals has been established: a sinusoidal base signal with fixed parameters. It logically follows that irregularity can be introduced by varying these parameters over time. This is precisely the definition of an irregular breathing pattern in this work: a sinusoidal base signal, whose main parameters

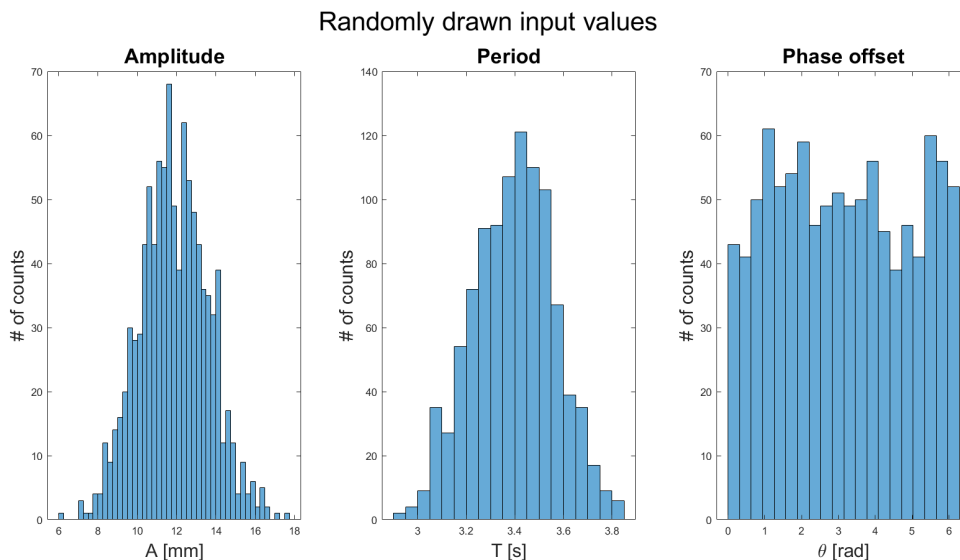


Figure 4.4: Histograms of the values of each of the variables used in generating regular sinusoidal breathing.

vary over the duration of the signal. Specifically, three parameters were allowed to vary: the reference phase A_{ref} , the amplitude A and the period T . The phase offset θ only impacts the signal instantaneously at the start, and thus was not considered a variable that was of clinical interest. The deflection d itself was also considered, since instantaneous changes such as coughing could be reflected by imposing disturbances on top of the base signal. However, only a minor portion (up to approximately 5 [s]) of the signal would be affected, so the impact was expected to be smaller than that of the other variables. Eventually, variation of d was discarded due to a lack of time.

4.3.1. Baseline shift

During a treatment fraction, a patient might relax, causing a decrease in the anterior-posterior (AP) diameter of the chest while increasing the lateral diameter under the influence of gravity [53], [100], [101]. This can be modelled by a variation of the reference phase. Relatively large patients that relax over the course of half an hour can see much larger shifts in average tumour position, so the maximum positive shift was set to 34 [mm], or a shift to an equilibrium position of 60 [mm]. This means the signal itself can actually have a d greater than 50 [mm] at times; in this case the dose will by default be plotted to phase 50 for as long as $d > 50$ [mm]. Since an increase in the AP direction is also technically possible but far less likely, the maximum negative baseline shift was to phase 20, i.e. a 6 [mm] change. Note, however, that the final baseline value is only obtained after 100 [s], while the longest irradiation time for any field was found to be 65 [s], so the irradiation always ended before the final value for the baseline shift was reached. Figure 4.5 shows a sample signal, in which the baseline shifts by 10 [mm]. In total, 40 shifts were considered: from 20 to 60 in 1 [mm] increments, passing over 26 since this would simply be a regular pattern again. For each shift, 13 signals were generated; each signal had a different amplitude, which remained constant, ranging from 6 to 18 [mm] in 1 [mm] increments. This range corresponds to the full range seen for the regular signals with random inputs. Period and starting phase offset were 3.4 and 0 in all cases. In total, there were therefore 520 signals generated with baseline shifts.

4.3.2. Amplitude change

The second parameter that can be varied throughout a signal is the amplitude. With setup and irradiation of several fields, a patient can often be on the treatment table for half an hour or longer. In that time, patients can start to breathe more deeply, sometimes even falling asleep. Conversely, they may also be anxious about what is occurring, leading to shallower breathing. To model this irregularity, the amplitude of the signal was

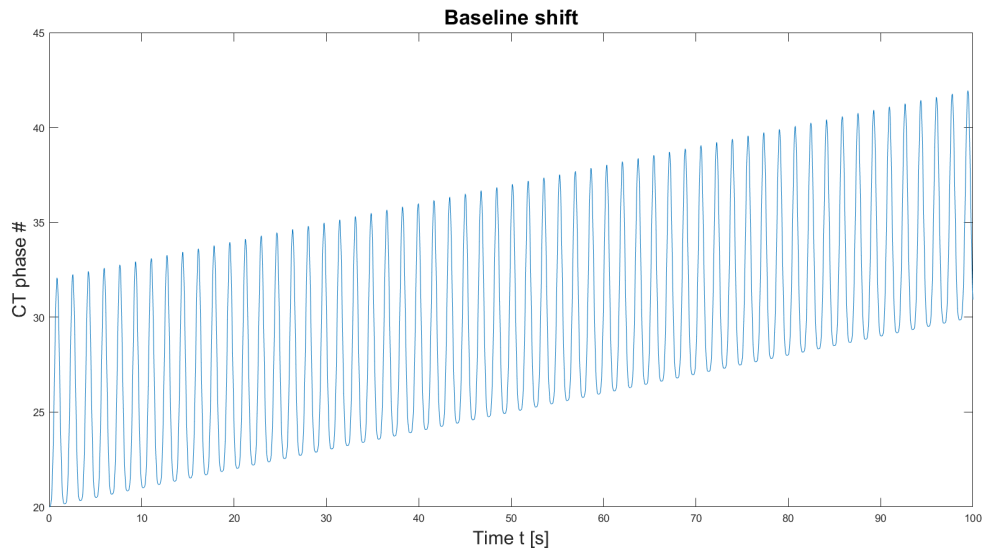


Figure 4.5: Example signal with baseline shift. Here, the baseline or equilibrium position shifts from 26 [mm] at the start to 36 [mm] at the end of the signal, with an amplitude of 12 [mm].

allowed to vary over time [100]–[102]. Figure 4.6 shows an example of such a signal. In this particular case, the amplitude at the start is 8 [mm] and this gradually increases to 15 [mm].

Overall, the start and end values of the amplitude ranged from 6 to 18 [mm] in 0.5 [mm] increments. Rejecting signals where the start and end amplitude were identical, this leads to $25 \times 24 = 600$ signals in total. For all signals, period T was kept constant at 3.4 [s] and phase offset θ was 0.

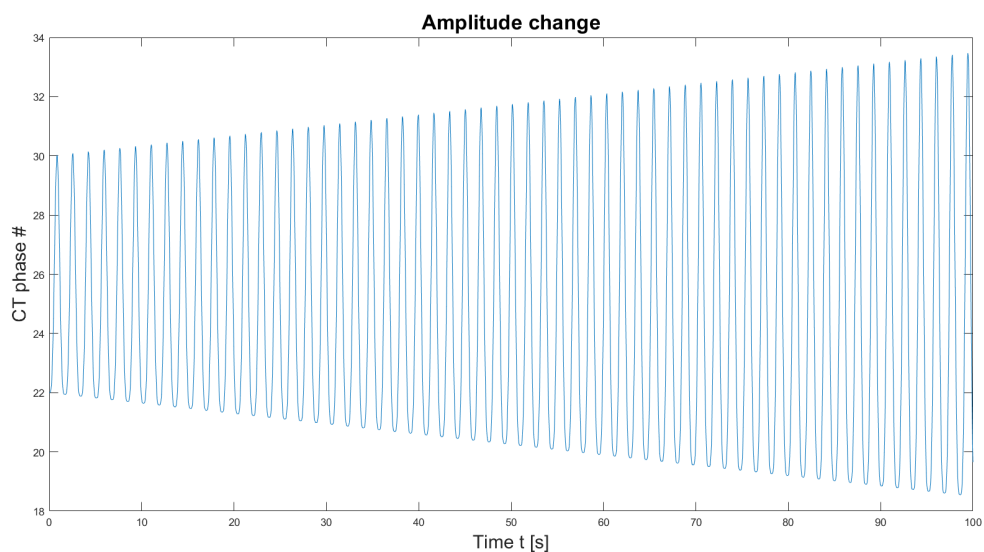


Figure 4.6: Example signal with varying amplitude. Here, the amplitude varies from 8 [mm] at the start to 15 [mm] at the end of the signal.

4.3.3. Period variation

Last, the period of the signal was varied. Shallower or deeper breathing does not only vary amplitude, in this case the breathing cycle length will naturally vary too. The data used for generating the randomised regular signals suggests $\mu_T = 3.4[s]$ and $\sigma_T = 0.17[s]$, but a larger range was selected, identical to the single variable analysis of the effect of varying the period: from 1.6 to 5.2 [s] in 0.3 [s] increments. The concept was the

same as for amplitude variation; each period value was matched with every other value to create a linearly changing value for the period. Figure 4.7 shows a signal with the period increasing from 1.6 [s] at the start to 5.2 [s] at the end, with a 12 [mm] amplitude. The starting phase offset θ was again set to zero. The amplitude was also constant, but since different breathing speeds often go hand-in-hand with a different amplitude, all signals were varied for five different amplitudes: 8 to 16 mm in 2 [mm] increments. In total, there were $13 \times 12 \times 5 = 780$ signals generated.

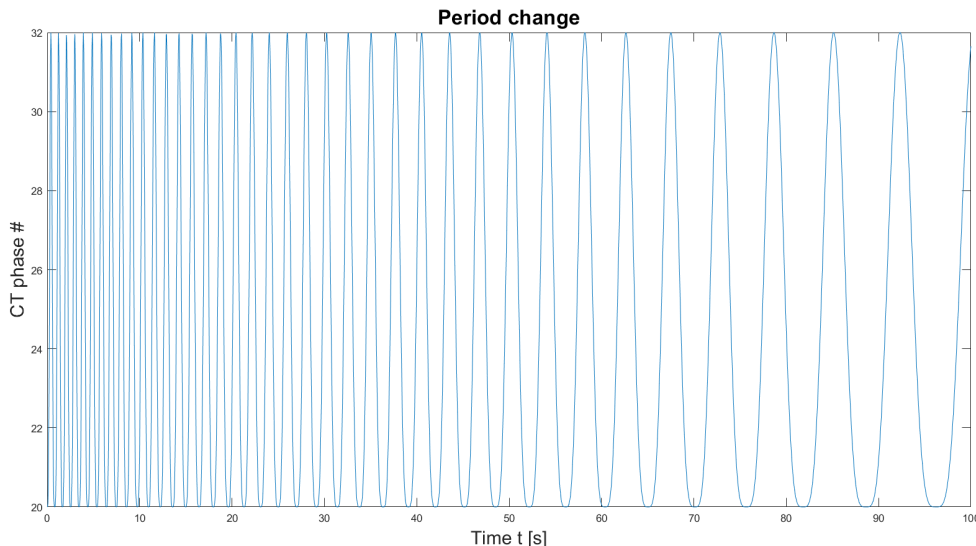


Figure 4.7: Example signal with a changing period. Here, the period changes from 1.6 [s] at the start to 5.2 [s] at the end of the signal, with an amplitude of 12 [mm].

4.4. Calculating 4D dose distributions

The program calculating the dose distributions is based on previous work at the WPE [38]. It is shown schematically in Figure 4.8 and takes two inputs: a treatment plan and a breathing signal. The treatment plan consists of a certain number of spots that need to be irradiated. The combination of their location and weight together create the irradiation pattern. Next, machine parameters are included: horizontal and vertical scan speed in [cm/s], energy layer switching time in [s] and inverse dose rate coefficients in [s/MU] allow the time model for the beam to be established, listing exactly which spot is irradiated at what instant. These machine parameters can be entered into the program or the plan can be irradiated, after which machine logs can be imported to replace the calculated beam time model. In this work, machine parameters were used, which were validated during previous work for the system at the WPE [57]. Normally, these are taken from a probability distribution, since they are generally not constant, but the variance for these parameters was set to zero to better isolate the effect of variations in breathing. For each beam, the beam time model was established separately, starting over from $t = 0$ in the breathing signal.

The other side of the pipeline concerns the anatomical data. A breathing signal and a phase-to-amplitude mapping file can be entered in the form of two comma-separated value files. The breathing signal is comprised of a series of time stamps in [s] and amplitudes in [mm]. The mapping file must contain a list of CT phase names and their corresponding amplitude in [mm]. The mapping file is specific to a certain 4DCT set, and therefore does not need to be changed unless the 4DCT is changed between calculations. In this work, only one phantom was used and thus only one phase-to-amplitude mapping file was required. The format is shown together with a sample breathing pattern in Figure 4.9. Together, the files define the anatomical motion over time.

Combining the anatomical motion and the beam time model, each spot is assigned to a CT phase based on the amplitude as indicated by the breathing signal at the time of irradiation. The program checks the amplitude of the breathing signal at a given time, compares it to the mapping file and selects the nearest

match as 'active'. Their contribution is then calculated using PBA, applying the beam for that single spot to the anatomy of the assigned CT phase to find the deposited dose distribution in that phase. Once the full beam time model has been processed and the dose distribution for each spot has been calculated on the phase in which it was deposited, the cumulative dose distributions are computed on each CT phase individually. Next, the distributions are transformed to the reference phase, where the cumulative disturbed dose distribution is calculated by summing the transformed contributions of the individual phases. The program was looped, so that a set of signals could be calculated concurrently without user intervention.

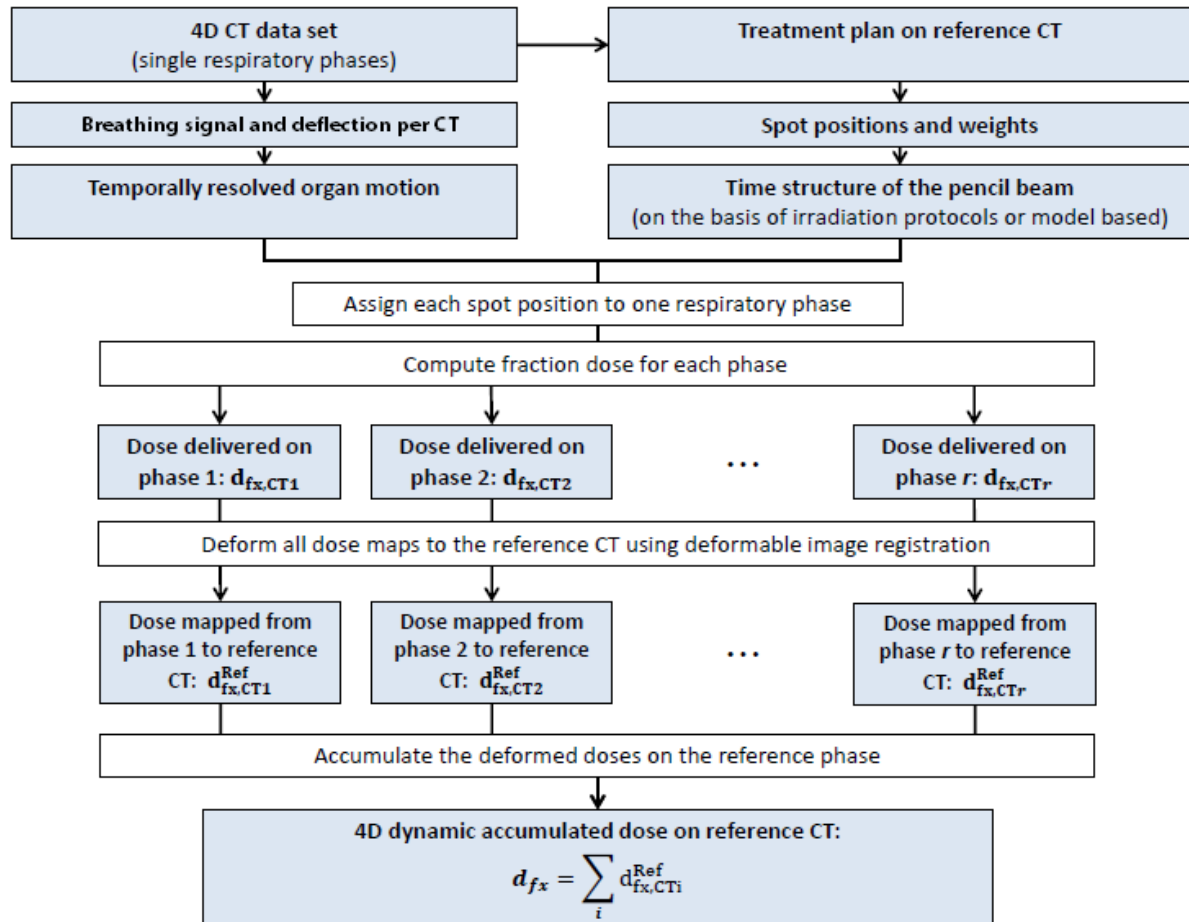


Figure 4.8: Schematic overview of the process used to calculate the dose distributions affected by the interplay effect.

1.csv	PhaseToAmplitude.csv
1 0;30.957	1 ATN_01; 1
2 0.04;31.095	2 ATN_02; 2
3 0.08;31.035	3 ATN_03; 3
4 0.12;30.779	4 ATN_04; 4
5 0.16;30.34	5 ATN_05; 5
6 0.2;29.74	6 ATN_06; 6
7 0.24;29.005	7 ATN_07; 7
8 0.28;28.17	8 ATN_08; 8
9 0.32;27.272	9 ATN_09; 9
10 0.36;26.348	10 ATN_10; 10
11 0.4;25.435	11 ATN_11; 11
12 0.44;24.566	12 ATN_12; 12
13 0.48;23.768	13 ATN_13; 13
14 0.52;23.063	14 ATN_14; 14
15 0.56;22.463	15 ATN_15; 15

Figure 4.9: Example of a breathing pattern input file (left) and the amplitude-to-phase mapping file (right).

4.5. Evaluation metrics

From the dose calculations, a total of eleven parameters were extracted:

- V_{107} : the fraction of the CTV that received more than 107% of the prescribed dose of 6300 cGy.
- V_{95} : the fraction of the CTV that received less than 95% of the prescribed dose of 6300 cGy.
- $D_{95\%}$: the maximum dose that covers 95% of the CTV in [cGy].
- $D_{5\%}$: the maximum dose that covers 5% of the CTV in [cGy].
- $D_{98\%}$: the maximum dose that covers 98% of the CTV in [cGy].
- $D_{2\%}$: the maximum dose that covers 2% of the CTV in [cGy].
- HI_5 : the 5% homogeneity index, calculated as $\frac{D_{5\%} - D_{95\%}}{D_{prescribed}}$
- HI_2 : the 2% homogeneity index, calculated as $\frac{D_{2\%} - D_{98\%}}{D_{prescribed}}$
- $V_{107/95}$: $V_{107} + (1 - V_{95})$
- D_{min} : Minimum dose received by any voxel in the CTV.
- D_{max} : Maximum dose received by any voxel in the CTV.

A common method for displaying a dose distribution is a dose-volume histogram (DVH). To clarify the parameters, V_{95} and $D_{5\%}$ are shown in Figure 4.10 for the nominal plan. Then $V_{107/95}$ is defined as the relative volume that falls outside the bounds of V_{107} and V_{95} . These two values are commonly used as clinical limits; the dose to the CTV may not be outside these limits [103]. Therefore, $V_{107/95}$ is the relative CTV volume that receives a clinically unacceptable dose. However, $V_{107/95}$ says nothing about how far outside of the bounds the volume is. A dose distribution where every voxel receives 107.1% of the prescribed dose would have a $V_{107/95}$ of 1, while a distribution where every voxel receives 106.9% has a $V_{107/95}$ of 0. This nuance is better captured by the homogeneity indices, HI_5 and HI_2 . They show the steepness of the DVH, as it falls from the top to the bottom end of the DVH. A very steep graph is desirable; it means the differences in received dose between different parts of the CTV are small, i.e. the dose is homogeneous. In that case, $D_{5\%}$ and $D_{95\%}$ (or $D_{2\%}$ and $D_{98\%}$) will be close to each other, so the homogeneity index will be close to zero. An ideal DVH would therefore look like an inverted step function, remaining horizontal at 100% volume until the prescribed dose value is reached, at which point it instantly drops to zero. Since both the 2/98% and 5/95% limits are commonly used in clinical practice, both sets of values were extracted from the calculated dose distributions.

It was noted that the results for $D_{5\%}$ and $D_{2\%}$, and for $D_{95\%}$ and $D_{98\%}$, are highly similar. This is to be expected, and since they are the inputs for HI_5 and HI_2 , these almost identical. More generally, it was noted that trends in the results are consistent for all eleven metrics. This also holds for each of the investigated signal types and for both the plans with and without repainting, so only the plotted results for two metrics are shown throughout the rest of the report for brevity: the fraction of over- and underdosed volume $V_{107/95}$ and the homogeneity index HI_5 . An additional advantage is that these metrics both naturally range from zero to unity, making comparison between various graphs more straightforward than between dose-based metrics, where the vertical axis can vary in range significantly between figures. The full data files, as well as plots for D_{max} and D_{min} and all relevant programs were uploaded to a repository [89].

4.6. Assumptions

Virtually all research done worldwide involves some assumptions on which the work is based. The assumptions supporting this work are listed here. Some assumptions are very minor and some potentially have a significant impact on the work, which is why the validity of these assumptions must be considered. The assumptions that were made, are:

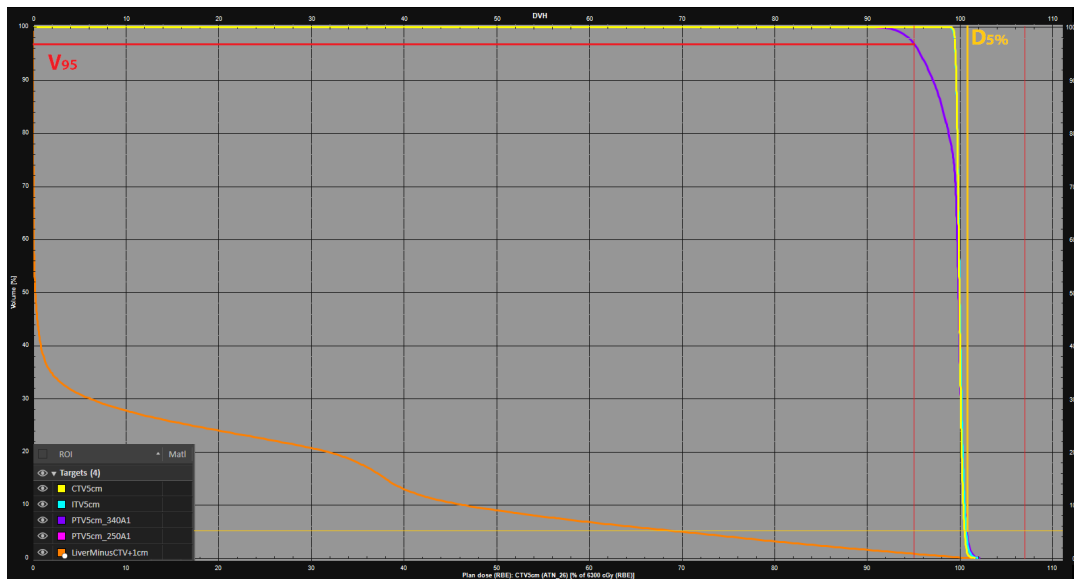


Figure 4.10: A DVH, showing dose relative to the prescribed dose level of 6300 [cGy] on the horizontal axis and relative volume of several regions of interest on the vertical axis. Volume-based metrics are read from the histogram by drawing a vertical line at the desired dose level, and then finding the intersection with the line of the desired ROI, after which the volume receiving that dose is read from the vertical coordinate, usually as fraction of the total ROI volume. For dose-based metrics, the process is inverted. This DVH corresponds to the static reference plan and shows examples for reading V_{95} and $D_{5\%}$ for ROI *PTV5cm_340A1*.

1. The anatomy generated by the XCAT software is accurate.
2. The tumour motion per XCAT phase is 1 [mm], meaning that no conversion factor is needed between the breathing patterns and the tumour motion entered into the interplay calculator.
3. The use of the PBA instead of the clinical standard MC does not adversely affect the results.
4. The transformation between phases is accurate.
5. All signals started with the equilibrium position of the signal equal to the planning reference phase (ATN_26).
6. Breathing signals were one-dimensional, referring to the motion of the diaphragm in the superior-inferior (SI) direction.
7. The effect of fractionation was not accounted for.
8. The beam time model accurately represents the properties of the WPE installation.

The first four assumptions were discussed in Chapter 3, the remaining four will be discussed here.

Constant starting equilibrium phase Every breathing pattern generated here has started with the planning reference phase as its equilibrium position. Aside from the signals with a non-zero starting phase shift, every pattern even started at this phase. This means that the first spots, which are also generally the spots with the largest weight and which also irradiate every layer on their way through, tend to be irradiated pretty close to their planned target. However, it is highly unlikely that the patient anatomy at the start of the irradiation is identical, or at least very similar, to the planning anatomy.

One-dimensional breathing This assumption is reasonable, since motion is often found to be notably larger in one direction than in the other two, with the SI direction commonly the most affected direction [54], [100], [104]. However, any motion orthogonal to the beam direction is likely to have a notable influence on the accuracy of spot delivery, so ideally a three-dimensional signal, or at the very least a two-dimensional

signal that accounts for all motion in the plane orthogonal to the beam path, should be considered. Results can then be compared with works such as this, based on one-dimensional signals, to establish the accuracy of the 1D assumption. With the current methodology, multi-dimensional breathing is only tangentially accounted for by rendering of the XCAT phantom, which distorts in all directions based on an input amplitude. However, this is again based on a one-dimensional input, since it requires only the average diaphragm location.

Fractionation Radiotherapy is commonly delivered in a fractionated regimen; that is, the full prescribed dose is cut up in smaller portions that are delivered over the course of several days or weeks [23], [105]. In general, one treatment fraction is delivered each working day, with more than one fraction per day being called hyperfractionation and delivery of only a few bigger fractions referred to as hypofractionated treatment. In essence, the magnitude of the interplay effect can cause both over- and underdosage to a given region, depending on a combination of input values such as starting breathing phase and amplitude. The combination for any given treatment fraction can be considered a random process to a certain extent, and thus this effectively means that a result is drawn from some distribution of possible effect sizes. Fractionation can then be seen as drawing from this distribution multiple times; the mean of the drawn results then naturally converges towards the mean of the distribution as the number of drawn results goes to infinity. This behaviour is important to note, since it means fractionation naturally counteracts debilitating effects of interplay [56], [106]. This was not accounted for in this research, so it can be assumed that in most clinical plans, the interplay effects described here will be less severe when the full treatment course is considered.

Beam time model Another important input into the interplay calculator is the beam time model. This takes the known inputs such as dose rate and energy layer switching time. One factor that is not considered is the effect of beam pausing. In clinical practise, irradiation does not always progress uninterrupted from start to finish. Starting with the ionisation of hydrogen and ending with the beam leaving the nozzle, many parameters of the beam delivery process need to be kept within limits. If one of these values falls outside of its tolerance values, this often results in a pause in the system, requiring user intervention to restart the irradiation process. Depending on how easily the error is resolved, this can lead to a delay of several seconds to sometimes as much as a minute, if cyclotron operator intervention is necessary to resolve the problem. For the plans without repainting, irradiation took roughly half a minute; for the 5x repainting plan, the irradiation time was approximately one minute. Therefore, beam delivery issues can have a notable effect on the beam time model. Since they will always lengthen the nominal irradiation time, it stands to reason that irregularities such as baseline drift or amplitude variation become more pronounced in this scenario as well. However, the current interplay calculator does not have the ability to implement such interruptions in beam delivery, and must thus be modified before their effect can be investigated.

Interplay effect with regular breathing

In this chapter, the results of calculations with regular input signals will be shown. Section 5.1 starts off with the individual parameter analyses. The results for the 1000 randomised signals follow in Section 5.2. The results are then analysed in Section 5.3 before a statistical analysis on the effect of repainting is carried out in Section 5.4.

5.1. Single variable analysis

The sinusoid in Section 4.2 contains three parameters that were varied independently to investigate their effect on the magnitude of the interplay effect. The results are shown here. The correlation of the magnitude with each parameter is shown by calculating the Pearson correlation coefficient [107].

5.1.1. Amplitude dependence

20 signals were generated, keeping period and starting phase offset constant at 3.4 [s] and 0 [rad] respectively, and varying amplitude from 1 to 20 [mm] in 1 [mm] increments. Figure 5.1 shows the amplitude dependence of the interplay effect, for the plan without repainting. Figure 5.2 shows the results for the plan with 5x layered repainting.

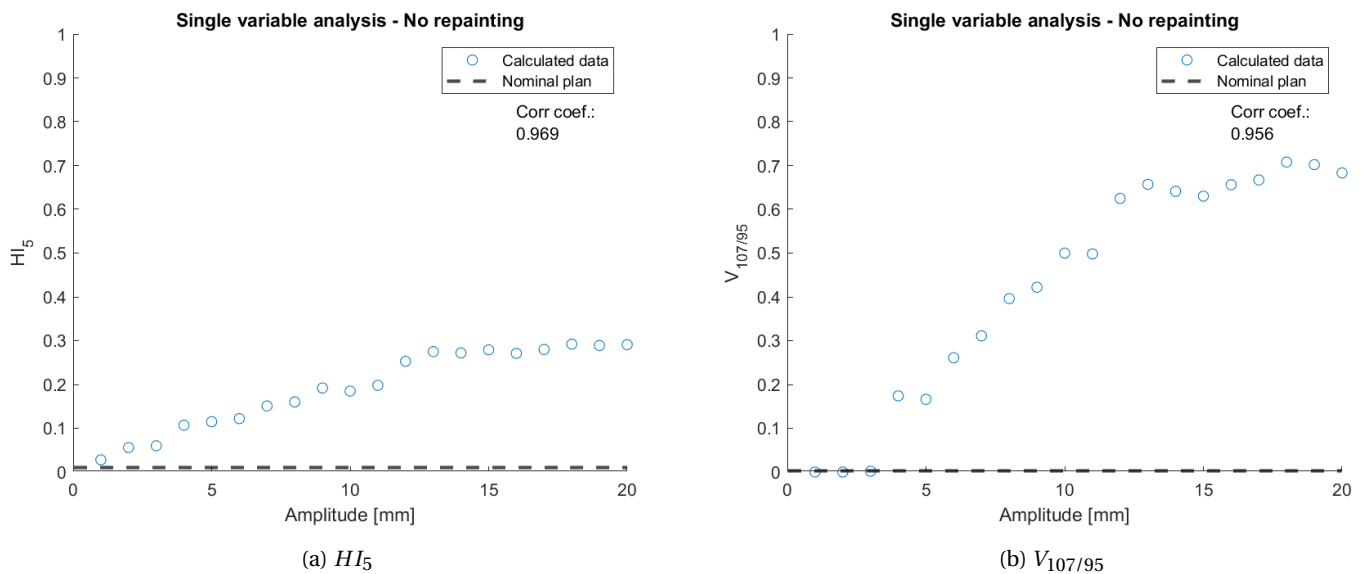


Figure 5.1: The values of HI_5 and $V_{107/95}$ as a function of varying amplitude. The Pearson correlation coefficient is also displayed.

5.1.2. Period dependence

13 signals were generated, keeping amplitude and starting phase offset constant at 12 [mm] and 0 [rad] respectively, and varying period from 1.6 to 5.2 [s] in 0.3 [s] increments. Figure 5.3 shows the period dependence of the interplay effect, for the plan without repainting. Figure 5.4 shows the results for the plan with 5x layered repainting.

[htb!]

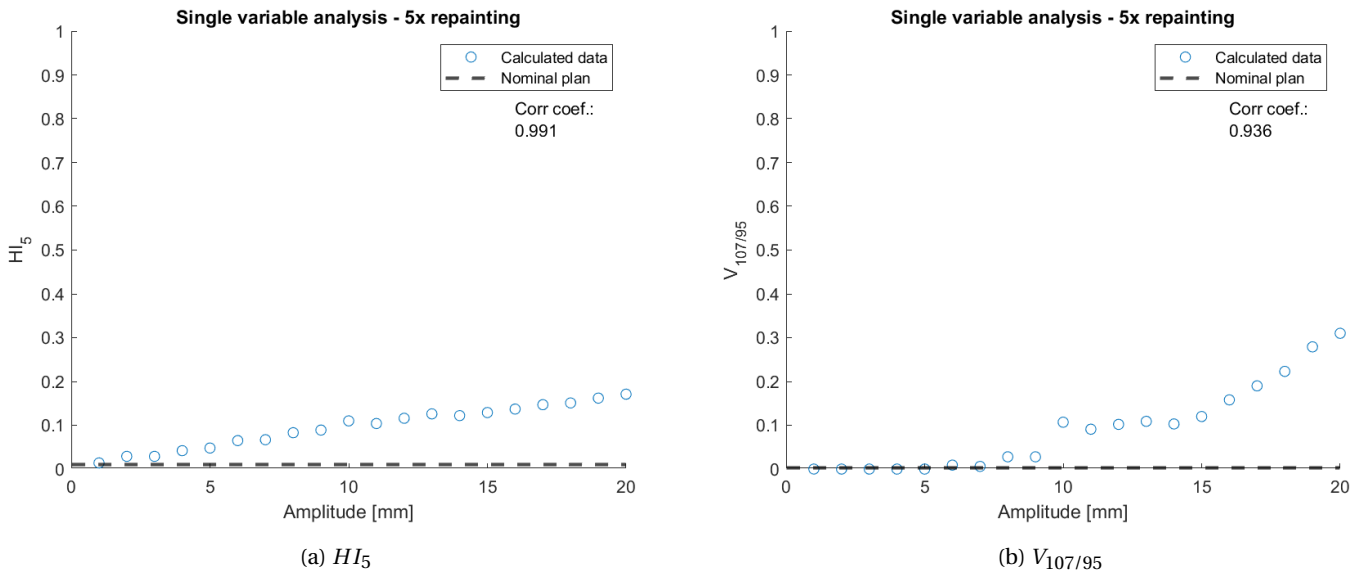


Figure 5.2: The values of HI_5 and $V_{107/95}$ as a function of varying amplitude, with 5x layered repainting applied. The Pearson correlation coefficient is also displayed.

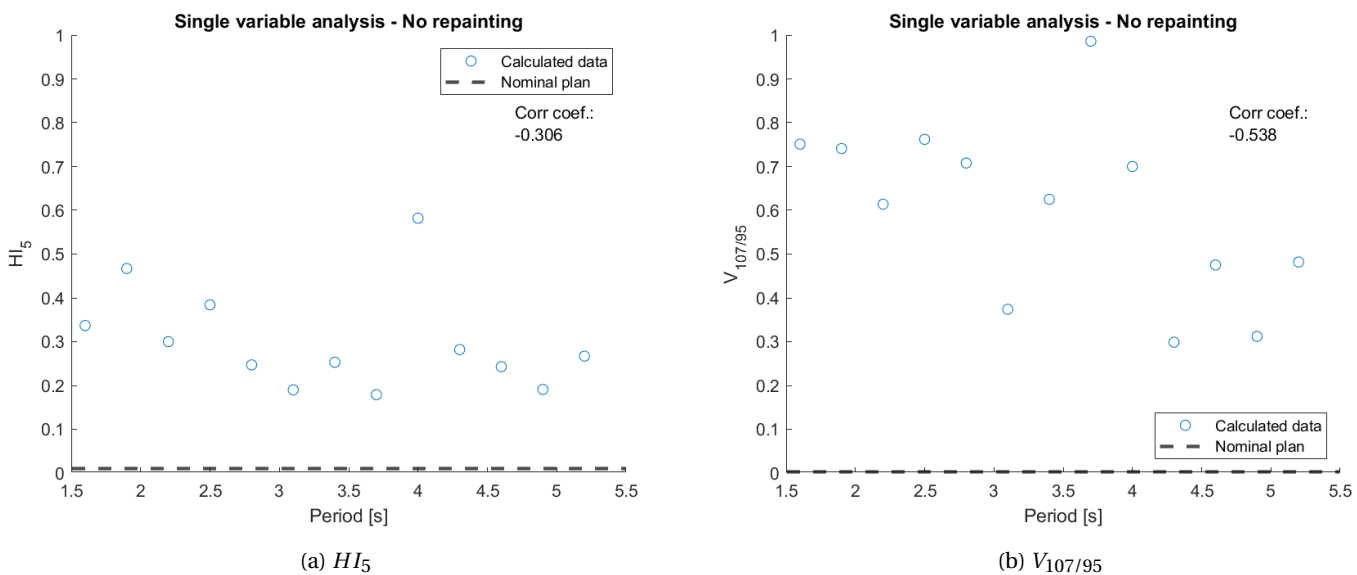


Figure 5.3: The values of HI_5 and $V_{107/95}$ as a function of varying period. The Pearson correlation coefficient is also displayed.

5.1.3. Phase dependence

21 signals were generated, keeping amplitude and period constant at 12 [mm] and 3.4 [s] respectively, and varying phase from 0 to 6.0 [rad] in 0.3 [rad] increments. Figure 5.5 shows the starting phase offset dependence of the interplay effect, for the plan without repainting. Figure 5.6 shows the results for the plan with 5x layered repainting.

5.2. Randomised signals

Next, the results for the 1000 randomised signals will be displayed. Table 5.1 shows the mean and standard deviation of both the plans with and without repainting, as well as those of the static plan, to give an indica-

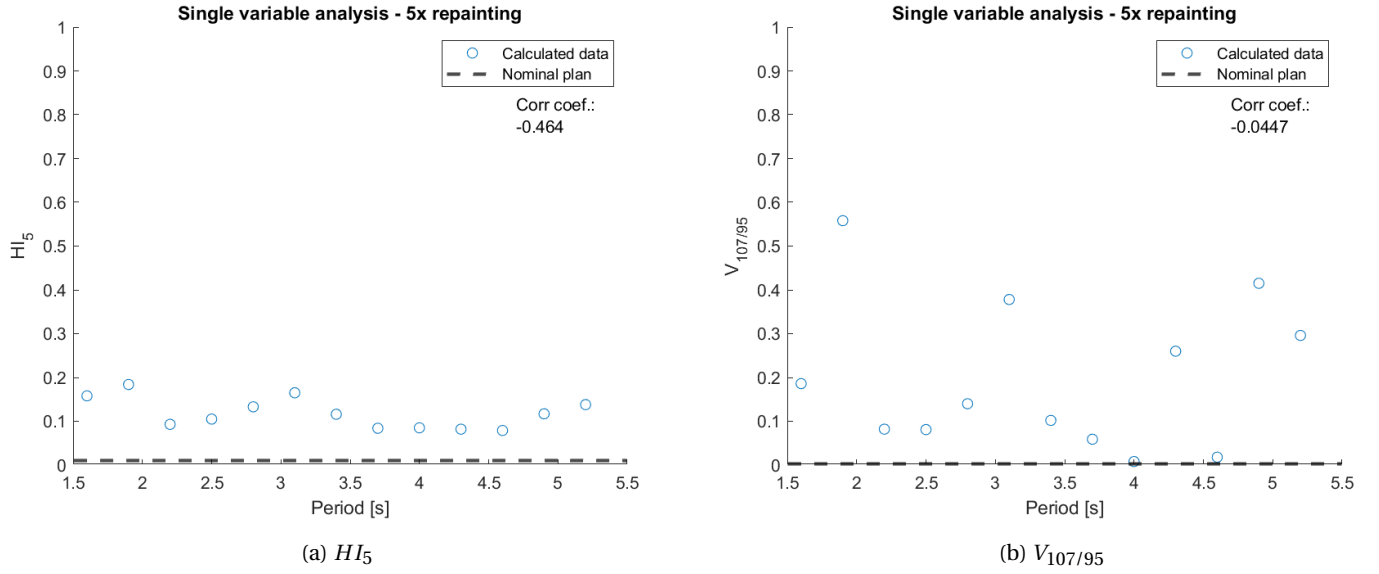


Figure 5.4: The values of HI_5 and $V_{107/95}$ as a function of varying period, with 5x layered repainting applied. The Pearson correlation coefficient is also displayed.

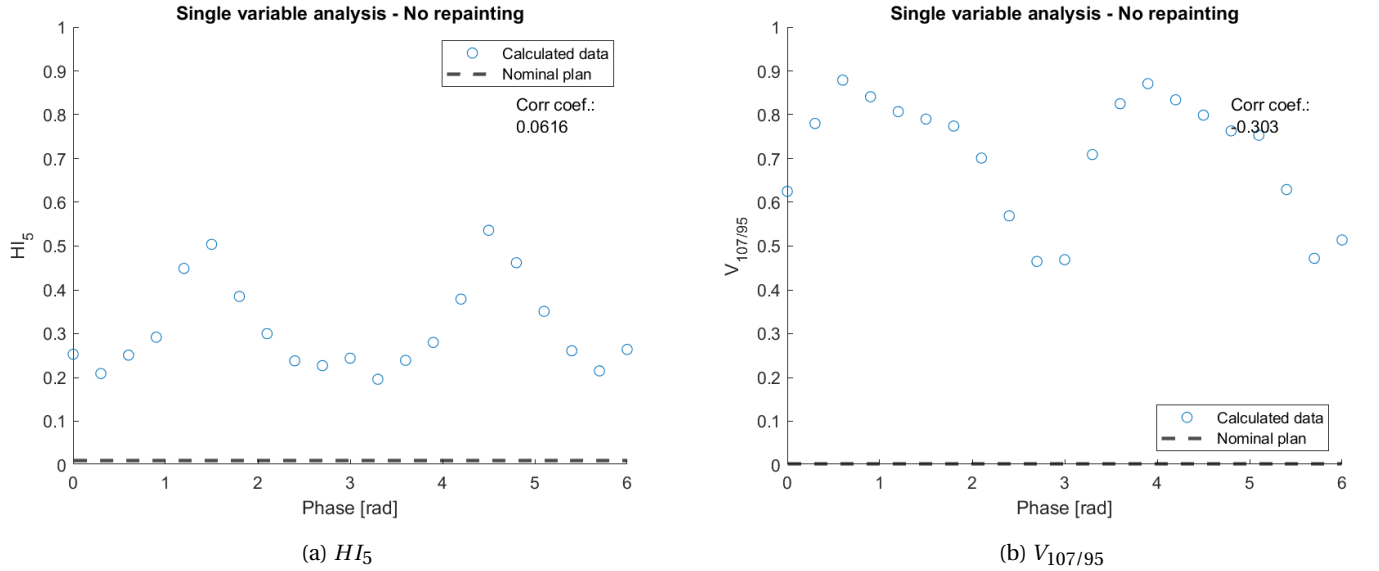


Figure 5.5: The values of HI_5 and $V_{107/95}$ as a function of varying starting phase offset. The Pearson correlation coefficient is also displayed.

tion of the general magnitude of the interplay effect. D_{min} and D_{max} are not always clearly related to the two main metrics, HI_5 and $V_{107/95}$, so they are included here, normalised with respect to the prescribed dose.

Plan	Mean value μ				Standard deviation σ			
	HI_5	$V_{107/95}$	D_{min}	D_{max}	HI_5	$V_{107/95}$	D_{min}	D_{max}
Static	0.01	0.00	0.99	1.02	-	-	-	-
No repainting	0.31	0.71	0.75	1.29	0.11	0.17	0.11	0.15
5x repainting	0.11	0.12	0.90	1.09	0.03	0.11	0.03	0.03

Table 5.1: The effects of interplay on the presented treatment plan. Values for the static plan are based on the dose distribution after optimisation. Values for the plans with and without repainting are averaged over the results for the 1000 randomised breathing signals, with standard deviation also calculated. Note that the values for D_{min} and D_{max} were normalised relative to the prescribed dose.

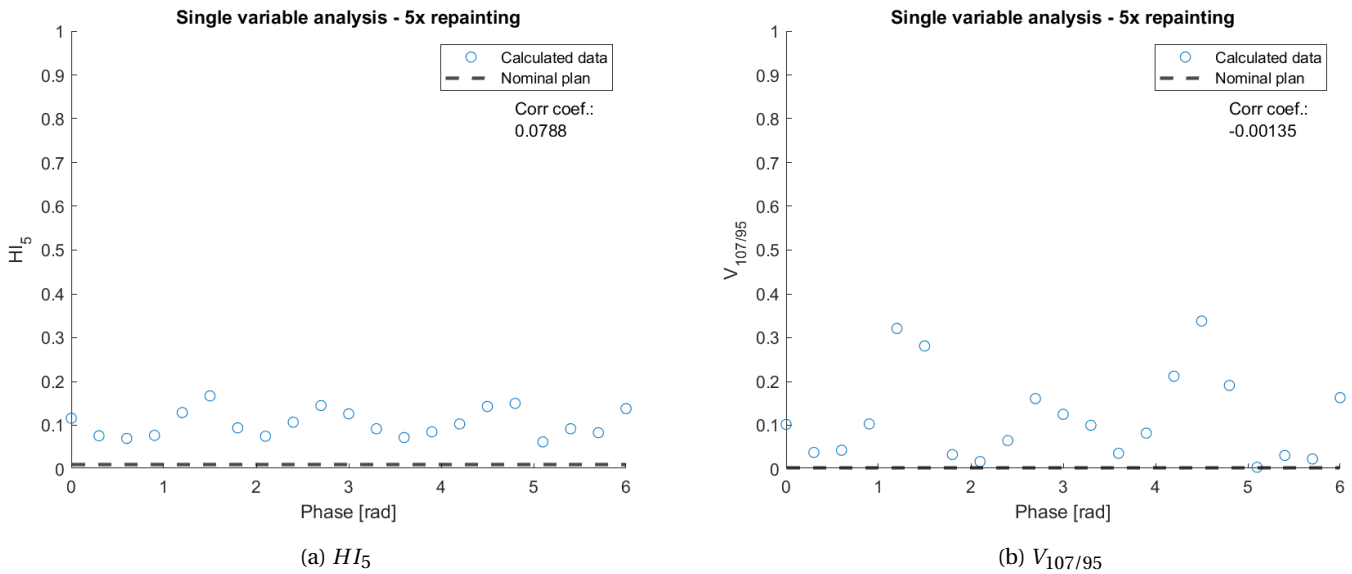


Figure 5.6: The values of HI_5 and $V_{107/95}$ as a function of varying starting phase offset, with 5x layered repainting applied. The Pearson correlation coefficient is also displayed.

5.2.1. Results without repainting

Figure 5.7 shows the results for the plan without repainting, sorted as a function of the amplitude of each input signal. Figures 5.8 and 5.9 display the same results, as functions of the period and starting phase offset of the signals, respectively.

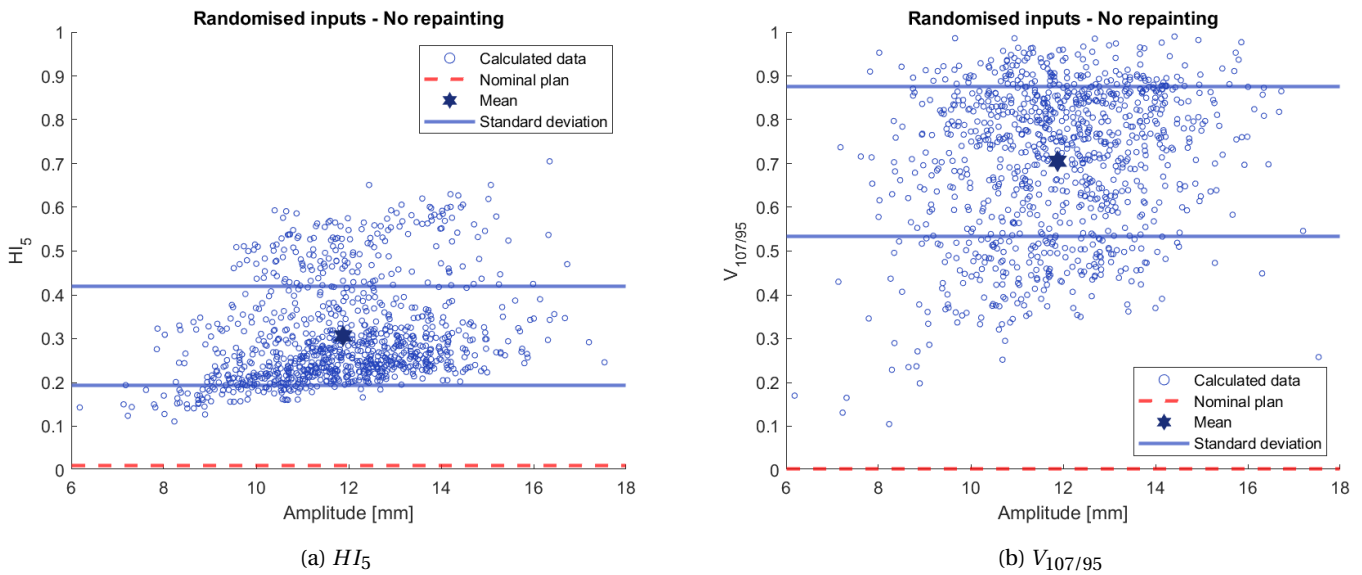


Figure 5.7: HI_5 and $V_{107/95}$ extracted from dose distributions calculated from 1000 randomly generated breathing patterns, sorted by amplitude of the breathing signal.

5.2.2. Results with 5x repainting

For the randomised breathing patterns, irradiated with 5x layered repainting, the results are shown in Figures 5.10 to 5.12, again sorted by amplitude, period and starting phase offset, respectively.

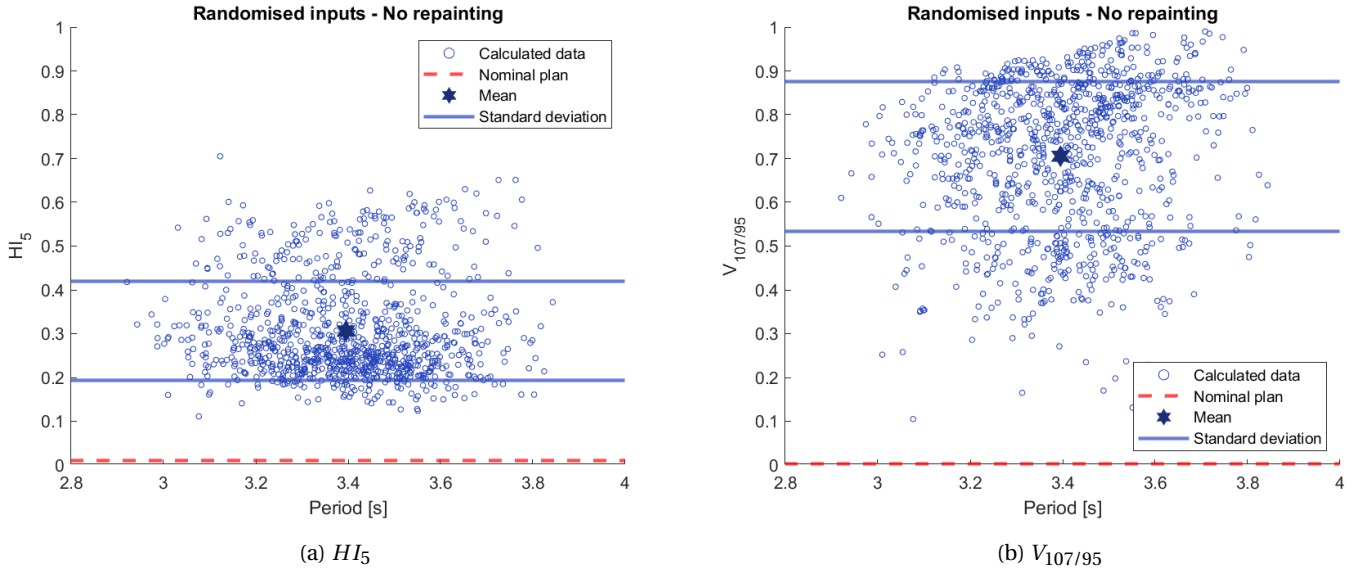


Figure 5.8: HI_5 and $V_{107/95}$ extracted from dose distributions calculated from 1000 randomly generated breathing patterns, sorted by period of the breathing signal.

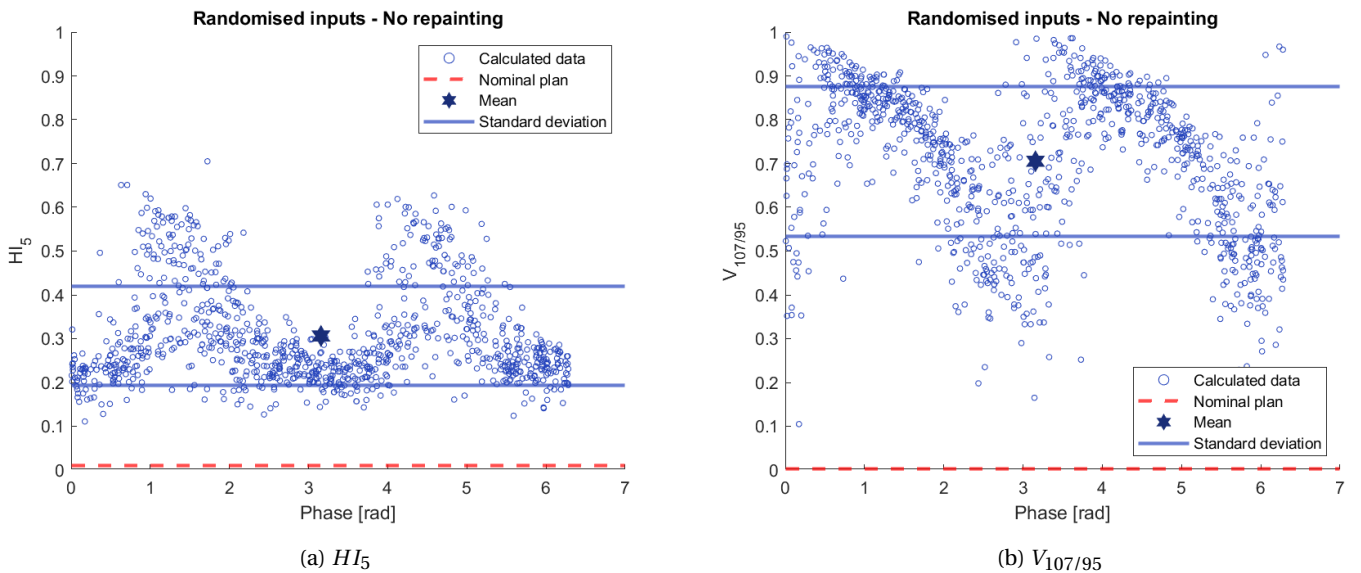


Figure 5.9: HI_5 and $V_{107/95}$ extracted from dose distributions calculated from 1000 randomly generated breathing patterns, sorted by starting phase offset of the breathing signal.

5.3. Discussion of results

Some correlations and patterns can be established based on the single variable breathing signals, after which the randomised signals can be evaluated with these relationships in mind.

5.3.1. Single variable analysis

Figure 5.1 shows a very strong correlation with amplitude, but the influence is actually comparatively small compared to that of the other two parameters. Figure 5.1a shows that even the slightest motion already leads to a decrease in dose homogeneity, and the magnitude of this effect rises fairly steadily until an amplitude of 13 [mm], after which a plateau is reached with an HI_5 of roughly 0.3. In Figure 5.1b, $V_{107/95}$ shows a similar

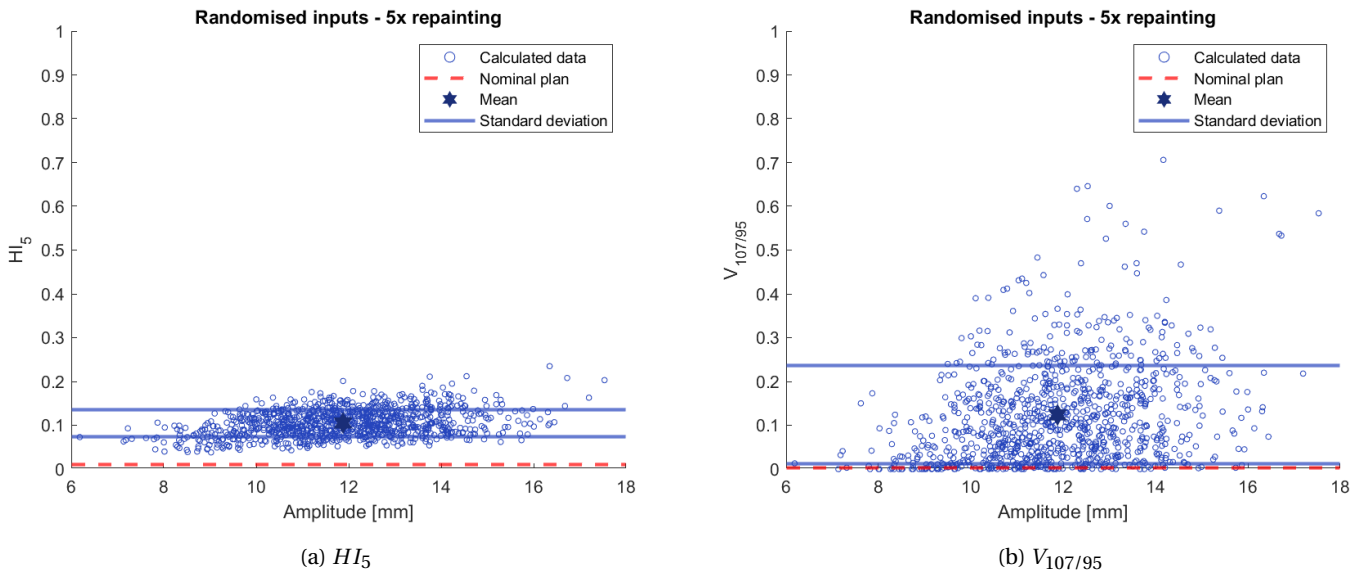


Figure 5.10: HI_5 and $V_{107/95}$ extracted from dose distributions calculated from 1000 randomly generated breathing patterns, sorted by amplitude of the breathing signal, with 5x layered repainting applied.

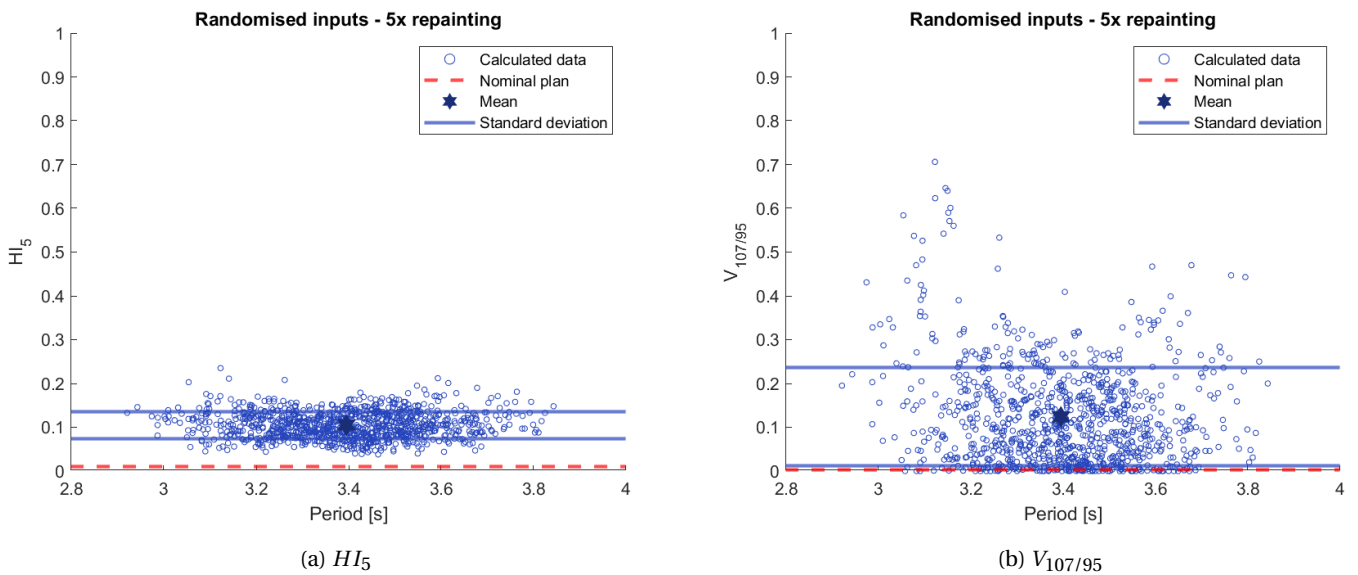


Figure 5.11: HI_5 and $V_{107/95}$ extracted from dose distributions calculated from 1000 randomly generated breathing patterns, sorted by period of the breathing signal, with 5x layered repainting applied.

trend but with some different details. Here, the binary effect of this metric shows very clearly; while HI_5 gradually climbs, $V_{107/95}$ shows no signs of dose deterioration until an amplitude of 4 [mm], at which point it suddenly jumps to 0.2, indicating that a notably portion of the CTV crosses the boundary at the same time. After this, it climbs steadily before also levelling off after 13 [mm] at 0.7. Note that despite the slightly more erratic behaviour of $V_{107/95}$, the Pearson correlation coefficient is almost identical for both metrics. There are also occasional dips in the trend, but these are fairly small and can likely be attributed to random effects, such as whether certain individual spots coincide or not.

The effect of the period length is far more obscure than that of the amplitude. However, it is important to note that although no correlation seems to exist, the variation of the effect is actually larger than that of amplitude. Figure 5.3a shows that HI_5 ranges from a minimum of 0.18 to a maximum of 0.58, for a total range of 0.4 - 33% larger than the range exhibited by HI_5 in Figure 5.1a. For $V_{107/95}$, the range of the data points

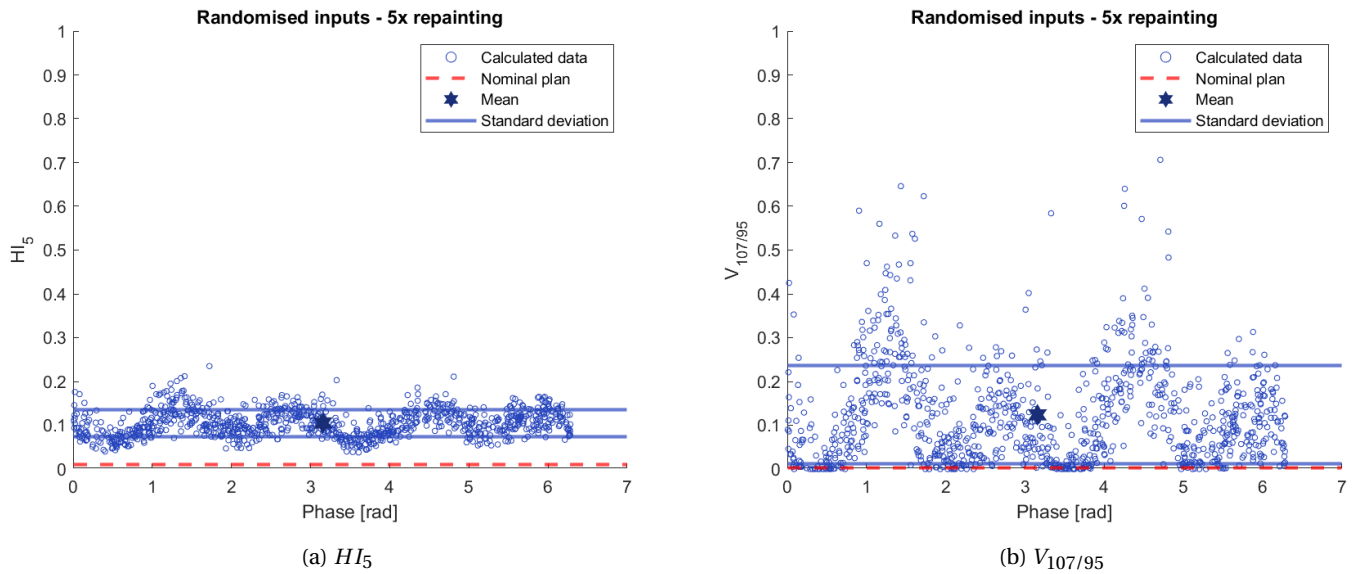


Figure 5.12: HI_5 and $V_{107/95}$ extracted from dose distributions calculated from 1000 randomly generated breathing patterns, sorted by starting phase offset of the breathing signal, with 5x layered repainting applied.

is still 0.7, but Figure 5.3a shows a minimum value of 0.3 and a maximum of 1. The maximal $V_{107/95}$ actually corresponds to the minimal value of HI_5 , with both occurring for a period of 3.7 [s]. This once more illustrates the importance of evaluating both metrics simultaneously, rather than focusing on one or the other. Such a result is most likely explained by a change which causes a significant portion to fall outside the 95% and 107% limits, but which occurs relatively constantly around the entire volume, keeping the dose inhomogeneity induced by this change relatively small. This reinforces the seemingly random effect of the period length on the magnitude of the interplay effect. The most likely explanation is that all values of the period cause a deterioration of the dose homogeneity, since these are all signals with a 12 [mm] amplitude, but some values might cause layer switching or scanning direction switches to move the beam in an unfavourable direction at a particularly inopportune moment.

Arguably the most interesting graph is that of the starting phase offset (Figure 5.5). At first glance, the correlation seems to be the smallest of the three variables, with Pearson correlation coefficients of 0.06 and 0.3. Moreover, the values for HI_5 , plotted in Figure 5.5a, seem to move inversely to those of $V_{107/95}$ in Figure 5.5b. The range of HI_5 is similar to that of the period dependence, while $V_{107/95}$ has a similar average of 0.7, but its range is slightly smaller than that of the period dependence in Figure 5.3b, going from 0.45 to 0.9. On closer inspection, however, it can be noted that the two peaks in HI_5 occur at approximately $\pi/2$ and $3\pi/2$. At this value, the irradiation starts with the maximum deflection, meaning the first layers are delivered at an anatomy that has the maximum offset found in the signal. Since the spots in the first layers pass through the entire tumour volume and also have the greatest weight, it stands to reason that delivering them with a large offset will have especially detrimental effects on the resulting dose distribution. This effect of special values of the phase offset can also be seen in $V_{107/95}$, albeit inversely. Since any non-zero starting phase offset means the first, heaviest spots are delivered to the wrong location, it is easy to see why a large portion of the dose is delivered inaccurately. Three dips in the pattern can be seen; perhaps unsurprisingly, they occur around values for which $\sin^4(\theta) = 0$: 0 , π and 2π . It could then be noted that for a phase offset which is essentially zero, the HI_5 values are still around 0.25, with $V_{107/95}$ at 0.5, which seem unexpectedly high. However, the amplitude is still 12 [mm] and the period 3.4 [s]. These values are actually consistent with those for a 12 [mm] amplitude in Figure 5.1 and for those at a period of 3.4 [s] in Figure 5.3.

Next, examining the results for repainting, displayed in Figures 5.2, 5.4 and 5.6, it can be noted that repainting in general does its job of counteracting the interplay-induced deterioration of the dose distributions. Specifically, Figure 5.2a shows that HI_5 decreases by about 1/3, to a maximum of 0.2. It is interesting to note that although the results rise more slowly, they do not reach any plateau like in Figure 5.1a. $V_{107/95}$ in Figure 5.1b resembles its counterpart without repainting even more closely. Again, the interplay effect is nullified, in

this case up to an amplitude of 7 [mm], after which a sudden jump is seen, followed by a steady rise for the remainder of the points. Considering HI_5 (Figure 5.4a) and $V_{107/95}$ (Figure 5.3b) for the period graphs, it is again difficult to notice a pattern. One notable feature, however, is that the three small peaks in HI_5 do correspond to outliers in $V_{107/95}$ this time, which may indicate a stronger interplay effect overall. Last, the phase offset shows more rapid variation. Figure 5.6a, showing HI_5 , and Figure 5.6b, showing $V_{107/95}$, show similar behaviour. The number of peaks increases, which seems to confirm that the deposition of the first layers has a large influence on this. These peaks could correspond to values for which at least one repainting passes starts with a sizeable anatomical offset.

5.3.2. Randomised inputs

Next, focussing on the results for the 1000 breathing signals with randomised inputs, calculated for the plan without repainting (Figures 5.7 to 5.9), it can be noted that there seems to be no clear dependence on any of the three input parameters of amplitude, period and starting phase offset. The correlation between amplitude and interplay effect magnitude is entirely obscured by the variance introduced by the period and starting phase offset. It should be pointed out that the results used to generate the three figures are always the same, the only change is in the parameter that is used to sort them along the horizontal direction. Hence, the vertical range is identical for each figure, meaning that examining Figures 5.7a and 5.7b yields all relevant information regarding the general magnitude of the interplay effect. From Figure 5.7a, it can be noted that the average HI_5 is 0.3. For a prescribed dose of 63 [Gy], this is a 19 [Gy] distance between D_5 and D_{95} , nowhere near the steep drop that was seen in the static reference plan DVH of Figure 4.10. The maximum value for HI_5 is significantly worse at 0.7, or a 44 [Gy] distance between D_5 and D_{95} , while the best result is an HI_5 of 0.12, corresponding to a 7.5 [Gy] distance. Similarly poor results are obtained for $V_{107/95}$, with a minimum value of 0.1. The average is 0.7; on average 70% of the CTV would be underdosed or overdosed due to interplay. In some scenarios, $V_{107/95}$ even runs as high as unity, meaning that the entire CTV receives a clinically unacceptable dose. None of these results would be allowed in clinical practise at the WPE. Note that a very poor result for $V_{107/95}$ does not automatically translate to an equally poor value for HI_5 ; as mentioned in Section 4.5, $V_{107/95}$ is very sensitive to small changes if a significant portion of the volume is close to either the 107% or the 95% limits.

Next, the effect of repainting can be investigated. As expected from the single variable analysis, a clear effect is seen in Figures 5.10 to 5.12: both the mean and the standard deviation decrease notably for both metrics. Figure 5.10a shows that for HI_5 , the average falls to 0.1. While this seems as if repainting is doing what it is supposed to, this means there is still a 6 [Gy] difference between D_5 and D_{95} . Even the minimum value of 0.05 is still roughly three times worse than that of the static plan. Looking at $V_{107/95}$ (Figure 5.10b), the results are similarly encouraging. The average also drops, in this case to 0.15, while the maximum drops to 0.7. That is still an unacceptable result, but the number of results worse than 0.5 is small. It is actually outweighed by the number of results smaller than 0.02, which is a common limit for clinical acceptance of a robustness analysis at the WPE.

5.4. Statistical analysis

By their nature, the 1000 randomised signals lend themselves well for a statistical analysis of their results. This is done in three steps:

1. Formulate null hypothesis H_0 to be tested.
2. Estimate underlying distribution of data.
3. Calculate statistical significance and effect size [108].

The null hypothesis that will be evaluated concerns the effect of applying 5x layered repainting on a dose distribution affected by the interplay effect. Specifically: the null hypothesis is that the set of results found when applying repainting is drawn from the same probability distribution as the results found without repainting, with a decision level of 0.05. That is, H_0 will be accepted if the difference in results can be attributed

to chance, meaning it cannot be reliably concluded that repainting affects the dose distribution. It will be rejected if the chance that the repainting results come from the same distribution is smaller than 5%, indicating that repainting does have an effect on the dose distribution.

Next, the underlying dose distribution must be estimated. To do this, the empirical cumulative density functions (CDFs) were plotted. These can be seen in Figure 5.13. They indicate that the results for the plan without repainting come from underlying normal distributions with the means displayed in Table 5.1. To show the similarity, the theoretical CDF for each of these was also plotted in Figure 5.13.

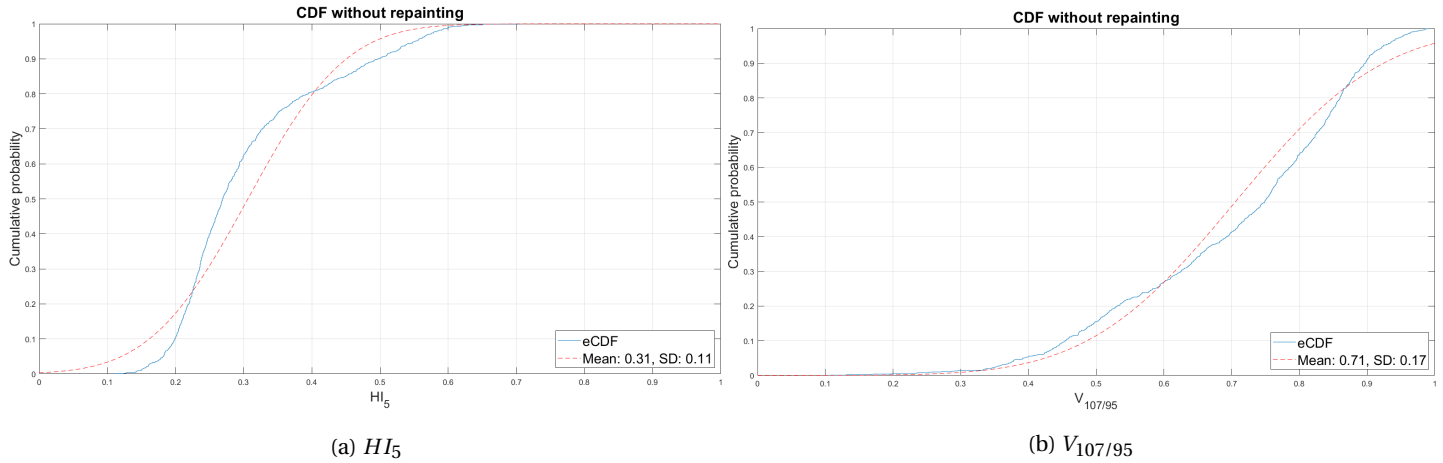


Figure 5.13: CDFs for HI_5 and $V_{107/95}$, indicating underlying normal distributions. The solid blue lines represent the empirical CDFs or eCDFs, with the estimated theoretical CDFs shown by the dashed red lines.

Assuming that the results are indeed normally distributed, a paired T-test can be carried out, comparing the results for both plans. This was done twice, once for HI_5 and once for $V_{107/95}$. The null hypothesis was rejected with $p < 0.0001$ for both metrics. The p-value indicates that it is all but certain that repainting does indeed have an effect on the resulting dose distribution. This effect can be quantified using the 95% confidence interval (CI). This was found to be $[0.1945, 0.2073]$ for HI_5 and $[0.5696, 0.5934]$ for $V_{107/95}$, or, realising that the difference in means from Table 5.1 corresponds to the centre of these intervals, 0.2009 ± 0.0064 for HI_5 and 0.5815 ± 0.0119 for $V_{107/95}$.

Interplay effect with breathing irregularities

This chapter will present the results from the interplay calculations for irregular breathing rhythms. Section 6.1 contains the results of the breathing patterns with baseline drift, Section 6.2 covers the signals with amplitude variation and Section 6.3 displays the results of varying periods. Since each breathing pattern is characterised by at least two variables, the figures shown in this chapter will use a colour map to show the value change of the metric being displayed as a function of the variables. To facilitate interpreting of the results, the range of the colour map has been kept constant for all figures. For each figure, the corresponding value of the metric for the nominal plan has also been included for reference. Once all results are presented, Section 6.4 discusses their significance, before Section 6.5 summarises the results of both the regular and irregular breathing patterns.

6.1. Baseline change

The breathing patterns with changing baseline are characterised by two variables: their equilibrium value at the end of the signal $A_{eq,end}$ and their amplitude A . The equilibrium position at the start of each signal was the reference phase ATN_{26} with a deflection of 26 [mm]. Figure 6.1 shows the results for the plan without repainting. Figure 6.2 shows the results for the plan with 5x layered repainting.

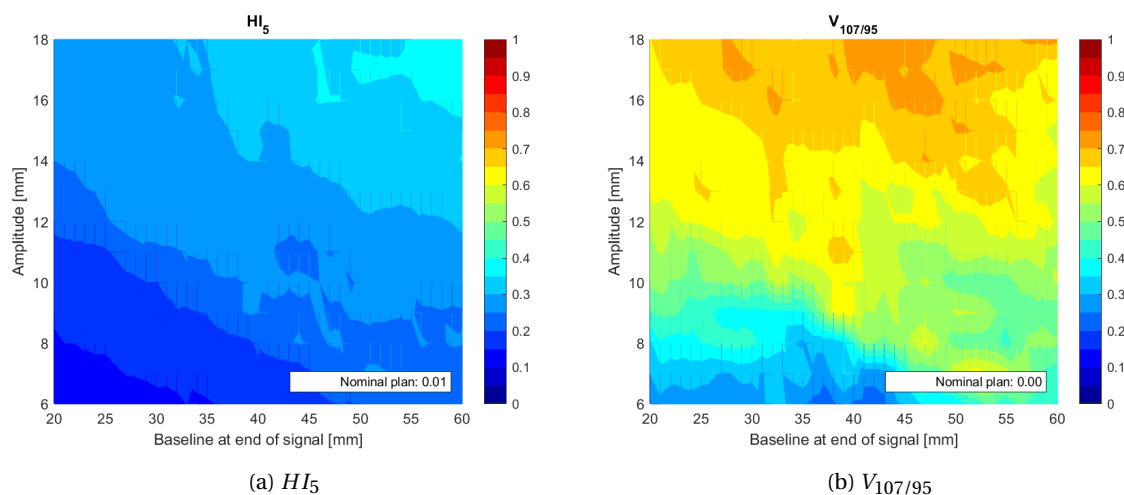


Figure 6.1: The values of HI_5 and $V_{107/95}$ as a function of varying amplitude and baseline drift, calculated for a plan without repainting.

6.2. Amplitude variation

The breathing patterns with varying amplitude are characterised by their amplitude at the start of the signal A_{start} and their amplitude at the end of the signal A_{end} . Figure 6.3 shows the results for the plan without repainting. Figure 6.4 shows the results for the plan with 5x layered repainting.

6.3. Period variation

The period variation signals have three variables: amplitude A , period at the start of the signal T_{start} and period at the end of the signal T_{end} . The results were obtained for amplitudes ranging from 8 to 16 [mm] in 2 [mm] increments; only the two extremes are shown here, with the additional plots added to the repository

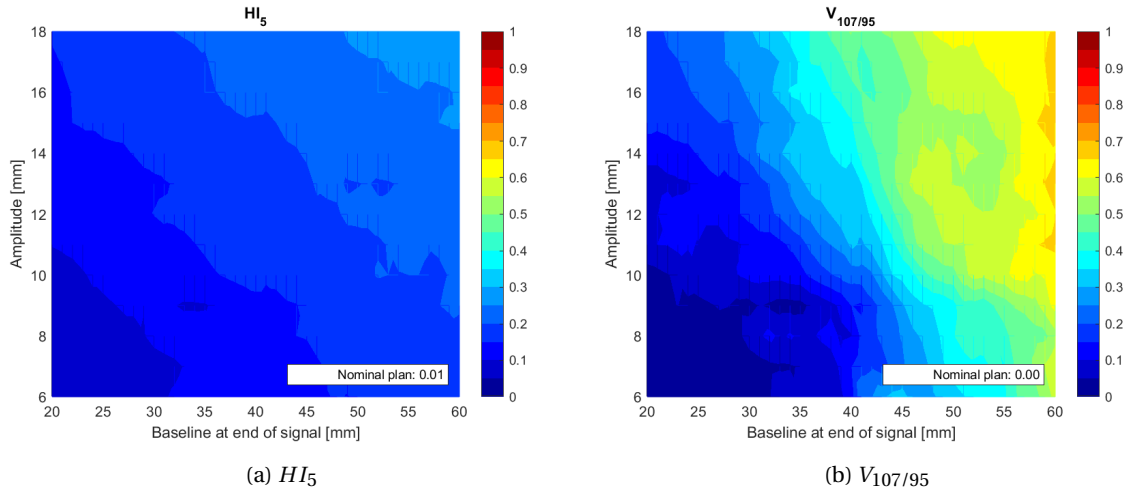


Figure 6.2: The values of HI_5 and $V_{107/95}$ as a function of varying amplitude and baseline drift, calculated for a plan with five times layered repainting.

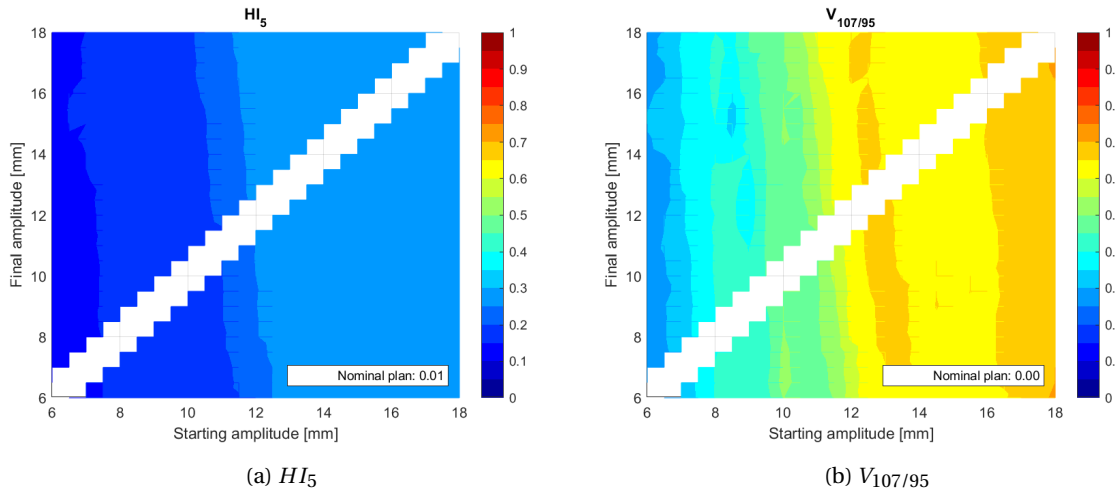


Figure 6.3: The values of HI_5 and $V_{107/95}$ as a function of increasing or decreasing amplitude, calculated for a plan without repainting.

[89]. Figure 6.5 shows the results for the plan without repainting, for a breathing amplitude of 8 [mm]. Figure 6.6 shows the results for the plan without repainting, for a breathing amplitude of 16 [mm]. Figure 6.7 shows the results for the plan with 5x layered repainting, for a breathing amplitude of 8 [mm]. Figure 6.8 shows the results for the plan with 5x layered repainting, for a breathing amplitude of 16 [mm].

6.4. Discussion of results

Looking at Figure 6.1, HI_5 seems more structured than $V_{107/95}$, but in both cases, the amplitude variation seems more influential than the baseline shift. Only for large shifts and comparatively small amplitudes does $V_{107/95}$ show some clear dependency on the magnitude of the drift. However, without repainting, irradiation times are half a minute, while the total time signal is 100 [s]. Therefore, the baseline drift will hardly be relevant for small and medium drift values. For example, if the baseline drifts from phase ATN_26 to ATN_40 in 100 [s], only 1/3 of this change, or 5 [mm], will have been realised by the end of the irradiation. This change is smaller than all the investigated amplitudes, so it should come as no surprise that the amplitude has a greater effect than the baseline change.

Figure 6.2 shows that when 5x layered repainting is applied, there is even less cause for concern. Even $V_{107/95}$ in Figure 6.2b shows relatively good behaviour. However, here the overall result does seem to depend more

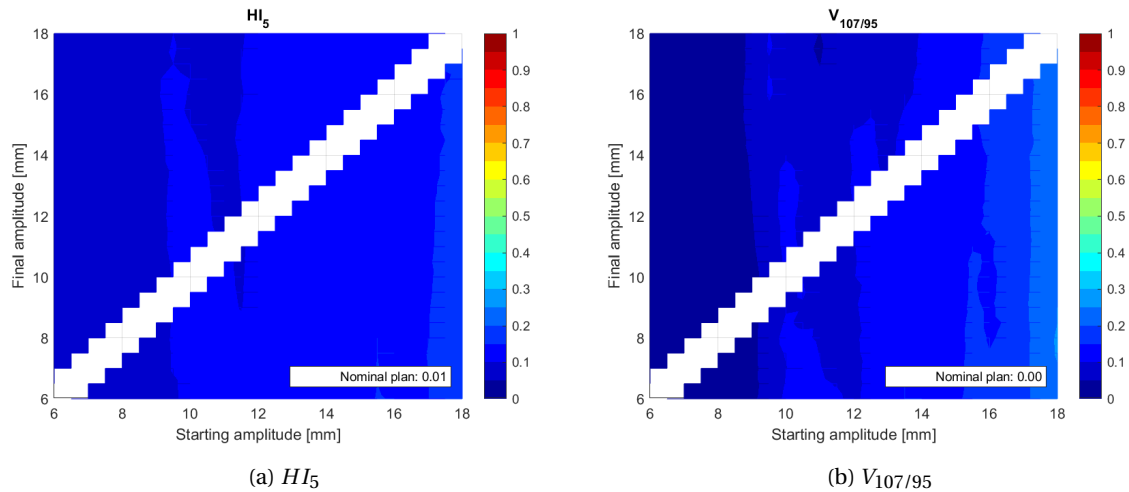


Figure 6.4: The values of HI_5 and $V_{107/95}$ as a function of increasing or decreasing amplitude, calculated for a plan with five times layered repainting.

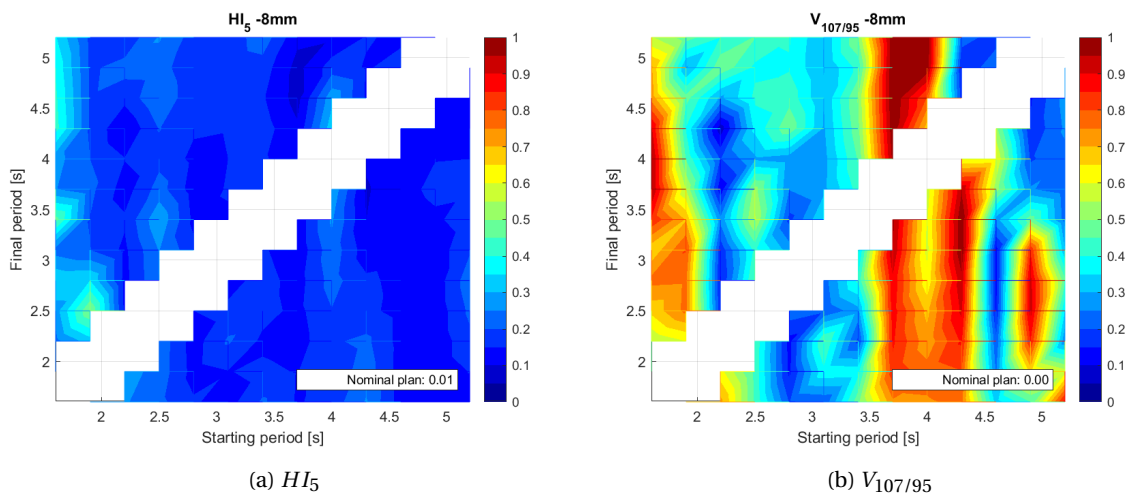


Figure 6.5: The values of HI_5 and $V_{107/95}$ as a function of varying period length, for an amplitude of 8 [mm], calculated for a plan without repainting.

strongly on the baseline drift. This is not too surprising; the concept behind repainting is that it diminishes interplay by giving the beam several chances to irradiate a spot accurately, effectively averaging the irradiated location. However, baseline drift causes the inaccuracy to only grow larger with time, meaning that the longer the beam is on, the larger the offset between reference phase and actual anatomy becomes, and thus the less accurately spots are delivered. Note, however, that the argument could be made that a significant part of the figures contains such large shifts that it is unlikely these will be seen in the span of 100 [s].

The results for amplitude variation, shown in Figure 6.3, are very consistent and clear across both metrics and the full range of starting and ending amplitudes. The only parameter that influences the outcome here, is the starting amplitude. The logic behind this pattern is easy to discern; since the end amplitude is only reached after 100 [s] and the irradiation lasts for roughly 1/3 of that time, the change in amplitude that the beam perceives in the time it is on is much smaller. As has been common throughout the results discussed so far, HI_5 shows a smaller absolute value than $V_{107/95}$. Repainting (Figure 6.4) takes about twice as long, so it would be reasonable to find more effect of the amplitude at the end of the signal here. However, both HI_5 and $V_{107/95}$ are so effectively minimised by the repainting, that the opposite is true. Comparing Figure 6.4 to Figure 6.2, it actually appears that repainting is particularly effective in nullifying the effect of amplitude, regardless of how large it is, but it seems a relatively ineffective strategy against large baseline shifts.

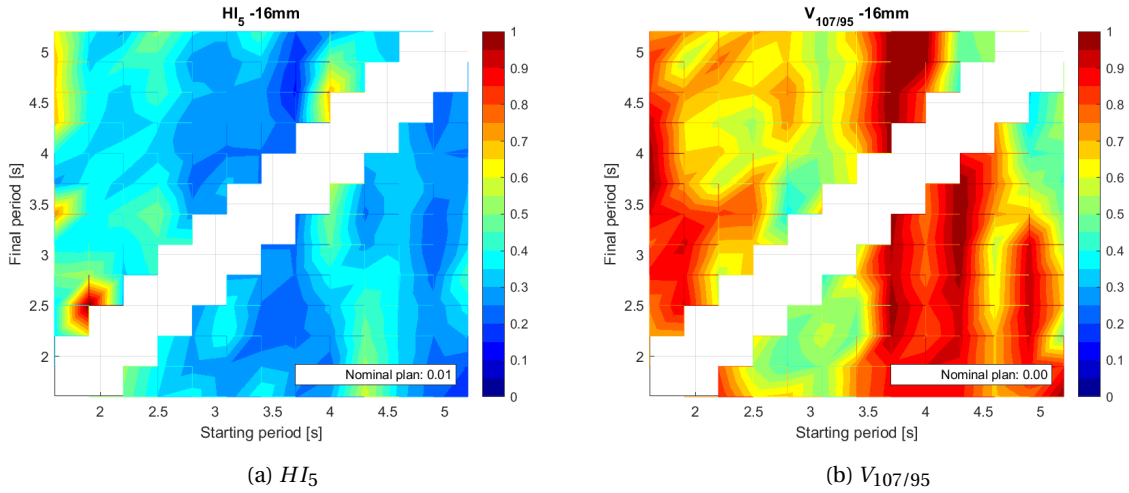


Figure 6.6: The values of HI_5 and $V_{107/95}$ as a function of varying period length, for an amplitude of 16 [mm], calculated for a plan without repainting.

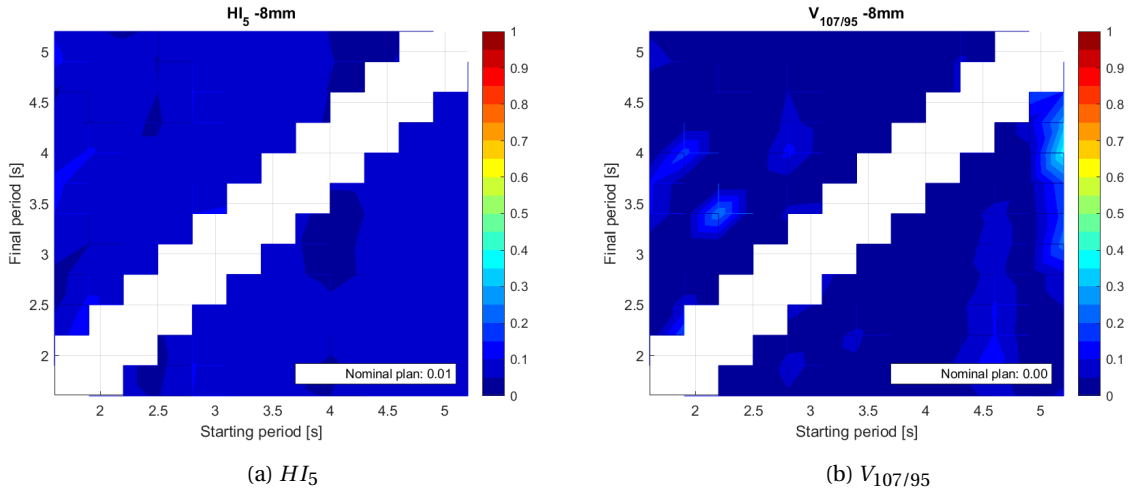


Figure 6.7: The values of HI_5 and $V_{107/95}$ as a function of varying period length, for a peak-to-peak amplitude of 8 [mm], calculated for a plan with five times layered repainting.

Last, the relatively chaotic behaviour of period dependence is shown very clearly yet again in both Figure 6.5 and Figure 6.6. However, as large as the variation in both figures is, it again appears to be largely dominated by the starting value. Similar to the first two types of irregularities, this is to be expected due to the relatively short irradiation time. Figure 6.5b indicates some synchronisation between beam and tumour motion for certain ranges of the starting period. This is similar to the conclusions drawn from Figure 5.3b, and the range of values for which the effect occurs most strongly is also the same - up to 2 [s] and from approximately 3.5 to 4.5 [s]. This effect is most strongly noticeable in $V_{107/95}$, but the corresponding results for HI_5 in Figures 6.5a and 6.6a do show some increase in inhomogeneity for both period ranges.

Once again, repainting has a very strong mitigating effect on the overall magnitude of the effect, significantly reducing both average magnitude and range of the interplay effect in Figures 6.7a and 6.8a. Increasing the amplitude still has the expected effect though; recalling Figure 5.2, the interplay effect was nearly completely cancelled out for an amplitude of 8 [mm], but for 16 [mm] only a partial reduction of the effect could be observed.

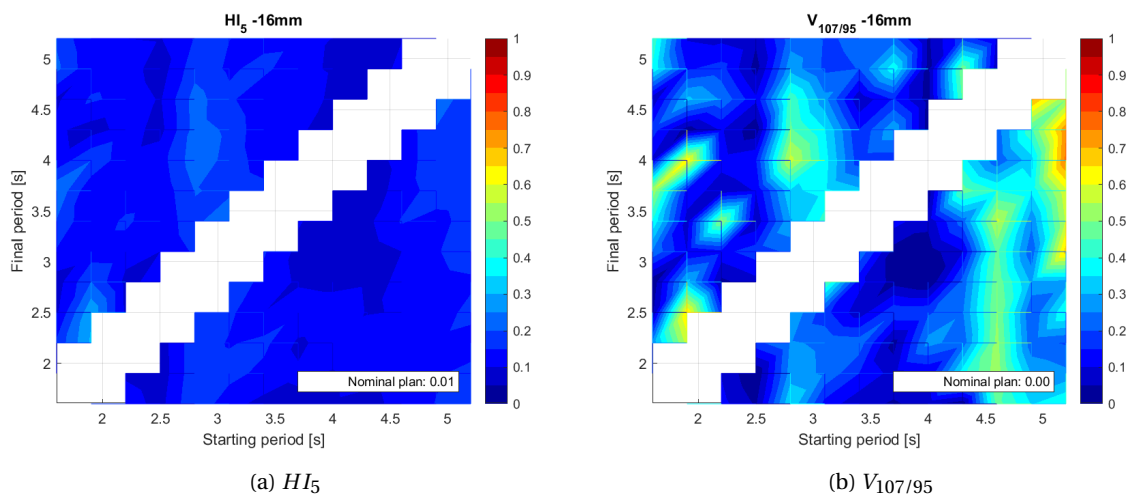


Figure 6.8: The values of HI_5 and $V_{107/95}$ as a function of varying period length, for a peak-to-peak amplitude of 16 [mm], calculated for a plan with five times layered repainting.

6.5. Summary of results

Since the irregular breathing patterns were generated systematically rather than randomly, no statistical analysis was carried out. However, their results also show a clear effect of repainting in reducing dose inhomogeneities and under-/overdosed volume fraction. Table 6.1 shows the mean of each metric for the full range of breathing patterns and for both plans. It also shows by which percentage repainting decreases the original effect. It should be noted that no allowances have been made for extreme cases in the irregular patterns; they are included and weighted the same as more realistic breathing patterns.

	Regular		Amplitude variation		Baseline shift		Period variation	
	HI_5	$V_{107/95}$	HI_5	$V_{107/95}$	HI_5	$V_{107/95}$	HI_5	$V_{107/95}$
No repainting	0.31	0.71	0.22	0.54	0.26	0.56	0.28	0.64
5x repainting	0.11	0.12	0.11	0.10	0.17	0.33	0.11	0.16
Difference [%]	-65.6	-82.5	-50.44	-81.8	-34.6	-41.2	-62.1	-75.0

Table 6.1: Average value of HI_5 and $V_{107/95}$ for the different breathing patterns. Both the results for the plan with and that without repainting are shown, as well as the reduction caused by repainting in percentages.

Conclusions

Now that all results have been processed, conclusions can be drawn. This will be done in Section 7.1, based on the research questions stated in Chapter 2. A comparison with the outcome of other related research is made in Section 7.2. Finally, recommendations for follow-up research are made in Section 7.3.

7.1. Evaluation of research questions

It is now time to look back on the research questions posed in Section 2.3. They will be discussed one by one.

What is the magnitude of the interplay effect for regular breathing? The interplay effect has a wide range of magnitudes. However, it is virtually always non-zero for breathing amplitudes greater than 6 [mm]. It has been shown that the homogeneity HI_5 of the dose is severely deprecated by interplay and that significant portions of the CTV can be dosed outside of clinically acceptable limits, both by under- and by overdosing. Results show that on average, 70% of the target volume will not receive a dose between 95% and 107% of the prescribed dose ($V_{107/95}$), while in some scenarios, this even extended to the entire CTV. The mean minimum and maximum dose were found to be more than 25% off from the prescribed dose.

Which parameters of a regular breathing pattern have the largest impact on the magnitude of the interplay effect? Three parameters were investigated: the amplitude, period and starting phase offset of the signal. The magnitude of the interplay effect on both dose homogeneity and the fraction of over-/underdosed volume is strongly correlated with the amplitude of the motion; the Pearson correlation coefficient is greater than 0.95 for both metrics. The interplay effect does not appear to be correlated with the period. However, some outliers were found that indicate that at certain values of the period, some synchronisation with the beam motion may occur. This will likely depend on machine characteristics and the plan itself, potentially making these outliers highly unpredictable. Varying the period did give a large variation in the results, indicating that a significant part of the variance of the interplay effect can be attributed to variations in period. Variance caused by varying the starting phase offset was of a similar magnitude, but more predictable. This parameter behaved roughly periodically, with peaks in dose inhomogeneity when the breathing signal started at maximum deflection. The phase offset at the start of irradiation is very important; implementing some type of gating at least for the starting point of irradiation could contribute to significantly limiting the magnitude of the interplay effect.

Which parameters should be varied over the duration of a breathing pattern to obtain realistic irregular breathing patterns? Most interest in literature goes towards baseline shifts and amplitude variation. These were duly investigated. For a systematic approach, variation in the period was also investigated. For both baseline shifts and period variation, signals were generated for a variety of different but constant amplitudes. All parameters were varied linearly.

What is the magnitude of the interplay effect when considering irregular breathing patterns? Irregularities seem to have little effect. For both metrics and for each type of irregular signal, the mean values found were smaller than the mean effect found for regular breathing. No representative population of signals was generated, however, so this result was not verified statistically. The smallest change is found in the signals with varying period. However, period was found to have a very unpredictable effect on the magnitude of the interplay effect. In all, no statistically significant conclusions can be drawn regarding the significance of breathing irregularities; randomised research would be needed before any such conclusions could be reached.

What is the magnitude of the interplay effect when applying clinical standards for mitigation of motion effects? Standard margins were applied. These were kept constant throughout the project, so no conclusion regarding their effectiveness can be drawn. Repainting works well against all types of breathing, dampening the interplay effect significantly for each of the investigated signal groups. It achieved improvements of more than 50% in HI_5 and 75% in $V_{107/95}$ for regular breathing and for signals with varying amplitude or period. It was found to be less effective against baseline shifts, but still achieved a one-third improvement in HI_5 and more than 40% improvement in $V_{107/95}$.

7.2. Comparison to other work

The outcomes of this work echo that of some other publications. There is some discussion regarding the accuracy of surrogates for modelling breathing motion of the tumour. For example, Petterson et al. found there is an intrafractional change in the relationship between tumour and external marker [47]. This is corroborated by the correlation shown in Figure 3.2, which indicates a linear relationship, but only for part of the breathing range. The topic was also discussed at the 4D treatment planning workshops in 2016 and 2017 [109]. Lambert et al. found that motion greater than 10 [mm] can cause 100% of the volume to receive a dose outside of the clinical limits of 95% and 107% [110], a result that was supported by unity values for $V_{107/95}$ that were found for some breathing patterns in this work. Pan et al. similarly found large deterioration of the dose under the interplay effect, using gamma pass rates as metric [111]. Poulsen et al. concluded that repainting can significantly improve the result, but similar to the repainting results presented here, still found a considerable fraction of the target volume to receive unacceptable dose levels [50]. This fits well with the earlier conclusion from Zenklusen et al. to implement repainting in conjunction with gating at the Paul Scherrer Institute to reduce required margins and improve overall results [52]. Interplay also introduces some limitations to the general planning process, leading Krieger et al. to recommend that variability in breathing be accounted for in planning [81], [112]. This is in line with earlier work by Liu et al., who recommend the use of 4D robust optimisation when planning for targets suffering from interplay [113].

If the interplay effect can on average cause underdosage of a target volume, a logical question would be where the remaining dose is absorbed. The most logical answer is in the surrounding tissue, meaning that along with a decrease in the probability of tumour control, the probability of adverse effects in the surrounding healthy tissue increases, as confirmed in [112]. This would undermine the main advantage of proton therapy, and as such must be thoroughly investigated to justify the use of protons in breathing motion-impacted locations. Changes in the dose to nearby OARs were not evaluated as part of this work. This is perhaps the first aspect of this work that should be properly investigated in any future research based on this work. The conformity number used in the work of Lee et al. could be calculated, for example [42]. A last note concerns the 4D data sets themselves. Zhang et al. highlighted the importance of temporal resolution for accurate breathing modelling, which is why this work was carried out with a very large number of CT phases [114]. That introduces other uncertainties, however, as image registration algorithms are not always reliable. This was seen in Section 3.2, and is confirmed by other works [71], [109].

7.3. Recommendations for future research

While many different breathing patterns were investigated in this project, there is still a large number of variables that were not considered. Some recommendations for follow-up studies will be presented here. Furthermore, important aspects of the work will be assessed critically, to identify potential sources of error or inaccuracies.

7.3.1. Testing assumptions

In order to ratify the conclusions and results, it is important that the assumptions are challenged, since incorrect assumptions can adversely impact the reliability and accuracy of the obtained data. Therefore, ways to challenge each of the assumptions will be considered. To start, it is important to use reliable tools. This refers to tools that are not developed in the course of the research. In this case, that includes the XCAT that was used

to model the anatomy, the RayStation (RS) software that was used for calculating transformations between phases and for planning, and the algorithm built into RS that was used to calculate the dose distributions.

As discussed in Section 4.6, there is a variety of settings that can be tweaked to vary the result of the deformation fields generated by RS to transform doses from one CT phase to another. For the purposes of this research, only the reliability of the transformation of the liver was verified. If other parts of the anatomy play a role, especially if a larger portion of the body is considered, the deformation fields must be closely monitored for their accuracy, and it is important to verify transformations for a larger and varied set of contours. Of course, a perfect transformation field exists for the XCAT phantom and other hybrid or fully mathematical phantoms, by reverse-engineering the equations that create and deform the anatomy in the first place. However, this would require access to the source code of proprietary software. Therefore, the most efficient route is likely still to take a heuristic approach and compare each set based on some objective measures that fit the research goal, or to set a pre-defined threshold for the desired accuracy. There is little point in spending a long time calculating an extremely accurate deformation field if other factors, such as imaging resolution or time resolution of the 4DCT, induce uncertainties that wipe out the gain in accuracy.

The full range of 50 [mm] of the XCAT phantom used here was based on patient breathing data, but this range covered breathing signals of more than an hour in length [115]. A structural way to investigate this could for example be the obtaining of breathing patterns for a patient over a complete fractionated treatment and examining this data for relevant parameters such as mean, maximum and minimum values of amplitude and period, as was done in [116]. An XCAT could then be created based on this patient's anatomy and breathing patterns. It is safe to assume that the required breathing amplitude range will be smaller than 50 [mm], leading to a more reliable rendering of the phantom. A drawback for this would be that this requires another assumption, namely that an external surrogate such as chest wall motion accurately represents tumour motion. However, the literature is conflicted about this and the only way to be sure would be to measure tumour motion directly [47], [97], [117]. Excluding options that require significant patient dose such as CT, the most viable modality for this would be MRI [106].

The value of careful consideration of the anatomical difference between patient breathing and modelled breathing was already discussed. However, there is another limit to the generated breathing patterns here, and that is the limited number of parameters that was varied simultaneously. Patient breathing signals have continuous baseline shifts and continuously changing periods and amplitudes, sometimes increasing and decreasing again within a relatively short time frame. This kind of real-life complexity and stacking of effects is very challenging to model, but it must be modelled accurately if the result is to be accurate. Therefore, it is recommended that at least a comparison with patient data is made to quantify the accuracy of the breathing model. Using the breathing signal of a patient similar to the planning anatomy would be even better, while of course a large volume of breathing data and a tailor-made phantom of a single patient would be the optimal setup. However, it should be noted that the discrete variation of irregularities allows for examining which type of irregularities are worth the most concern. This is similar to how the single parameter evaluation showed that the large spread of the results of the 1000 randomised signals was mostly due to the effect of period and starting phase variation, with a limited contribution of the amplitude to the overall magnitude of the interplay effect.

Another type of irregularity that might be of interest is random, short spikes in the breathing amplitude. Such spikes could be caused by coughing, for example. Breathing signals were actually generated to investigate this type of breathing irregularity, but were eventually disregarded due to time constraints on the work. Generating additional data was deemed of lower importance than accurate analysis and reporting on the already gathered data. However, especially frequent coughing such as in a patient with a cold or other illness, or perhaps patients suffering from side-effects of their treatment, could still yield notable offsets. The effect might be most notable if this occurs in the first few layers, since that boils down once again to the importance of notable anatomical offsets in the irradiation of the most heavily weighted spots.

7.3.2. Increasing generality

A wide variety of breathing patterns has been evaluated in this work. However, that is the only aspect of which a wide range of different possibilities have been considered. Many parameters were disregarded or

fixed, and in order to draw more definitive conclusions about the importance of accounting for breathing irregularities, their full range must also be considered. The set of parameters to vary can be roughly split in patient parameters and tumour parameters.

The current research focused on a healthy adult male phantom. The XCAT provides the flexibility to investigate female anatomies as well as male. This would not be immediately relevant for liver tumours, as the only notable difference in thoracic anatomy between genders is the amount of breast tissue. As the breast is not in the beam path anyway, the difference is negligible in this instance. However, for lung tumours and more inferior abdominal organs, the differences in anatomy are certainly worth exploring.

A more influential patient characteristic would be the age. Children and even babies might have smaller motion ranges, but the OARs are also closer together, incurring a greater penalty for any dose inaccuracies. Long-term effects are also of greater concern for this group. A potentially relevant difference would for example be the effect of bone density, which generally varies with age and can have significant influence on the penetration depth of a beam [118]. The investigation of the influences of gender and age should not be limited to the anatomical changes they cause, their influence on breathing patterns also needs to be considered [119], [120]. The effects of body type could also be investigated, for example varying anatomy based on a metric such as the Body Mass Index (BMI).

So far, only one tumour has been investigated. While a liver tumour is certainly a fairly representative case for interplay-affected tumours, there are many other organs that suffer from interplay. Most notably the lungs, but pancreatic, kidney and prostate tumours also suffer from breathing motion-induced degradation of the dose distribution [27], [29], [106]. Moreover, liver tumours are usually close to spherical, which means that the most distal layers pass through the entire tumour and their build-up dose is likely to be deposited within the target volume, even if this does not happen exactly where it was planned to. However, other tumour shapes may see not just the Bragg peak, but also the build-up dose deposited in healthy tissue.

Tumour size must also be considered. The 5 [cm] diameter here is a realistic value for hepatocellular carcinoma, but the range of the size for these kinds of tumours is quite large. Size can also affect the size of the interplay effect [121]. This stands to reason as larger tumours will have more and larger layers, leading to longer irradiation times, which in turn gives the interplay effect more time to affect the resulting dose distribution. Longer irradiation would also give irregularities a bigger window to affect the magnitude of the dose degradation, so it certainly seems worthwhile to investigate the effect of varying tumour size.

Other organs and their tumours may also move in different primary directions, or at the very least the beams would be coming in from different angles, so the perceived motion from a beam's eye view (BEV) would be different. Since the scanning pattern is usually primarily horizontal, scanning a full row of spots before moving vertically to the next row, an organ seeing lateral motion from a BEV perspective could potentially see a very different interplay effect from one experiencing primarily vertical motion, although literature on the topic is inconclusive [90].

7.3.3. Further recommendations

Once the effect of breathing irregularities has been adequately robustly quantified, the next question is how to minimise these effects. A starting point could be to investigate a variety of different repainting strategies. The available framework at the WPE already allows for this, being able to consider a varying number of repainting passes of the beam as well as the two main time-structures: volumetric and layered repainting. In this work, only 5x layered repainting was considered, while the effect of lengthening treatment times was discussed, which is a side-effect of the application of repainting. For volumetric repainting, this effect is even stronger than for layered repainting. Changing the number of repainting passes would affect the spot weights, thereby varying the time structure of the beam. It is evident that this could have an influence on the magnitude of the interplay effect. There exists an optimum strategy for any given plan, and while this optimal solution would vary for every single plan, perhaps some general guidelines can be established based on motion range, tumour size and location and some other basic parameters of the problem [50], [52].

Of course, repainting is not the only motion mitigation strategy available, as discussed previously in Section 2.2. Each method in isolation has been investigated already, but a relatively unexplored field is the po-

tential of combinations of various techniques. For example, it stands to reason that while neither training patients to control their breathing in a relatively shallow range, nor repainting on its own will completely eradicate the interplay effect, in combination the methods may have the potential to keep the dose inhomogeneities within the clinical limits of 95% and 107%. Similarly, gating in conjunction with repainting would lengthen irradiation considerably, but if this significantly limits the motion range that must be accounted for, it is again conceivable that clinical dose limits could be met even with interplay. An example of the effectiveness of combining motion mitigation techniques is shown in Figure 7.1 [122], [123].

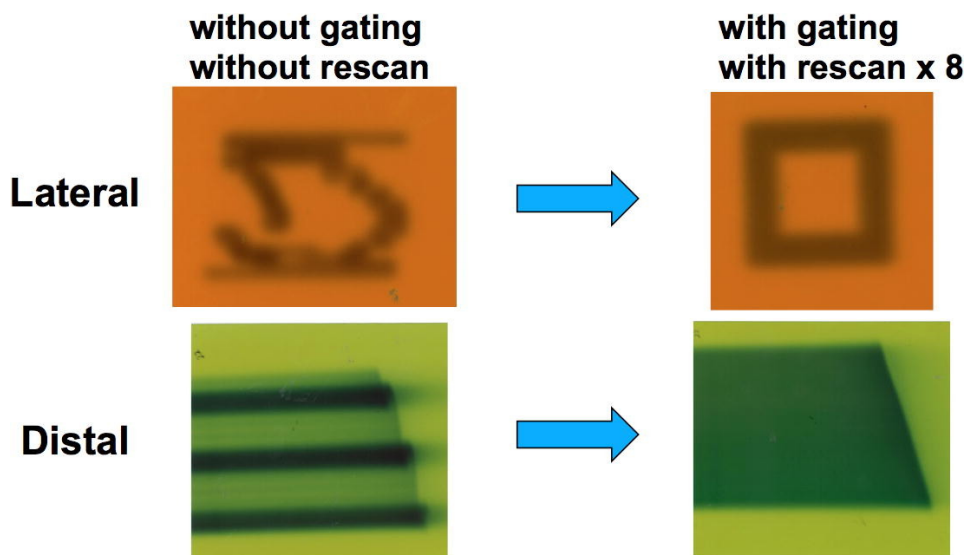


Figure 7.1: Motion mitigation techniques in carbon ion therapy. The two images on the left show the dose distribution of a scanned carbon ion beam if motion is present and left unaccounted for. The images on the right show the same beam and motion, but now irradiated with fast rescanning and gating applied to mitigate the motion effects. The lateral image shows that rescanning and gating help irradiate a target structure more accurately, while the distal image shows that the dose in a layer is distributed more uniformly than without applying motion mitigation techniques. Source: [122]

The last recommendation concerns the irradiation with heavier particles. As shown in Figure 1.3, these are known to have a sharper Bragg peak. This means they are even more susceptible to both the range and spot location uncertainties caused by the interplay effect. Since the sharper Bragg peak requires energy layers to be spaced closer together, resulting in an increased number of layers and spots, irradiation times also typically increase. Combining these considerations, it is easy to see how heavy ion plans might not only be susceptible to regular interplay, but also be affected even more than proton plans by the impact of irregularities in the breathing pattern driving the motion [124], [125].

Bibliography

- [1] Freddie Bray, Jacques Ferlay, Isabelle Soerjomataram, et al. "Global cancer statistics 2018: GLOBOCAN estimates of incidence and mortality worldwide for 36 cancers in 185 countries". In: *CA: A Cancer Journal for Clinicians* 68.6 (2018), pp. 394–424. DOI: 10.3322/caac.21492.
- [2] World Health Organization. *Cancer*. URL: <https://www.who.int/news-room/fact-sheets/detail/cancer> (visited on 03/06/2020).
- [3] Cancer Research UK. *Worldwide cancer incidence statistics | Cancer Research UK*. URL: <https://www.cancerresearchuk.org/health-professional/cancer-statistics/worldwide-cancer-incidence> (visited on 03/06/2020).
- [4] C.P. Wild, E Weiderpass, and B.W. Stewart. *World Cancer Report: Cancer Research for Cancer Prevention*. Tech. rep. Lyon, France: International Agency for Research on Cancer, 2020. URL: <http://publications.iarc.fr/586>.
- [5] World Health Organization. *Cancer*. URL: <https://www.who.int/cancer/prevention/en/> (visited on 03/21/2020).
- [6] National Cancer Institute. *Cancer Causes and Prevention*. URL: <https://www.cancer.gov/about-cancer/causes-prevention> (visited on 03/21/2020).
- [7] Our World in Data. *Cancer*. URL: <https://ourworldindata.org/cancer%7B%5C%7Dall-charts-preview> (visited on 05/08/2020).
- [8] H Lodish, A Berk, SL Zipursky, et al. *Molecular Cell Biology*. 4th ed. New York: W. H. Freeman, 2000. Chap. 8.1. URL: <https://www.ncbi.nlm.nih.gov/books/NBK21578/>.
- [9] Cancer Treatment Centers of America. *What's the difference? Benign and malignant tumors | CTCA*. URL: <https://www.cancercenter.com/community/blog/2017/12/whats-the-difference-benign-and-malignant-tumors> (visited on 03/22/2020).
- [10] Shahzina Kanwal, Yann Fardini, Patrick Pagesy, et al. "O-GlcNAcylation-Inducing Treatments Inhibit Estrogen Receptor α Expression and Confer Resistance to 4-OH-Tamoxifen in Human Breast Cancer-Derived MCF-7 Cells". In: *PLOS ONE* 8.7 (July 2013). DOI: 10.1371/journal.pone.0069150.
- [11] National Cancer Institute. *Types of Cancer Treatment*. URL: <https://www.cancer.gov/about-cancer/treatment/types> (visited on 03/24/2020).
- [12] Abigail T. Berman and Jordan Kharofa. *Introduction to Radiation Oncology*. 2014. URL: https://www.astro.org/uploadedfiles/affiliates/arro/future_residents/introtoro.pdf.
- [13] SR Mehta, V Suhag, M Semwal, et al. "Radiotherapy: Basic Concepts and Recent Advances". In: *Medical Journal Armed Forces India* 66.2 (2010), pp. 158–162. DOI: 10.1016/S0377-1237(10)80132-7.
- [14] Sevnaz Nourollahi and Archis Ghate. "Optimal modality selection in external beam radiotherapy". In: *Mathematical Medicine and Biology: A Journal of the IMA* 36 (2019), pp. 361–380. DOI: 10.1093/imammb/dqy013.
- [15] Elaine M Zeman, Eric C. Schreiber, and Joel E. Tepper. "Basics of Radiation Therapy". In: *Abeloff's Clinical Oncology*. Ed. by John E. Niederhuber, James O. Armitage, Michael B. Kastan, et al. 6th ed. Elsevier, 2020. Chap. 27, pp. 431–460. ISBN: 978-0-323-47674-4. DOI: 10.1016/B978-0-323-47674-4.00027-X.
- [16] Jack F Fowler. "Brief summary of radiobiological principles in fractionated radiotherapy". In: *Seminars in Radiation Oncology* 2.1 (1992), pp. 16–21. DOI: 10.1016/S1053-4296(05)80045-1.
- [17] A Kaiser, J G Eley, N E Onyeuku, et al. "Proton Therapy Delivery and Its Clinical Application in Select Solid Tumor Malignancies". In: *Journal of Visualized Experiments* 144 (2019), e58372. DOI: 10.3791/58372.

- [18] Radiology Oncology Systems. *Linear Accelerators with Photon Energies*. URL: www.oncologysystems.com/resources/linear-accelerator-guides/photon-energies (visited on 03/27/2020).
- [19] Seo Hyun Park and Jin Oh Kang. "Basics of particle therapy I: physics". In: *Radiation Oncology Journal* 29.3 (2011), pp. 135–146. DOI: 10.3857/roj.2011.29.3.135.
- [20] Z Francis, E Seif, S Incerti, et al. "Carbon ion fragmentation effects on the nanometric level behind the Bragg peak depth". In: *Physics in Medicine and Biology* 59.24 (2014), pp. 7691–7702. DOI: 10.1088/0031-9155/59/24/7691.
- [21] Arnold Pompos, Marco Durante, and Hak Choy. "Heavy ions in cancer therapy". In: *JAMA Oncology* 2.12 (2016), pp. 1539–1540. DOI: 10.1001/jamaoncol.2016.2646.
- [22] Harald Paganetti. *Proton Therapy Physics*. Boca Raton, FL: CRC Press, 2012. ISBN: 9781439836453.
- [23] Harald Paganetti. *Proton beam therapy*. IOP Publishing Ltd, 2017. ISBN: 9780750313704. DOI: 10.1088/978-0-7503-1370-4.
- [24] David Jette and Weimin Chen. "Creating a spread-out Bragg peak in proton beams". In: *Physics in Medicine and Biology* 56.11 (2011), N131–N138. DOI: 10.1088/0031-9155/56/11/n01.
- [25] Hsiao-Ming Lu and Hanne Kooy. "Optimization of current modulation function for proton spread-out Bragg peak fields". In: *Medical Physics* 33.5 (2006), pp. 1281–1287. DOI: 10.1118/1.2188072.
- [26] M Krämer and M Durante. "Ion beam transport calculations and treatment plans in particle therapy". In: *European Physical Journal D* 60 (2010), pp. 195–202. DOI: 10.1140/epjd/e2010-00077-8.
- [27] K. M. Langen and D. T.L. Jones. "Organ motion and its management". In: *International Journal of Radiation Oncology Biology Physics* 50.1 (2001), pp. 265–278. DOI: 10.1016/S0360-3016(01)01453-5.
- [28] D. A. Jaffray, D. Yah, and J. W. Wong. "Managing geometric uncertainty in conformal intensity modulated radiation therapy". In: *Seminars in Radiation Oncology* 9.1 (1999), pp. 4–19. DOI: 10.1016/S1053-4296(99)80051-4.
- [29] Zhouguang Hui, Xiaodong Zhang, George Starkschall, et al. "Effects of interfractional motion and anatomic changes on proton therapy dose distribution in lung cancer". In: *International Journal of Radiation Oncology Biology Physics* 72.5 (2008), pp. 1385–1395. DOI: 10.1016/j.ijrobp.2008.03.007.
- [30] Heming Lu, Hui Lin, Guosheng Feng, et al. "Interfractional and intrafractional errors assessed by daily cone-beam computed tomography in nasopharyngeal carcinoma treated with intensity-modulated radiation therapy: a prospective study". In: *Journal of Radiation Research* 53 (2012), pp. 954–960. DOI: 10.1093/jrr/rrs041.
- [31] Feng Xu, Jin Wang, Sen Bai, et al. "Interfractional and intrafractional setup errors in radiotherapy for tumors analyzed by cone-beam computed tomography". In: *Chinese Journal of Cancer* 27.10 (2008), pp. 372–376.
- [32] Cynthia S. Ross, David H. Hussey, Edward C. Pennington, et al. "Analysis of movement of intrathoracic neoplasms using ultrafast computerized tomography". In: *International Journal of Radiation Oncology Biology Physics* 18.3 (1990), pp. 67–677. DOI: 10.1016/0360-3016(90)90076-V.
- [33] H Paganetti, H Jiang, and A Trofimov. "4D Monte Carlo simulation of proton beam scanning: modelling of variations in time and space to study the interplay between scanning pattern and time-dependent patient geometry". In: *Physics in Medicine and Biology* 50 (2005), pp. 983–990. DOI: 10.1088/0031-9155/50/5/020.
- [34] Christoph Bert, Sven O. Grözinger, and Eike Rietzel. "Quantification of interplay effects of scanned particle beams and moving targets". In: *Physics in Medicine and Biology* 53.9 (2008), pp. 2253–2265. DOI: 10.1088/0031-9155/53/9/003.
- [35] Joao Seco, Daniel Robertson, Alexei Trofimov, et al. "Breathing interplay effects during proton beam scanning: simulation and statistical analysis". In: *Physics in Medicine and Biology* 54 (2009), p. 294. DOI: 10.1088/0031-9155/54/14/N01.
- [36] Clemens Grassberger, Stephen Dowdell, Antony Lomax, et al. "Motion interplay as a function of patient parameters and spot size in spot scanning proton therapy for lung cancer". In: *International Journal of Radiation Oncology Biology Physics* 86.2 (2013), pp. 380–386. DOI: 10.1016/j.ijrobp.2013.01.024.

- [37] Ye Zhang, Isabel Huth, Martin Wegner, et al. "An evaluation of rescanning technique for liver tumour treatments using a commercial PBS proton therapy system". In: *Radiotherapy and Oncology* 121.2 (2016), pp. 281–287. DOI: 10.1016/J.RADONC.2016.09.011.
- [38] Tina Pfeiler. "Dynamic evaluation of 4D robust optimisation for motion management in scanned proton therapy of hepatocellular carcinoma". PhD Thesis. Technische Universität Dortmund, 2018, p. 13.
- [39] Yune Kwong, Alexandra Olimpia Mel, Greg Wheeler, et al. "Four-dimensional computed tomography (4DCT): A review of the current status and applications". In: *Journal of Medical Imaging and Radiation Oncology* 59.5 (2015), pp. 545–554. DOI: 10.1111/1754-9485.12326.
- [40] Christian Heinz, Michael Reiner, Claus Belka, et al. "Technical evaluation of different respiratory monitoring systems used for 4D CT acquisition under free breathing". In: *Journal of Applied Clinical Medical Physics* 16.2 (2015), pp. 334–349. DOI: 10.1120/jacmp.v16i2.4917.
- [41] S. Mori, A.C. Knopf, and K. Umegaki. "Motion management in particle therapy". In: *Medical Physics* 45.11 (2018), e994–e1010. DOI: <https://doi.org/10.1002/mp.12679>.
- [42] Eunsin Lee, Daniel Perry, Joseph Speth, et al. "Measurement-based study on characterizing symmetric and asymmetric respiratory motion interplay effect on target dose distribution in the proton pencil beam scanning". In: *Journal of Applied Clinical Medical Physics* (2020), pp. 1–9. DOI: 10.1002/acm2.12846.
- [43] Martijn Engelsman, Stanley J. Rosenthal, Susan L. Michaud, et al. "Intra- and interfractional patient motion for a variety of immobilization devices". In: *Medical Physics* 32.11 (2005), pp. 3468–3474. DOI: 10.1118/1.2089507.
- [44] Aurora Fassi, Joel Schaerer, Mathieu Fernandes, et al. "Tumor tracking method based on a deformable 4D CT breathing motion model driven by an external surface surrogate". In: *International Journal of Radiation Oncology Biology Physics* 88.1 (2014), pp. 182–188. DOI: 10.1016/j.ijrobp.2013.09.026.
- [45] Philippe Giraud, Esra Morvan, Line Claude, et al. "Respiratory gating techniques for optimization of lung cancer radiotherapy". In: *Journal of Thoracic Oncology* 6.12 (2011), pp. 2058–2068. DOI: 10.1097/JT0.0b013e3182307ec2.
- [46] Kathleen Malinowski, Thomas J. McAvoy, Rohini George, et al. "Incidence of changes in respiration-induced tumor motion and its relationship with respiratory surrogates during individual treatment fractions". In: *International Journal of Radiation Oncology Biology Physics* 82.5 (2012), pp. 1665–1673. DOI: 10.1016/j.ijrobp.2011.02.048.
- [47] Niclas Pettersson, Oluwaseyi M. Oderinde, James Murphy, et al. "Intrafractional relationship changes between an external breathing signal and fiducial marker positions in pancreatic cancer patients". In: *Journal of Applied Clinical Medical Physics* 21.3 (2020), pp. 153–161. DOI: 10.1002/acm2.12841.
- [48] Mitsuhiro Nakamura, Keiko Shibuya, Takehiro Shiinoki, et al. "Positional Reproducibility of Pancreatic Tumors Under End-Exhalation Breath-Hold Conditions Using a Visual Feedback Technique". In: *International Journal of Radiation Oncology Biology Physics* 79.5 (2011), pp. 1565–1571. DOI: 10.1016/j.ijrobp.2010.05.046.
- [49] Xin Wang, Renming Zhong, Sen Bai, et al. "Lung tumor reproducibility with active breath control (ABC) in image-guided radiotherapy based on cone-beam computed tomography with two registration methods". In: *Radiotherapy and Oncology* 99.2 (2011), pp. 148–154. DOI: 10.1016/j.radonc.2011.05.020.
- [50] Per Rugaard Poulsen, John Eley, Ulrich Langner, et al. "Efficient Interplay Effect Mitigation for Proton Pencil Beam Scanning by Spot-Adapted Layered Repainting Evenly Spread out Over the Full Breathing Cycle". In: *International Journal of Radiation Oncology Biology Physics* 100.1 (2018), pp. 226–234. DOI: 10.1016/j.ijrobp.2017.09.043.
- [51] Ye Zhang, D. Boye, C. Tanner, et al. "Respiratory liver motion estimation and its effect on scanned proton beam therapy". In: *Physics in Medicine and Biology* 57.7 (2012), pp. 1779–1795. DOI: 10.1088/0031-9155/57/7/1779.
- [52] S. M. Zenklusen, E. Pedroni, and D. Meer. "A study on repainting strategies for treating moderately moving targets with proton pencil beam scanning at the new gantry 2 at PSI". In: *Physics in Medicine and Biology* 55.17 (2010), pp. 5103–5121. DOI: 10.1088/0031-9155/55/17/014.

- [53] Seishin Takao, Naoki Miyamoto, Taeko Matsuura, et al. "Intrafractional baseline shift or drift of lung tumor motion during gated radiation therapy with a real-time tumor-tracking system". In: *International Journal of Radiation Oncology Biology Physics* 94.1 (2016), pp. 172–180. DOI: 10.1016/j.ijrobp.2015.09.024.
- [54] Shinichi Shimizu, Hiroki Shirato, Shigeaki Ogura, et al. "Detection of lung tumor movement in real-time tumor-tracking radiotherapy". In: *International Journal of Radiation Oncology Biology Physics* 51.2 (2001), pp. 304–310. DOI: 10.1016/S0360-3016(01)01641-8.
- [55] RaySearch Laboratories. *Treatment Planning System - Raystation*. 2020. URL: www.raysearchlabs.com/raystation/ (visited on 02/18/2020).
- [56] Tina Pfeiler, Dalia Ahmad Khalil, Myriam Ayadi, et al. "Motion effects in proton treatments of hepatocellular carcinoma - 4D robustly optimised pencil beam scanning plans versus double scattering plans". In: *Physics in Medicine and Biology* 63.23 (2018). DOI: 10.1088/1361-6560/aaecfc.
- [57] Tina Pfeiler, C. Bäumer, Erik Engwall, et al. "Experimental validation of a 4D dose calculation routine for pencil beam scanning proton therapy". In: *Zeitschrift für Medizinische Physik* 28.2 (2018), pp. 121–133. DOI: 10.1016/j.zemedi.2017.07.005.
- [58] T Pfeiler, D Ahmad Khalil, C Bäumer, et al. "4D robust optimization in pencil beam scanning proton therapy for hepatocellular carcinoma". In: *Journal of Physics: Conference Series* 1154 (2019). DOI: 10.1088/1742-6596/1154/1/012021.
- [59] A. F. Abdelnour, S. A. Nehmeh, T. Pan, et al. "Phase and amplitude binning for 4D-CT imaging". In: *Physics in Medicine and Biology* 52.12 (2007), pp. 3515–3529. DOI: 10.1088/0031-9155/52/12/012.
- [60] W. Paul Segars, Benjamin M.W. Tsui, E. C. Frey, et al. "Extension of the 4D NCAT phantom to dynamic X-ray CT simulation". In: *IEEE Nuclear Science Symposium Conference Record* 5 (2003), pp. 3195–3199. DOI: 10.1109/nssmic.2003.1352577.
- [61] James M. Garrity, W. Paul Segars, Stephen B. Knisley, et al. "Development of a Dynamic Model for the Lung Lobes and Airway Tree in the NCAT Phantom". In: *IEEE Transactions on Nuclear Science* 50.3 (2003), pp. 378–383. DOI: 10.1109/TNS.2003.812445.
- [62] The International Commission on Radiological Protection. *Basic Anatomical and Physiological Data for Use in Radiological Protection: Reference Values*. Tech. rep. 2002. DOI: 10.1016/S0960-894X(03)00438-4.
- [63] The National Library of Medicine. *The National Library of Medicine's Visible Human Project*. URL: https://www.nlm.nih.gov/research/visible/visible%7B%5C_%7Dhuman.html (visited on 05/10/2020).
- [64] Les Piegl and Wayne Tiller. *The NURBS Book*. 1st ed. Springer-Verlag Berlin Heidelberg, 1995. ISBN: 978-3-642-97385-7. DOI: 10.1007/978-3-642-97385-7.
- [65] Hugues Hoppe, Tony DeRose, Tom Duchamp, et al. "Piecewise Smooth Surface Reconstruction". In: *Proceedings of the 21st Annual Conference on Computer Graphics and Interactive Techniques*. 1994, pp. 295–302. DOI: 10.1145/192161.192233.
- [66] W. P. Segars, M. Mahesh, T. J. Beck, et al. "Realistic CT simulation using the 4D XCAT phantom". In: *Medical Physics* 35.8 (2008), pp. 3800–3808. DOI: 10.1118/1.2955743.
- [67] W. P. Segars, G. Sturgeon, S. Mendonca, et al. "4D XCAT phantom for multimodality imaging research". In: *Medical Physics* 37.9 (2010), pp. 4902–4915. DOI: 10.1118/1.3480985.
- [68] Sonja Dieterich, Eric Ford, Dan Pavord, et al. "Respiratory Motion Management for External Beam Radiotherapy". In: *Practical Radiation Oncology Physics*. Elsevier, 2016. Chap. 19, pp. 252–263. DOI: 10.1016/b978-0-323-26209-5.00019-5.
- [69] Craig W. Stevens, Reginald F. Munden, Kenneth M. Forster, et al. "Respiratory-driven lung tumor motion is independent of tumor size, tumor location, and pulmonary function". In: *International Journal of Radiation Oncology Biology Physics* 51.1 (2001), pp. 62–68. DOI: 10.1016/S0360-3016(01)01621-2.
- [70] Stewart Gaede, Gregory Carnes, Edward Yu, et al. "The use of CT density changes at internal tissue interfaces to correlate internal organ motion with an external surrogate". In: *Physics in Medicine and Biology* 54.2 (2009), pp. 259–273. DOI: 10.1088/0031-9155/54/2/006.

- [71] Björn Eiben, Jenny Bertholet, Martin J. Menten, et al. “Consistent and invertible deformation vector fields for a breathing anthropomorphic phantom: a post-processing framework for the XCAT phantom”. In: *Physics in Medicine and Biology* (2020). DOI: 10.1088/1361-6560/ab8533.
- [72] Lee R. Dice. “Measures of the amount of ecologic association between species”. In: *Ecology* 26.3 (1945), pp. 297–302. DOI: 10.2307/1932409.
- [73] Juha Korhonen, Mika Kapanen, Jani Keyriläinen, et al. “A dual model HU conversion from MRI intensity values within and outside of bone segment for MRI-based radiotherapy treatment planning of prostate cancer”. In: *Medical Physics* 41.1 (2013). DOI: 10.1118/1.4842575.
- [74] Mika Kapanen and Mikko Tenhunen. “T1/T2*-weighted MRI provides clinically relevant pseudo-CT density data for the pelvic bones in MRI-only based radiotherapy treatment planning”. In: *Acta Oncologica* 52.3 (2013), pp. 612–618. DOI: 10.3109/0284186X.2012.692883.
- [75] Adam Johansson, Mikael Kalsson, and Tufve Nyholm. “CT substitute derived from MRI sequences with ultrashort echo time”. In: *Medical Physics* 38.5 (2011), pp. 2708–2714. DOI: 10.1118/1.3578928.
- [76] T. Landberg, J. Chavaudra, J. Dobbs, et al. “ICRU Report 50: Prescribing, Recording and Reporting Photon Beam Therapy”. In: *Journal of the International Commission on Radiation Units and Measurements* os26.1 (1993), pp. 1–72. DOI: 10.1093/jicru/os26.1.Report50.
- [77] T. Landberg, J. Chavaudra, J. Dobbs, et al. “ICRU Report 62: Prescribing, Recording and Reporting Photon Beam Therapy (Supplement to ICRU Report 50)”. In: *Journal of the International Commission on Radiation Units and Measurements* os32.1 (1999), pp. 1–52. DOI: 10.1093/jicru/os32.1.Report62.
- [78] Søren M. Bentzen, Louis S. Constine, Joseph O. Deasy, et al. “Quantitative Analyses of Normal Tissue Effects in the Clinic (QUANTEC): An Introduction to the Scientific Issues”. In: *International Journal of Radiation Oncology Biology Physics* 76.3 (2010), S1–S160. DOI: 10.1016/j.ijrobp.2009.09.040.
- [79] Ashutosh Mukherji. “Basics of Planning and Management of Patients during Radiation Therapy: A Guide for Students and Practitioners”. In: Singapore: Springer Singapore, 2018. Chap. Planning a Patient, Deciding on the Volumes and Fields and Plan Verification, pp. 79–107. DOI: 10.1007/978-981-10-6659-7_9.
- [80] “ICRU report 78: Prescribing, Recording, and Reporting Proton-Beam Therapy”. In: *Journal of the ICRU* 7.2 (2007). URL: <https://academic.oup.com/jicru/issue/7/2>.
- [81] M Krieger, A Giger, D C Weber, et al. “Consequences of respiratory motion variability in lung 4DMRI datasets”. In: *ESTRO 38 Abstract book*. 2019, pp. 231–232.
- [82] Joe Y. Chang, Xiaodong Zhang, Antje Knopf, et al. “Consensus Guidelines for Implementing Pencil-Beam Scanning Proton Therapy for Thoracic Malignancies on Behalf of the PTCOG Thoracic and Lymphoma Subcommittee”. In: *International Journal of Radiation Oncology Biology Physics* 99.1 (2017), pp. 41–50. DOI: 10.1016/j.ijrobp.2017.05.014.
- [83] Harald Paganetti, K. Parodi, H. Jiang, et al. “Comparison of pencil-beam and Monte Carlo calculated dose distributions for proton therapy of skull-base and para-spinal tumors”. In: *IFMBE Proceedings*. Vol. 14. 1. Springer Verlag, 2007, pp. 2219–2222. DOI: 10.1007/978-3-540-36841-0_560.
- [84] A Mairani, T. T. Böhlen, A. Schiavi, et al. “A Monte Carlo-based treatment planning tool for proton therapy”. In: *Physics in Medicine and Biology* 58 (2013), pp. 2471–2490. DOI: 10.1088/0031-9155/58/8/2471.
- [85] Francesco Tommasino, Francesco Fellin, Stefano Lorentini, et al. “Impact of dose engine algorithm in pencil beam scanning proton therapy for breast cancer”. In: *Physica Medica* 50 (2018), pp. 7–12. DOI: 10.1016/j.ejmp.2018.05.018.
- [86] Sheng Huang, Kevin Souris, Siyang Li, et al. “Assessing the clinical impact of TPS dose calculation for proton PBS treatment using fast Monte Carlo algorithm”. In: *PTCOG*. 2018. URL: <http://hdl.handle.net/2078.1/210766>.
- [87] RaySearch Laboratories AB. *Proton Monte Carlo Dose Calculation in RayStation*. Tech. rep. 2017. URL: <https://www.raysearchlabs.com/proton-therapy-treatment-planning/>.
- [88] J.R. McPeake, J.G. O’Grady, S. Zaman, et al. “Liver transplantation for primary hepatocellular carcinoma: tumor size and number determine outcome”. In: *Journal of Hepatology* 18 (1993), pp. 226–234.

- [89] Erik den Boer. *Repository*. Tech. rep. 2020. DOI: 10.5281/zenodo.3819582.
- [90] G. Fattori, G. Klimpki, J. Hrbacek, et al. “The dependence of interplay effects on the field scan direction in PBS proton therapy”. In: *Physics in Medicine and Biology* 64.9 (2019). DOI: 10.1088/1361-6560/ab1150.
- [91] K. Bernatowicz, A. J. Lomax, and A. Knopf. “Comparative study of layered and volumetric rescanning for different scanning speeds of proton beam in liver patients”. In: *Physics in Medicine and Biology* 58.22 (2013), pp. 7905–7920. DOI: 10.1088/0031-9155/58/22/7905.
- [92] Jean Pierre Bissonnette, Kevin N. Franks, Thomas G. Purdie, et al. “Quantifying Interfraction and Intrafraction Tumor Motion in Lung Stereotactic Body Radiotherapy Using Respiration-Related Cone Beam Computed Tomography”. In: *International Journal of Radiation Oncology Biology Physics* 75.3 (2009), pp. 688–695. DOI: 10.1016/j.ijrobp.2008.11.066.
- [93] Anthony E Lujan, Edward W Larsen, James M Balter, et al. “A method for incorporating organ motion due to breathing into 3D dose calculations”. In: *Medical Physics* 26.5 (1999), pp. 715–720. DOI: 10.1118/1.598577.
- [94] Kristy K. Brock and Laura A. Dawson. “Adaptive Management of Liver Cancer Radiotherapy”. In: *Seminars in Radiation Oncology* 20.2 (2010), pp. 107–115. DOI: 10.1016/j.semradonc.2009.11.004.
- [95] Geoffrey D. Hugo, Jian Liang, Jonathan Campbell, et al. “On-Line Target Position Localization in the Presence of Respiration: A Comparison of two Methods”. In: *International Journal of Radiation Oncology Biology Physics* 69.5 (2007), pp. 1634–1641. DOI: 10.1016/j.ijrobp.2007.08.023.
- [96] Jochem W.H. Wolthaus, Christoph Schneider, Jan Jakob Sonke, et al. “Mid-ventilation CT scan construction from four-dimensional respiration-correlated CT scans for radiotherapy planning of lung cancer patients”. In: *International Journal of Radiation Oncology Biology Physics* 65.5 (2006), pp. 1560–1571. DOI: 10.1016/j.ijrobp.2006.04.031.
- [97] Anna Kirilova, Gina Lockwood, Perry Choi, et al. “Three-Dimensional Motion of Liver Tumors Using Cine-Magnetic Resonance Imaging”. In: *International Journal of Radiation Oncology Biology Physics* 71.4 (2008), pp. 1189–1195. DOI: 10.1016/j.ijrobp.2007.11.026.
- [98] David P. Gierga, George T.Y. Chen, Jong H. Kung, et al. “Quantification of respiration-induced abdominal tumor motion and its impact on IMRT dose distributions”. In: *International Journal of Radiation Oncology Biology Physics* 58.5 (2004), pp. 1584–1595. DOI: 10.1016/j.ijrobp.2003.09.077.
- [99] E. Engwall, L. Glimelius, and E. Hynning. “Effectiveness of different rescanning techniques for scanned proton radiotherapy in lung cancer patients”. In: *Physics in Medicine and Biology* 63.9 (2018). DOI: 10.1088/1361-6560/aabb7b.
- [100] Zhiwen Liang, Hongyuan Liu, Jun Xue, et al. “Evaluation of the intra- and interfractional tumor motion and variability by fiducial-based real-time tracking in liver stereotactic body radiation therapy”. In: *Journal of Applied Clinical Medical Physics* 19.3 (2018), pp. 94–100. DOI: 10.1002/acm2.12292.
- [101] Jennifer Dhont, Jef Vandemeulebroucke, Manuela Burghelca, et al. “The long- and short-term variability of breathing induced tumor motion in lung and liver over the course of a radiotherapy treatment”. In: *Radiotherapy and Oncology* 126.2 (2018), pp. 339–346. DOI: 10.1016/j.radonc.2017.09.001.
- [102] Keiichi Harada, Norio Katoh, Ryusuke Suzuki, et al. “Evaluation of the motion of lung tumors during stereotactic body radiation therapy (SBRT) with four-dimensional computed tomography (4DCT) using real-time tumor-tracking radiotherapy system (RTRT)”. In: *Physica Medica* 32.2 (2016), pp. 305–311. DOI: 10.1016/j.ejmp.2015.10.093.
- [103] “ICRU report 83: Prescribing, Recording, and Reporting Photon-Beam Intensity-Modulated Radiation Therapy (IMRT)”. In: *Journal of the ICRU* 10.1 (2010). DOI: 10.1093/jicru/10.1.Report83.
- [104] A. M. Henry, W. D.J. Ryder, C. Moore, et al. “Chemoradiotherapy for Locally Advanced Pancreatic Cancer: a Radiotherapy Dose Escalation and Organ Motion Study”. In: *Clinical Oncology* 20.7 (2008), pp. 541–547. DOI: 10.1016/j.clon.2008.03.004.
- [105] G. W. Barendsen. “Dose fractionation, dose rate and iso-effect relationships for normal tissue responses”. In: *International Journal of Radiation Oncology, Biology, Physics* 8.11 (1982), pp. 1981–1997. DOI: 10.1016/0360-3016(82)90459-X.

- [106] Kai Dolde, Ye Zhang, Naved Chaudhri, et al. “4DMRI-based investigation on the interplay effect for pencil beam scanning proton therapy of pancreatic cancer patients”. In: *Radiation Oncology* 14.1 (2019), pp. 1–13. DOI: 10.1186/s13014-019-1231-2.
- [107] The Mathworks Inc. *Correlation coefficients - MATLAB corrcoef*. URL: <https://de.mathworks.com/help/matlab/ref/corrcoef.html> (visited on 02/14/2020).
- [108] Gail M Sullivan and Richard Feinn. “Using Effect Size-or Why the P Value Is Not Enough”. In: *Journal of Graduate Medical Education* (Oct. 2012), pp. 279–282. DOI: 10.4300/JGME-D-12-00156.1.
- [109] Petra Trnkova, Barbara Knäusl, Oxana Actis, et al. “Clinical implementations of 4D pencil beam scanned particle therapy: Report on the 4D treatment planning workshop 2016 and 2017”. In: *Physica Medica* 54 (2018), pp. 121–130. DOI: <https://doi.org/10.1016/j.ejmp.2018.10.002>.
- [110] J Lambert, N Suchowerska, D R McKenzie, et al. “Intrafractional motion during proton beam scanning”. In: *Physics in Medicine and Biology* 50.20 (2005), pp. 4853–4862. DOI: 10.1088/0031-9155/50/20/008.
- [111] Chia Hsin Pan, An Cheng Shiau, Kai Chiun Li, et al. “The irregular breathing effect on target volume and coverage for lung stereotactic body radiotherapy”. In: *Journal of Applied Clinical Medical Physics* 20.7 (2019), pp. 109–120. DOI: 10.1002/acm2.12663.
- [112] Miriam Krieger, Alina Giger, Rares Salomir, et al. “Impact of internal target volume definition for pencil beam scanned proton treatment planning in the presence of respiratory motion variability for lung cancer: A proof of concept”. In: *Radiotherapy and Oncology* 145 (2020), pp. 154–161. DOI: 10.1016/j.radonc.2019.12.001.
- [113] Wei Liu, Steven E. Schild, Joe Y. Chang, et al. “Exploratory Study of 4D versus 3D Robust Optimization in Intensity Modulated Proton Therapy for Lung Cancer”. In: *International Journal of Radiation Oncology Biology Physics* 95.1 (2016), pp. 523–533. DOI: 10.1016/j.ijrobp.2015.11.002.
- [114] Ye Zhang, Isabel Huth, Damien Charles Weber, et al. “Dosimetric uncertainties as a result of temporal resolution in 4D dose calculations for PBS proton therapy”. In: *Physics in Medicine and Biology* 64 (2019). DOI: 10.1088/1361-6560/ab1d6f.
- [115] Floris Ernst. *Compensating for quasi-periodic motion in robotic radiosurgery*. New York, NY: Springer Science+Business Media, LLC, 2012. ISBN: 9781461419129. DOI: 10.1007/978-1-4614-1912-9. URL: https://signals.rob.uni-luebeck.de/index.php/Signals%7B%5C_%7D@%7B%5C_%7DROB.
- [116] R. George, S. S. Vedam, T. D. Chung, et al. “The application of the sinusoidal model to lung cancer patient respiratory motion”. In: *Medical Physics* 32.9 (2005), pp. 2850–2861. DOI: 10.1118/1.2001220.
- [117] Juan Yang, Jing Cai, Hongjun Wang, et al. “Is diaphragm motion a good surrogate for liver tumor motion?” In: *International Journal of Radiation Oncology Biology Physics* 90.4 (2014), pp. 952–958. DOI: 10.1016/j.ijrobp.2014.07.028.
- [118] Paul J. Kelly, Tuan Nguyen, John Hopper, et al. “Changes in axial bone density with age: A twin study”. In: *Journal of Bone and Mineral Research* 8.1 (1993), pp. 11–17. DOI: 10.1002/jbmr.5650080103.
- [119] María Ragnarsdóttir and Ella Kolbrun Kristinsdóttir. “Breathing Movements and Breathing Patterns among Healthy Men and Women 20–69 Years of Age”. In: *Respiration* 73.1 (2006), pp. 48–54. DOI: 10.1159/000087456.
- [120] Verônica F Parreira, Carolina J Bueno, Danielle C França, et al. “Breathing pattern and thoracoabdominal motion in healthy individuals: influence of age and sex”. In: *Revista brasileira de fisioterapia* 14.5 (2010), p. 416.
- [121] Chie Toramatsu, Norio Katoh, Shinichi Shimizu, et al. “What is the appropriate size criterion for proton radiotherapy for hepatocellular carcinoma? A dosimetric comparison of spot-scanning proton therapy versus intensity-modulated radiation therapy”. In: *Radiation Oncology* 8.48 (2013). DOI: 10.1186/1748-717X-8-48.
- [122] T. Furukawa, Y. Hara, K. Mizushima, et al. “Development of NIRS pencil beam scanning system for carbon ion radiotherapy”. In: *Nuclear Instruments and Methods in Physics Research Section B: Beam Interactions with Materials and Atoms* 406 (2017), pp. 361–367. DOI: <https://doi.org/10.1016/j.nimb.2016.10.029>.

- [123] Daniel K Ebner, Hiroshi Tsuji, Shigeo Yasuda, et al. "Respiration-gated fast-rescanning carbon-ion radiotherapy". In: *Japanese Journal of Clinical Oncology* 47.1 (2017), pp. 80–83. DOI: 10.1093/jjco/hyw144.
- [124] Filippo Ammazzalorso, Sebastian Graef, Uli Weber, et al. "Dosimetric consequences of intrafraction prostate motion in scanned ion beam radiotherapy". In: *Radiotherapy and Oncology* 112 (2014), pp. 100–105. DOI: 10.1016/j.radonc.2014.03.022.
- [125] Daniel Richter, Christian Graeff, Oliver Jäkel, et al. "Residual motion mitigation in scanned carbon ion beam therapy of liver tumors using enlarged pencil beam overlap". In: *Radiotherapy and Oncology* 113 (2014), pp. 290–295. DOI: 10.1016/j.radonc.2014.11.020.